UNIVERSITÀ
DEGLI STUDI
DI PADOVA

Sede Amministrativa: Università degli Studi di Padova

Dipartimento di Ingegneria dell'Informazione

SCUOLA DI DOTTORATO DI RICERCA IN: Ingegneria dell'Informazione

INDIRIZZO: Bioingegneria

CICLO: XXV

DEVELOPMENT OF A GAIT ANALYSIS DRIVEN FINITE ELEMENT MODEL OF THE DIABETIC FOOT

Direttore della Scuola : *Ch.mo Prof. Matteo Bertocco*

Supervisore : *Ch.mo Prof. Claudio Cobelli*

Dottorando :

Annamaria Guiotto

Contents

List of Figures

List of Tables

Abstract

Diabetic foot is an invalidating complication of diabetes mellitus, a chronic disease increasingly frequently encountered in the aging population. The global prevalence of diabetes is predicted to double by the year 2030 from 2.8% to 4.4%. The prevalence of foot ulceration among patients with diabetes mellitus ranges from 1.3% to 4.8%.

Several studies have highlighted that biomechanical factors play a crucial role in the aetiology, treatment and prevention of diabetic foot ulcers. Recent literature on the diabetic foot indicates that mechanical stresses, high plantar pressures or/and high tangential stresses, acting within the soft tissues of the foot can contribute to the formation of neuropathic ulcers. While it is important to study the in-vivo diabetic foot-to-floor interactions during gait, models for simulations of deformations and stresses in the diabetic plantar pad are required to predict high risk areas or to investigate the performance of different insoles design for optimal pressure relief.

The finite element (FE) models allow taking into account the critical aspects of the diabetic foot, namely the movement, the morphology, the tissue properties and the loads.

Several 2-dimensional (2D) and 3-dimensional (3D) foot models were developed recently to study the biomechanical behavior of the human foot and ankle. However, to the author knowledge, a geometrically detailed and subject specific 3D FE model of the diabetic neuropathic foot and ankle has not been reported. Furthermore 2D and 3D state-of-the-art FE foot models are rarely combined with subject specific gait analysis data both in term of ground reaction forces and kinematics as input parameters and plantar pressure for validation purposes.

The purpose of the study herein presented was to simulate the biomechanical behavior of both an healthy and a diabetic neuropathic foot in order to predict the area characterized by excessive stresses on the plantar surface. To achieve this, it has been developed an FE model of the foot by means of applying the loading

and boundary conditions given by subject-specific integrated and synchronized kinematic-kinetic data acquired during gait analysis trials to a subject specific FE model (geometry was obtained through subject specific magnetic resonance images - MRI). Thus, an integrated kinematic-kinetic protocol for gait analysis which evaluates 3D kinematics and kinetics of foot subsegments together with two comprehensive FE models of an healthy and a diabetic neuropathic foot and ankle were described herein.

In order to establish the feasibility of the former approach, a 2D FE model of the hindfoot was first developed, taking into account the bone and plantar pad geometry, the soft tissues material properties, the kinematics and the kinetics of both an healthy and a diabetic neuropathic foot acquired during three different phases of the stance phase of gait. Once demonstrated the advantage of such an approach in developing 2D FE foot models, 3D FE models of the whole foot of the same subjects were developed and the simulations were run in several phases of the stance phase of gait.

The validation of the FE simulations were assessed by means of comparison between the simulated plantar pressure and the subject-specific experimental ones acquired during gait with respect to different phases of the stance phase of gait.

A secondary aim of the study was to drive the healthy and the diabetic neuropathic FE foot models with the gait analysis data respectively of 10 healthy and 10 diabetic neuropathic subjects, in order to verify the possibility of extending the results of the subject specific FE model to a wider population. The validity of this approach was also established by comparison between the simulated plantar pressures and the subject-specific experimental ones acquired during gait with respect to different phases of the stance phase of gait. Comparison was also made between the errors evaluated when the FE models simulations was run with the subject specific geometry (obtained from MRI data) and the errors estimated when the FE simulations were run with the data of the 20 subjects.

Sommario

Il diabete mellito è una malattia cronica sempre più frequente. Fra le complicanze ad esso associate vi è il cosiddetto piede diabetico. L'incidenza del diabete a livello mondiale è destinata a raddoppiare entro il 2030 passando dal 2.8% al 4.4% della popolazione ed il numero di pazienti affetti da diabete mellito che sviluppano ulcera podalica oscilla tra l'1.3% ed il 4.8%.

Numerosi studi hanno evidenziato come i fattori biomeccanici giochino un ruolo fondamentale nell'eziologia, nel trattamento e nella prevenzione delle ulcere del piede diabetico. La letteratura recente sul piede diabetico indica che le sollecitazioni meccaniche, ossia le elevate pressioni plantari e/o gli elevati sforzi tangenziali, che agiscono all'interno dei tessuti molli del piede possono contribuire alla formazione di ulcere. È quindi importante studiare le interazioni piede-suolo durante il cammino nei pazienti diabetici, ma si rendono anche necessari dei modelli per la simulazione di sollecitazioni e deformazioni nel tessuto plantare del piede diabetico che permettano di predire le aree ad alto rischio di ulcerazione o di valutare l'efficacia di ortesi plantari nel ridistribuire in modo ottimale le pressioni plantari.

I modelli agli elementi finiti consentono di tenere conto degli aspetti critici del piede diabetico, vale a dire il movimento, la morfologia, le proprietà dei tessuti e le sollecitazioni meccaniche. Di recente sono stati sviluppati diversi modelli bidimensionali (2D) e tridimensionali (3D) del piede con lo scopo di studiare il comportamento biomeccanico di piede e caviglia. Tuttavia, per quanto appurato dall'autore, in letteratura non è stato riportato un modello 3D agli elementi finiti del piede diabetico neuropatico con geometria dettagliata e specifica di un soggetto. Inoltre, i modelli 2D e 3D agli elementi finiti del piede presenti in letteratura sono stati raramente combinati con i dati del cammino specifici dei soggetti, sia in termini di forze di reazione al suolo e cinematica (come parametri di input) che in termini di pressioni plantari per la validazione.

L'obiettivo dello studio qui presentato è stato quello di simulare il comporta-

mento biomeccanico sia del piede di un soggetto sano che del piede di un soggetto diabetico neuropatico per prevedere l'area della superficie plantare caratterizzata da eccessive sollecitazioni. A tal scopo, sono stati sviluppati due modelli agli elementi finiti di piede e caviglia, utilizzando le geometrie specifiche dei piedi dei due soggetti (uno sano ed uno diabetico neuropatico) ottenute attraverso immagini di risonanza magnetica (MRI). Quindi sono state effettuate delle simulazioni mediante l'applicazione di carichi e di condizioni al contorno, ottenuti da dati di cinematica e cinetica, integrati e sincronizzati, acquisiti durante il cammino, specifici dei due soggetti sui rispettivi modelli agli elementi finiti. Pertanto in questa tesi sono stati descritti un protocollo integrato di cinematica-cinetica per l'analisi del cammino che permette di valutare la cinematica e la cinetica 3D dei sottosegmenti del piede e due modelli completi agli elementi finiti di un piede sano e di un piede diabetico neuropatico.

Per stabilire la fattibilit di tale approccio, sono stati inizialmente sviluppati due modelli 2D agli elementi finiti del retropiede di un soggetto sano e di un soggetto diabetico neuropatico, tenendo conto della geometria ossea e del cuscinetto plantare, delle proprietà dei materiali dei tessuti molli, della cinematica e della cinetica. Questi ultimi sono stati acquisiti durante tre istanti della fase di appoggio del ciclo del passo. Una volta dimostrato il vantaggio di un simile approccio nello sviluppo di modelli 2D agli elementi finiti del piede, sono stati sviluppati i modelli 3D agli elementi finiti del piede intero degli stessi soggetti e sono state eseguite le simulazioni in vari istanti della fase di appoggio.

La validazione delle simulazioni è stata effettuata attraverso il confronto tra le pressioni plantari simulate e quelle acquisite sperimentalmente durante il cammino degli stessi soggetti, nei corrispondenti istanti della fase di appoggio.

Un secondo scopo dello studio qui presentato è stato quello di effettuare simulazioni del modello del piede del soggetto sano e di quello del soggetto neuropatico con dati di analisi del cammino rispettivamente di 10 soggetti sani e 10 diabetici neuropatici, al fine di verificare la possibilit di estendere i risultati dei modelli specifici dei due soggetti ad una popolazione più ampia. La validit di questo approccio stata valutata tramite il confronto tra le pressioni plantari simulate e quelle sperimentali specifiche di ogni soggetto, acquisite durante il cammino. Inoltre gli errori delle simulazioni eseguite con i dati dei 20 soggetti sono stati confrontati con gli errori effettuati quando le simulazioni dei modelli avevano previsto l'utilizzo di dati di cammino specifici dei due soggetti la cui geometria podalica era stata ottenuta da MRI.

Chapter 1

Introduction

1.1 Overview

Diabetic neuropathy is common throughout the world and it has been estimated that around 40% of older diabetic patients have risk factors for foot ulceration. Foot ulceration can be highly debilitating and has been found to precede 84% of lower extremity amputations [19].

Peripheral neuropathy is one of the most insidious chronic complications of diabetes. It has been observed that dynamic changes in gait are usually associated with the peripheral neuropathy somatosensory deficits. Biomechanical studies have highlighted that dynamic gait evaluation can identify functional alterations. They are also useful as a complimentary routine in the clinic treatment of diabetes and its further long-term complications [100].

Normal walking requires sensory input to adapt and modify motor patterns. Fully functioning joints and bones, combined with adequate muscle strength, are also needed. The result of this activity is also coupled with local soft tissue mechanics affecting the foot-ground interface [118]. However in diabetic neuropathy these functionalities are affected by the pathology (paragraphs 2.2 and 2.4).

It should be mentioned that mechanical forces acting within the soft tissues of the foot can contribute to the formation of neuropathic ulcers [94]. It has been demonstrated that plantar ulcers occur at locations of high plantar pressures or/and high tangential stresses (paragraph 2.3.3). The measurement of pressure and ground reaction forces during gait using tools developed and refined in the field of biomechanics has been shown to be a valuable asset to the management of the foot at risk for ulceration [28].

While it is important to study the in-vivo diabetic foot-to-floor interactions

during gait [101, 102, 103, 104] (paragraph 2.3.1), models for simulations of deformations and stresses in the diabetic plantar pad are required to predict high risk areas or to investigate the performance of different insoles design for optimal pressure relief [57, 31, 47, 7].

Existing finite element (FE) models of the foot, and in some cases footwear, were developed by a number of groups [6, 31, 29, 36, 54, 57] to provide estimates of quantities that cannot be directly measured or to perform simulations that would be onerous or dangerous for human subjects [27]. The FE models allow taking into account the critical aspects of the diabetic foot, namely the movement, the morphology, the tissue properties and the loads. However they have been developed under certain simplifications and assumptions such as a simplified or partial foot shape, assumptions of linear material properties, infinitesimal deformation and linear boundary conditions [33] (paragraph 2.5.2).

Although several 2-dimensional (2D) and 3-dimensional (3D) foot models were developed recently to study the biomechanical behavior of the human foot and ankle, to the author knowledge, a geometrically detailed and subject specific 3D FE model of the diabetic neuropathic foot and ankle has not been reported. Furthermore 2D and 3D state-of-the-art FE foot models are rarely combined with subject specific gait analysis data both in term of ground reaction forces and kinematics as input parameters and plantar pressure for validation purposes.

1.2 Aims of the thesis

The aim of this thesis was to simulate the biomechanical behavior of both an healthy and a diabetic neuropathic foot in order to predict the area characterized by excessive stresses on the plantar surface. To achieve this, it has been developed an FE model of the foot by means of applying the loading and boundary conditions given by subject-specific integrated and synchronized kinematic-kinetic data acquired during gait analysis trials to a subject specific FE model (geometry was obtained through subject specific magnetic resonance images - MRI). Thus, an integrated kinematic-kinetic protocol for gait analysis which evaluates 3D kinematics and kinetics of foot subsegments together with two comprehensive FE models of an healthy and a diabetic neuropathic foot and ankle have been developed and described herein.

In order to establish the feasibility of the former approach, a 2D FE model of the hindfoot was first developed, taking into account the bone and plantar pad

geometry, the soft tissues material properties, the kinematics and the kinetics of both an healthy and a diabetic neuropathic foot. Once demonstrated the advantage of such an approach in developing 2D FE foot models, 3D FE models of the whole foot of the same subjects were developed.

The validation of the FE simulation was assessed by means of comparison between the simulated plantar pressure and the subject-specific experimental ones acquired during gait with respect to different phases of the stance phase of gait.

A secondary aim of the study was to drive the simulations of the healthy and the diabetic neuropathic FE foot models with the gait analysis data respectively of 10 healthy and 10 diabetic neuropathic subjects, in order to verify the possibility of extending the results of the subject specific FE model to a wider population. The validity of this approach was also established by comparison between the simulated plantar pressures and the subject-specific experimental ones acquired during gait with respect to different phases of the stance phase of gait. Comparison was also made between the differences recorded between experimental and simulated plantar pressure in the case of FE model simulations driven with the subject specific geometry (obtained from MRI data) or when this was not available.

1.3 Outlines

This thesis is organized as follows: the second chapter presents the diabetic foot problem, its study through the gait analysis and the state-of-the-art of the FE models of the foot reported in literature.

The third and fourth chapters focus respectively on the 2D model of the heel and the 3D model of the whole foot and ankle of both an healthy and a diabetic neuropathic subject. The description of the materials and methods are given first, presenting the workflow for the creation of the models, the boundary conditions and loads extraction from the gait analysis data and the application of the former to the FE models. Then the results and the discussion of the simulations are reported.

Conclusions and future developments are the objects of the fifth chapter.

Chapter 2

State of the art

2.1 Introduction

Diabetic foot is an invalidating complication of diabetes mellitus, a chronic disease increasingly frequently encountered in the aging population. Several methodologies have been developed in order to define successful prevention therapies. In this chapter an overview of the state of the art biomechanics approaches to diabetic foot prevention has been reported.

First of all the epidemiology of diabetes and diabetes complications has been reported (World Health Organization), together with the state of the art on risk factors for foot ulceration and ulcer prevention therapies.

Then the gait analysis discipline has been presented, focusing on state of the art simultaneous three-dimensional (3D) kinematics, kinetics and plantar pressure analysis, and how these can provide identification of the foot pathological alterations related to diabetes.

Finally, an overview on the finite element (FE) modelling technique applied to foot biomechanics is given, describing the state of the art of foot FE models focusing on diabetic foot FE models.

2.2 The diabetic foot

2.2.1 Diabetes and its complications [3]

Diabetes is a chronic disease that occurs either when the pancreas does not produce enough insulin or when the body cannot effectively use the insulin it produces. Insulin is a hormone that regulates blood sugar. Hyperglycaemia, or

raised blood sugar, is a common effect of uncontrolled diabetes and over time leads to serious damage to many of the body's systems, especially the nerves and blood vessels.

Type 1 diabetes is characterized by deficient insulin production and requires daily administration of insulin. The cause of type 1 diabetes is not known and it is not preventable with current knowledge.

Type 2 diabetes results from the body's ineffective use of insulin. Type 2 diabetes comprises 90% of people with diabetes around the world, and is largely the result of excess body weight and physical inactivity.

- Over time, diabetes can damage the heart, blood vessels, eyes, kidneys, and nerves.

- Diabetes increases the risk of heart disease and stroke. 50% of people with diabetes die of cardiovascular disease (primarily heart disease and stroke).

- Combined with reduced blood flow, neuropathy in the feet increases the chance of foot ulcers and eventual limb amputation.

- Diabetic retinopathy is an important cause of blindness, and occurs as a result of long-term accumulated damage to the small blood vessels in the retina. After 15 years of diabetes, approximately 2% of people become blind, and about 10% develop severe visual impairment.

- Diabetes is among the leading causes of kidney failure. 10-20% of people with diabetes die of kidney failure.

- Diabetic neuropathy is damage to the nerves as a result of diabetes, and affects up to 50% of people with diabetes. Although many different problems can occur as a result of diabetic neuropathy, common symptoms are tingling, pain, numbness, or weakness in the feet and hands.

- The overall risk of dying among people with diabetes is at least double the risk of their peers without diabetes.

The main underlying risk factors for foot ulcers in diabetic patients are peripheral neuropathy and ischemia [21].

Figure 2.1: Diabetic foot ulcer.

Neuropathy [92]

Chronic hyperglycaemia in diabetic patients leads to the loss of nerve function. In fact the hyperglycemia induces metabolic derangements that directly affect the Schwann cells (myelin) and nodes of Ranvier (axons) [53]. This neuropathy affects the motor, autonomic, and sensory components of the nervous system.

Damage to the innervations of the intrinsic foot muscles leads to an imbalance between flexion and extension of the affected foot. This produces anatomic foot deformities that create abnormal bony prominences and pressure points, which gradually cause skin breakdown and ulceration.

Autonomic neuropathy leads to dry skin, loss of sweating, and the development of fissures and cracks that promote infections.

Peripheral sensory neuropathy disables the protection mechanism that is normally activated when the plantar soft tissue is damaged [53]. This sensory loss worsen the situation as when trauma occurs or bony structure changes, patients do not feel the problem on their lower extremities. As a result, many wounds go unnoticed, they are unable to take appropriate corrective measures and the affected area is continuously subjected to repetitive pressure and shear forces from ambulation and weight bearing.

Ischemia

Another contributing factor to the development of foot ulcers is peripheral vascular disease. It is a condition characterized by atherosclerotic occlusive disease of the lower extremities and commonly affects the tibial and peroneal arteries. In

fact hyperglycemia affects the structure and function of endoneurial microvessels, thereby altering the blood-nerve barrier and causing local hypoxia or ischemia [53].

The abnormal metabolic state accompanying diabetes results in changes in the state of arterial structure and function which include increases in vascular inflammation and derangements in the cellular components of the vasculature, as well as alterations in blood cells and haemostatic factors [9]. Cumulatively, this leads to occlusive arterial disease that results in ischemia in the lower extremity and an increased risk of ulceration or worsening of wounds in diabetic patients.

Effects on soft tissues [53]

Hyperglycemia cause also an increased stiffening of collagen-rich soft tissues. A number of studies identified alterations in collagen structure and function as related to the glucose-exposure. Increased fibril diameter, closer packing of fibrils and local fusion of adjacent fibrils are the abnormalities observed in those studies. Cross-linking of adjacent collagen fibrils and nonenzymatic glycosylation of keratin occur with the glycation, causing substantial stiffening of the affected tissues, including hyperkeratosis and formation of thickened callus in the plantar skin. This mechanism has an overall effect of mechanically stiffening the plantar diabetic tissue, and consequently under heel and metatarsal heads soft tissues becomes less elastic and less able to spread the pressures. Hence, the 'cushioning' property of the plantar soft tissue, especially at high-pressure sites such as those under the medial metatarsals and the heel, is damaged [53].

2.2.2 Incidence and prevalence

The global prevalence of diabetes is predicted to double by the year 2030 from 2.8% to 4.4%. Of individuals with diabetes, a substantial number will develop lower extremity disease including peripheral neuropathy, foot ulcers, and peripheral arterial disease [115].

The prevalence of foot ulceration among patients with diabetes mellitus ranges from 1.3% to 4.8% in the community, to as high as 12% in hospital [18]. This represents considerable patient morbidity, and is associated with substantial healthcare costs.

The pathophysiology of diabetic foot ulceration is multifactorial, but peripheral neuropathy is thought to be responsible for most cases. The loss of perception

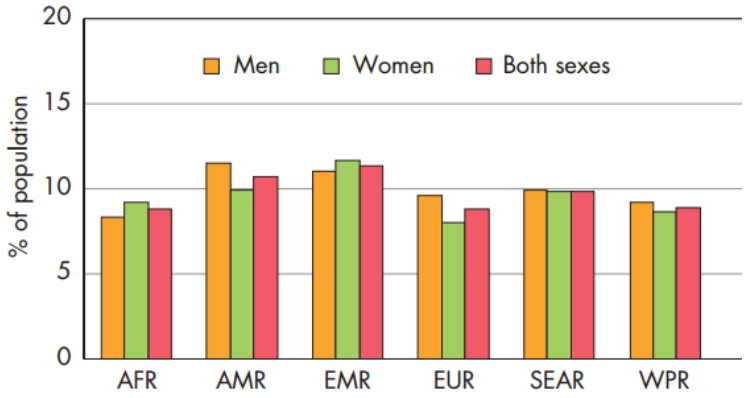

Figure 2.2: Age-standardized prevalence of diabetes in adults aged 25+ years, by WHO Region, 2008 [3, 116].

of pain results in the development of what should be preventable foot lesions in many patients. It has been estimated that around 40% of older type 2 diabetic neuropathic patients have risk factors for foot ulceration. As neuropathy is silent in up to 50% of patients, all diabetic patients should receive an annual screening by careful examination of the lower limbs for evidence of any sensory loss [19].

2.2.3 Prevention and treatment of the diabetic foot

To prevent foot ulceration and amputation, clinical guidelines recommend early identification of risk, based on annual foot screening of all diabetic patients, with targeting of preventive and treatment interventions to 'high risk' individuals [9, 40]. Therefore, preventive care should mainly aim at reducing foot pressures and shear. This can be performed through callus debridement as well as provision of pressure-reducing insoles and therapeutic footwear. A major goal of therapeutic footwear is frequently to relieve areas of elevated pressure underneath bony prominences such as metatarsal heads or the heel [115].

2.3 Diabetic foot biomechanics

Several studies have highlighted that biomechanical factors play a crucial role in the aetiology, treatment and prevention of diabetic foot ulcers. Recent literature on the diabetic foot indicates that mechanical stress concentrations in deep tissues of the plantar pad of the foot, which develop directly under bony

prominences (particularly under the calcaneous and metatarsal heads), play a dominant role in the mechanism of diabetic foot injuries and may lead to foot ulceration [120]. However, the association between kinematic-kinetic and the internal stresses is less investigated in the diabetic foot. This is because of the difficulties in quantifying the in-vivo bone and soft tissue stresses with the in-vitro studies: the loading conditions are often different from the real physiological loading situations.

Some techniques have been explored to study this mechanical interaction between the external and the internal stresses and strains. They can be subdivided in two categories: experimental and numerical. From an experimental point of view, the motion analysis technique presented on paragraph 2.3.1 is one among the possibilities to quantify biomechanical variables directly measurable in-vivo. Researchers have also used magnetic resonance imaging, or computed tomography imaging together with pressure analysis to quantify the links between internal structures and external pressures on the foot [29, 47, 52, 96]. While experimental analyses are limited solely to measurements of interfacial variables, a reliable numerical model can provide both the interfacial pressures and insight into internal stresses and strains tolerated by the plantar tissue [120].

2.3.1 Gait analysis [25]

In the last twenties, researchers have used the so called *gait analysis* in order to quantify the alterations in the diabetic foot. The aforementioned variables (the plantar pressures, the kinematic and the ground reaction forces) can be registered during static and walking trials with a non-invasive instrumentation setup.

The gait analysis can be subdivided in:

- Kinematic analysis studies the positions of the body segments in space, their velocity, acceleration and joint angles through stereophotogrammetric systems or electrogoniometers or inertial sensors;
- Kinetic analysis includes the study of ground reaction forces, moments and pressures recorded through force plates and pressure mats devices;
- Electromyographic analysis studies the muscle activation through an EMG device.

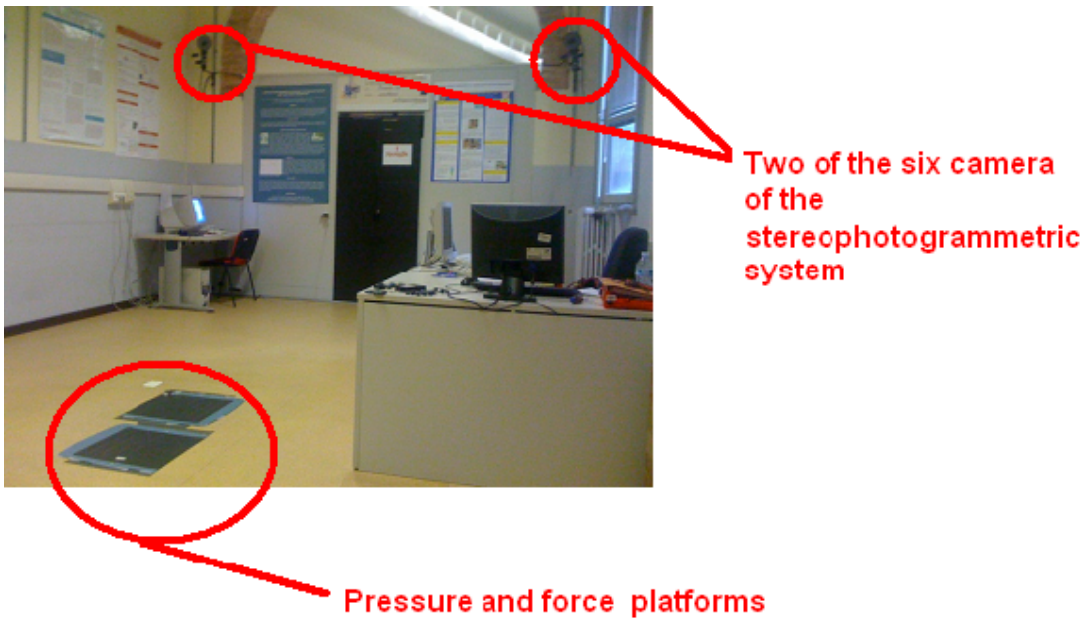

Figure 2.3: The laboratory with the streophotogrammetric system and the pressure and force plates.

The gait cycle [93]

"Walking uses a repetitious sequence of limb motion to move the body forward while simultaneously maintaining stance stability" [93]. During the body progression, a limb acts as support while the other progresses to the next support. The repetition of this sequence is performed by each limb alternatively. Every single sequence is called "gait cycle" and it is conventionally assumed to start at the first contact of the foot with the ground and to finish when the same foot touches the ground again.

In order to study the biomechanics of the gait, the "gait cycle" is usually taken as reference and every biomechanical variable is reported in the 100% of the gait cycle.

According to Perry [93], the normal gait cycle can be subdivided into two phases, the stance (approximately 0-60%) and the swing (approximately 60-100%), according to the functional activity of the lower limb. During the stance the foot is in contact with the ground while during the swing the foot is raised and progressing.

Several subphases can also be identified [93] (figure 2.4):

- *Initial contact* or *heel strike*: The phase when the foot impact with the

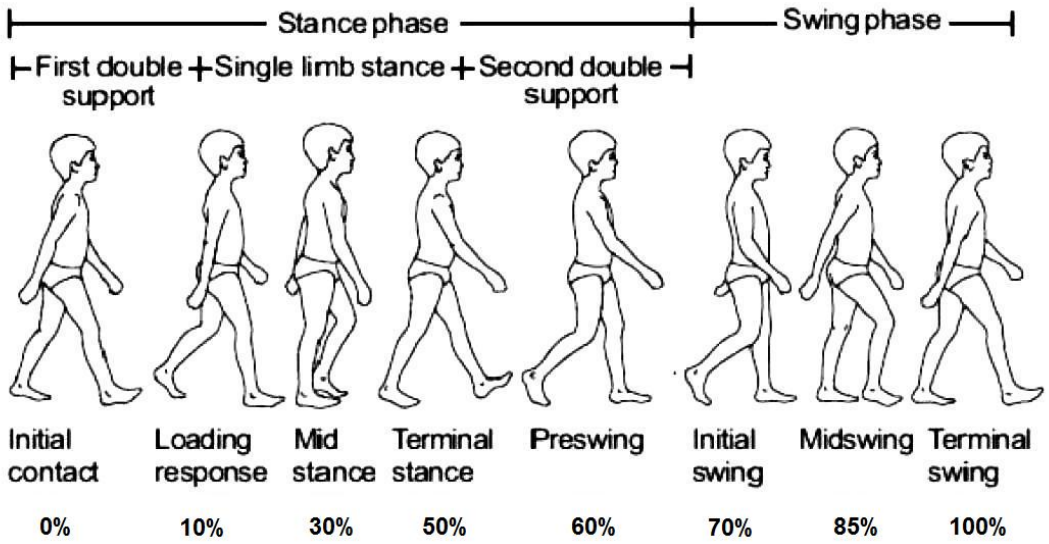

Figure 2.4: Normal gait cycle phases [114].

ground is around the 0-2% of the gait cycle.

- *Loading response*: The initial double support stance period which is defined from initial contact (0%) to 10% of the gait cycle.

- *Mid stance*: The first half of the single support from 10 to 30% of the gait cycle and is defined from the time the opposite limbs leaves the floor until body weight is aligned over the forefoot. Sometimes the term midstance is adopted also for the 30% instant alone.

- *Terminal stance*: The second half of the single support from 30 to 50% of the gait cycle and is defined as the time from heel rise until the other limb makes contact with the floor. During this phase body weight moves ahead of the forefoot.

- *Pre-swing*: The final double support stance period which is defined from the time of initial contact with the contralateral limb to ipsilateral toe-off (50-60%).

- *Initial swing*: The initial third of the swing phase from 60 to 73% of the gait cycle as defined from toe-off to when the swing limb foot is opposite the stance limb.

- *Mid swing*: The middle third of the swing phase from 73 to 87% of the gait

cycle as defined from the time the swing foot is opposite the stance limb to when the tibia is vertical.

- *Terminal swing*: The final third of the swing phase from 87 to 100% of the gait cycle as defined from the time when the tibia is vertical to initial contact.

Another phase not defined by Perry but relevant for the study of the diabetic foot biomechanics is the *push-off* phase. It is the period in late stance (between approximately 50% and *toe-off*) when the foot pushes toward the ground to help advance the limb into swing phase.

2.3.2 Gait analysis instrumentation [25]

In this paragraph only the instrument setup an protocols adopted for this thesis is presented.

Kinematic

Most commonly used systems for the estimation of human movement are the optoelectronic systems that use cameras operating in the range of the visible or near infrared. They ensure high accuracy even though they can provide only an estimate and not the direct measure of the kinematic variables. The use of cameras with infrared emitters together with passive markers is called *stereophotogrammetry*.

Figure 2.5: Camera with infrared illuminators.

The passive markers are small plastic balls covered with reflector film. In contrast to the active ones they do not have a led that generate light thus they need an additional lighting device with specific wavelengths (780-820 nm). Their

sphericity guarantees the best reflection of infrared rays and with cameras provided of an appropriate optical filter, they are immediately recognizable from the background.

Movements are thus acquired from a stereophotogrammetric system and the data are processed by an elaboration software that can detect markers. The result is a sequence of images. Before starting the acquisition the cameras have to be calibrated so their geometrical parameters have to be settled. The reference system of the laboratory has to be determined and also the internal parameters of the cameras as the optic has to be fixed. After these steps the system algorithm can reconstruct the position of a point in the 3D space.

For this thesis, a stereophotogrammetric setup have been adopted and passive markers have been double-side taped to the skin at various anatomical landmarks of the feet, according to the protocol described in [101, 104].

At the Bioengineering of Movement Laboratory (DEI - University of Padova) a 60-120 Hz 6 cameras stereophotogrammetric system (BTS S.r.l, Padova) have been used. Sensors of the cameras are CCD (1/2" F 1.4/4.5 mm) with IR filters. The video resolution is 640 x 480 pixel while the lens are 3.5mm and 6-12mm.

Ground reaction forces

Force platforms are measuring instruments that detect the ground reaction forces generated by a body standing on or moving across them, to quantify balance, gait and other parameters of biomechanics. Measures are given according to the reference system associated with the platform and usually provided by the constructor. More advanced and most commonly used devices measure the 3D components of the single equivalent force applied to the surface and its point of application, usually called the centre of pressure, as well as the vertical moment of force.

The most common technologies used for the realization of force transducers are based on strain gauge or piezoelectric crystals. The latter are not suitable for measuring static loads, because the electric charge disperses over time. The strain gauge sensors have a frequency response lower than the piezoelectric crystals but they are cheaper and they can be used for the posturographic examination.

For this thesis two strain gauge force platform (FP4060-10, Bertec Corporation, USA) have been used. The technical characteristics of the platforms are reported in table 2.1.

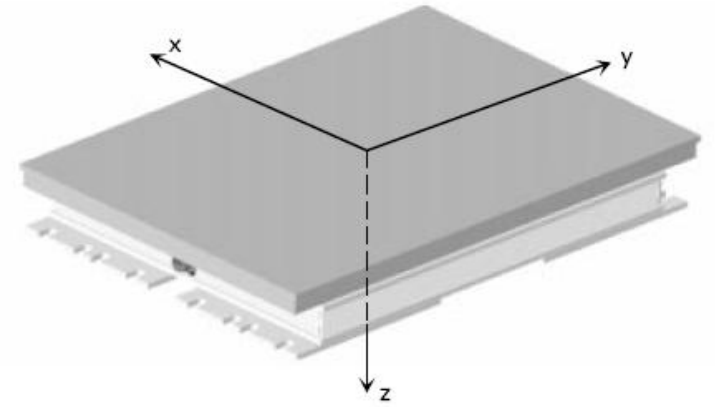

Figure 2.6: Bertec force plate with its reference system [14]

Size (mm)			**Weight (kg)**	**Rated Load (kN)**			**Natural Frequency (Hz)**		
L	W	H		Fx	Fy	Fz	Fx	Fy	Fz
600	400	83	28	5	5	10	550	540	340

	Fx	**Fy**	**Fz**	**Mx**	**My**	**Mz**
RATED LOAD (kN, kN*m)	5	5	10	3	2	1.5
OVERLOAD FACTOR (%)	50	50	50	50	50	50

Table 2.1: Technical details of the force plate-item 4060-80 (*Data sheet* [14]).

Plantar pressures

During locomotion forces between the human body and the ground are spread over various structures.

The force plates does not give the information on how loads distributes under the foot and so different technologies have been developed. To be able to detect the real map of loads, multiple sensors that measure only the vertical component of the force are used. Once the area of the sensor is known and the vertical force is measured, it is possible to calculate the pressure on it. Systems realized in this way provide measurement of the pressure distribution on a bearing surface with a detail that can be established in the construction phase according to requirements. Typically the pressure sensors are arranged in arrays to form platforms of pressure or they can be arranged in foot sole shapes to form insoles.

The latter have the advantage that they can be inserted inside a shoe thus allowing within shoes foot pressures measurements. However they are less accurate than the pressure platforms due to deformation that can occur on the sensors due to their adaptation to the shoe shape and to possible movements or misplacements inside the shoe.

The relevant characteristics of a pressure system are:

- spatial resolution, that is the distance between the centres of two adjacent sensors. It is important for the suitability to provide the information below smaller structures, such as the metatarsal heads;

- area of the sensor. Ideally, sensors should be point. In the reality the actual pressure is measured as the average force/area. The greater the surface is, the greater is the resulting error;

- sampling frequency. It should be the highest as possible but usually the limit is the quantity of data to register.

- type of sensors. They can be piezoelectric, resistive or capacitive.

The Bioengineering of Movement Laboratory (DEI - University of Padova) is provided with two plantar pressure systems (Imagortesi, Piacenza, produced by Medicapteurs, France - figure 2.7). The technical characteristics are reported in tables 2.2 and 2.3.

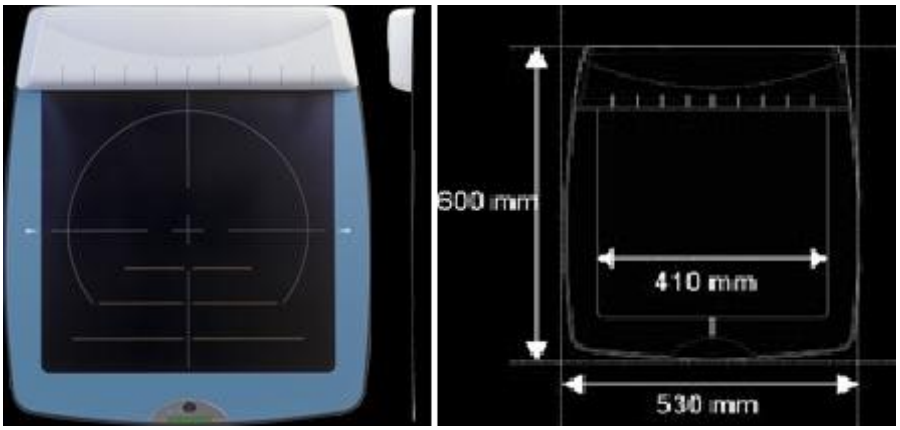

Figure 2.7: Winpod Pressure platform and its size [1].

Size (length/depth/height)	530 x 600 x 45mm
Thickness of the sensors	4mm
Detectable area	382 x 382mm
Weight	6,8kg

Table 2.2: Structural characteristics of the plantar pressure systems [1]).

Sensors	Sensors resistive
Sensor size	8mm x 8mm
Sensor thickness	0,15mm
Number of sensors in the platform	2304 = 48 x 48
Resistor	$> 1M\Omega$
Sensor accuracy	$\pm 5\%$
Rise time	da 1 a 2ms
Operating temperature	da -40 a +85C
Average life time of sensors	> 1 M of activations
Minimum pressure detectable	4 N/cm^2
Maximum pressure detectable / sensor	100 N/cm^2
PC connection	USB
Power supply	External transformer 12V DC
Frame rate (sampling frequency)	≤ 150 Hz
Analogical/digital conversion	8 bit, 255 valori

Table 2.3: Electronic characteristics of the plantar pressure systems [1]).

2.3.3 Gait analysis of the diabetic foot

The three main functions of the human foot and ankle are: shock absorption, weight bearing stability, and progression [93].

The aforementioned diabetic complications cause alterations in foot structure, affecting foot function, subsequently leading to increased plantar foot pressure, which is a predictive risk factor for the development of diabetic foot ulceration [113].

Several studies have been conducted in the last decade to investigate diabetic foot biomechanics alterations in order to evaluate subjects at risk for ulcer formation and the danger zone for developing an ulcer on their foot [15, 28, 39, 56, 55, 69, 81, 85, 97, 98, 101, 102, 103, 104, 106].

The influence of anatomical structure and type of foot on foot function in term of kinematics and kinetics has also been investigated in neuropathic subjects and important alterations were found with respect to controls [8, 15, 16, 56, 61, 69, 74, 75, 73, 81, 107, 112]. Some authors [74, 61] investigated diabetic subjects taking into account foot structure and foot deformities and demonstrated close relationships between foot morphological alterations and plantar ulcerations. Other studies indicate that mechanical stress concentrations in deep tissues of the plantar pad of the foot, which develop directly under bony prominences (particularly under the calcaneus and metatarsal heads) play a dominant role in the mechanism of diabetic foot injuries and may lead to foot ulceration [28, 47, 91, 120].

In the following paragraphs a detailed description of the specific role of different factors in altering the diabetic foot biomechanics is reported.

Plantar pressures

As reported above, the measure of the plantar pressure is important to prevent the breakdown of the plantar tissues. This can be initiated by three main mechanisms:

1. increased duration of pressures which includes application of relatively low pressures for a long period of time resulting in ischemia. If the latter is prolonged, it leads to cell death and injury. There is an inverse relationship between time and pressure that means that in several days pressure ulcers can also occur at a very low level;

2. increased magnitude of pressures which comprises the application of high

pressures in a short period of time. This only occurs if a large force is applied to a relatively small area of skin;

3. increased number of pressure which leads to failure of the biological structure for the continuous repetition of loads.

Studies on plantar pressures demonstrated an important correlation between the sites displaying high plantar pressures and the presence of callosities on diabetic neuropathic subjects [8, 56, 69]. Stresses were found to be relatively higher and located closer to the skin surface where skin breakdown was most likely to occur [23, 27, 85, 56, 112].

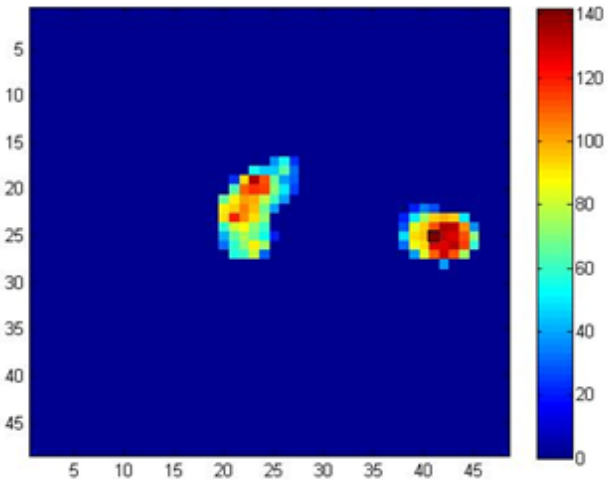

Figure 2.8: Output of the plantar pressure platform - diabetic subject.

Others demonstrated an association between higher peak plantar pressures and morphological foot alterations in diabetic neuropathic subjects.

Ahroni et al. evidenced that the plantar pressure increase under a rigid hallux [8] while Mueller et al. highlighted an increased peak plantar pressure at the plantar aspect of the metatarsal heads in feet with hammer toes [83]. Recent studies have suggested that peak plantar pressure may only be 65% specific for the development of ulcers [29]. These limitations are at least partially due to surface pressures not being representative of the complex mechanical stresses that developed inside the subcutaneous plantar soft-tissue, which are more likely to be the cause of tissue breakdown. In 2003 Lavery et al. confirmed that high plantar pressures are risk factor for foot ulceration but he also stated that studying the plantar pressures alone is not enough for a reliable prediction [69].

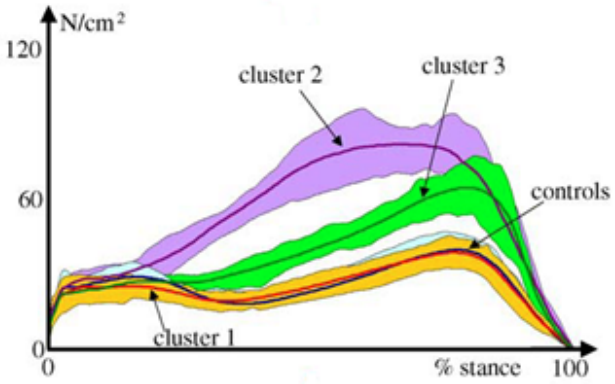

Figure 2.9: Peak pressure curves. 50% of diabetics of cluster 3 ulcerated few months after the tests [56].

Shear forces

A number of authors found that increased tangential stress is also an important determinant of tissue breakdown in diabetic neuropathic subjects [104, 112]. However their exact role in the aetiology of diabetic foot has not been understood yet. The antero-posterior forces decrease with the increase of the severity of the disease [112], while the high medio-lateral forces are correlated to the sites of ulceration, in particular at the sub-metatarsal areas [43, 107, 112].

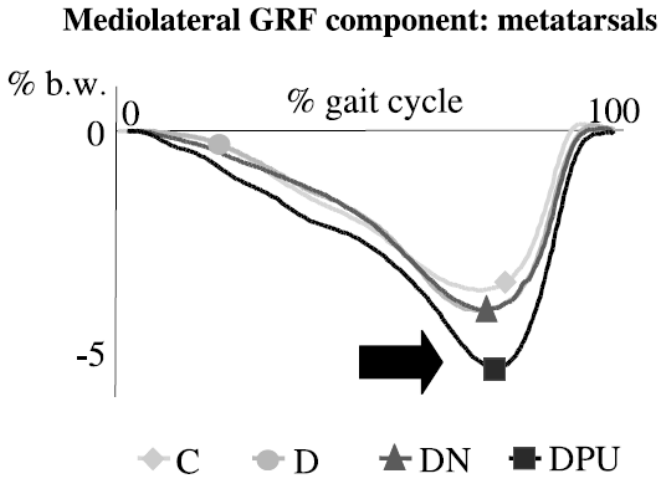

Figure 2.10: Averaged temporal evolution of the mediolateral ground reaction force component under the metatarsals, for all classes of patients (C=controls, D=diabetics, DN=diabetic neuropathics, DPU=diabetic with previous ulceration) [112].

Kinematics

Several foot protocols have been proposed in literature in the last twenties in order to estimate the 3D multisegment foot kinematics [46] mainly through the stereophotogrammetry. Although this technique has some weaknesses related to skin motion artifact [87], it has the advantage to measure more than the single-segment foot models, which are often used in conventional clinical gait analysis (for example the full body or lower limb models [45]). In this case if the foot is a bidimensional body segment thus only the ankle dorsi-plantarflexion can be measured while the 3D tibio-talar angles can be calculated if the foot is a 3D segment [102].

The 3D multisegment foot models are proposed for a specific evaluation of the foot subsegments kinematic and provide more informations on foot joint mobility. These informations have been demonstrated to be very useful in the assessment of the diabetic foot. Some authors demonstrated that diabetic subjects' gait is characterized by an altered kinematics [97, 101, 102, 103]. A displacement of the fulcrum of the step from the tibio-tarsal to the coxofemoral joint has been registered, accompanied by posture modifications [4]. Limited joint mobility has been found mainly at 1st metatarsophalangeal and subtalar joints and it has been hypothesized that is caused by additional alterations of the soft tissues, tendons and ligaments [15]. In diabetic subjects the plantar fascia behaves like one rigid lever during the step and this results in a reduction of the adaptability to the ground [43, 84]. Some authors observed significant alterations especially in correspondence of diabetic neuropathic subjects' forefoot triplanar angles [97, 101, 102, 103]. Mueller et al. demonstrated that the a limited ankle and subtalar dorsi-plantarflexion reduce the ability of the foot to absorb the strikes, contributing to the pathogenesis of plantar lesions [82].

It has also been shown that limited joint mobility may contribute to increased foot subsegments loading by limiting foot flexibility and restraining the forward progression of body weight during the stance phase of gait [98, 104]. Fernando et al. highlighted a correlation between the foot joint mobility and the increased plantar pressures [51]. However the causes and consequences of foot morphology on limited joints mobility in diabetic subjects with neuropathy are still under investigation.

2.3.4 Gait analysis protocols for simultaneous acquisition of foot kinematics, kinetics and plantar pressures

Plantar pressures and ground reaction forces are largely used in gait analysis coupled with foot kinematics measurements in order to better characterize normal and abnormal functionality of the foot. The combination of all these data provides an exhaustive and detailed view of foot loading during gait.

A synchronized set of data from different devices is important because it allows to study the dynamics of locomotion in a more complete way and it can be used to distinguish between normal and pathological foot function, to differentiate between the various levels of impairment and to assess quantitatively the recovery of normal function after treatment. In this context Giacomozzi at al. [55] developed a pressure-force-kinematic measuring system which consisted in: a pressure platform made of a matrix of 81 x 121 resistive sensors, 5 mm spaced in both directions, which was incorporated in the piezo-dynamometric platform and the data were transferred to a personal computer through a dedicated board. The pressure platform was rigidly fastened on top of a commercial 0.4 x 0.6 m force platform. The ELITE stereophotogrammetric system was used to track foot bone positions and the 3D foot kinematics protocol developed by Leardini et al. [71] was applied.

Also in Mac Williams et al. [78] a 3D foot kinematics, kinetics and plantar pressure synchronized acquisition have been proposed. Nineteen 10 mm diameter reflective markers were used to identify eight segments of the foot plus the shank. Six cameras were used to record the spatial positions of the markers throughout the stance phase of gait. In this work two separate sets of data were collected: in the first subjects walked over a pedobarograph system and so foot pressure and kinematic data were simultaneously collected; in the second one, subjects walked over a force plate and so ground reaction force and kinematic data were simultaneously collected.

In the work of Stebbins et al. [108] data of a synchronized kinematics and plantar pressure acquisition have been reported in order to obtain automatic foot sub-area definition on plantar pressure measurement by means of projecting the anatomical landmark position of the kinematics simultaneously acquired. They used a 12 cameras stereophotogrammetric system to collect the 3D kinematic data, and they adopted the protocol developed by Carson et al. [26] and a piezo-resistive pressure platform with a spatial resolution of 5 mm, sampling at 100 Hz. This was rigidly mounted to AMTI force plate, with a minimum sampling

frequency of 500 Hz and temporally synchronized with it.

The methodology adopted in this thesis has been proposed by Sawacha et al. and is described in [104]. The former allows the simultaneous assessment of kinematics, kinetics and plantar pressure on foot subareas of diabetic subjects by means of combining three commercially available systems. A four segments 3D foot kinematics model as proposed in [101] was adopted for the subsegments angles estimation together with a three segment model for the plantar sub-area definition during gait.

Movement analysis was carried on using a 6 cameras stereofotogrammetric system (60-120 Hz, BTS S.r.l, Padova, Italy), 2 force plates (FP4060-10, Bertec Corporation, USA), 2 plantar pressure systems (410x410 x 0.5 mm, 0.64 cm^2 resolution, 150 Hz, Imagortesi, Piacenza). The signals coming from all systems were temporally and spatially synchronized in post processing thus avoiding the need of modifying either the hardware or the software of the employed systems. The stereophotogrammetric system was used either to perform the automatic footprint subareas subdivision or to compute the 3D foot subsegment kinematics.

The synchronization between the force plates and motion capture system was provided by the motion capture company while the temporal synchronization of pressure and force plates is achieved normalizing the output of the devices with respect to stance phase of gait. Hence either the variables extracted from the plantar pressure system or the ones extracted from the force plates were normalized to 100% of stance phase of gait. Plantar pressure and force plates: each plantar pressure system was mounted onto each force plates by means of double-sided tape and the spatial alignment of the two platforms was assured by comparing the 2 centre of pressures. This was performed by defining a coefficient k=8 which measures the relationship between the PP system spatial resolution (each sensors = 8 mm x 8mm) and the motion capture system one (1 mm).

A four segments 3D foot kinematics model was adopted for the subsegments angles estimation during gait according to [101]. Skin markers were double-sided taped on 13 anatomical landmarks for each foot and leg (table 2.4). Model segments and joints rotation angles were calculated according to Cardan convention (table 2.5).

A three segments model for the plantar sub-area definition was obtained by means of projecting the anatomical landmarks of the kinematics protocol onto the footprint. The following foot subareas were defined:

- hindfoot: the area between the line connecting both the vertical projec-

Foot subsegment	Anatomical landmark	Acronym
TIBIA	Head of fibula	HF
	Tibial Tuberosity	TT
	Lateral Malleolus	LM
	Medial malleolus	MM
HINDFOOT	Calcaneus	CA
	Sustentaculum Talii	ST
	Peroneal Tubercle	PT
MIDFOOT	Navicular tuberosity	NT
	Fifth Metatarsal Base	VMB
	Cuboid	C
FOREFOOT	Fifth Metatarsal Head	VMH
	First Metatarsal Head	IMH
	Proximal epiphysis of Second Toe phalanx	IIT

Table 2.4: Markerset for the foot kinematic protocol.

SEGMENT	AXIS JOINT	COORDINATE SYSTEM
Tibia	y	The two malleoli and the head of fibula define a quasi frontal plane, the y axis is parallel to the line connecting the midpoint between LM and MM and the projection of the tibial tuberosity (TT) on this plane with its positive direction upward.
	x	The line connecting lateral and medial malleoli (LM e MM) and y axis define a plane: x is orthogonal to that plane with its positive direction forward (obtained as product between the two above described lines).
	z	Product between axis x and y.
	Origin	Midpoint between LM and MM.
Hindfoot	z	Parallel to the line connecting ST and peroneal tubercle PT with its positive direction from left to right.
	y	The line connecting calcaneus (CA) and substentaculum talii (ST) and the z axis define a plane: y axis is orthogonal to that plane with its positive direction upward (obtained as product between the two above described lines).
	x	Product between axis y and z.
	Origin	CA.
Midfoot	z	Parallel to the line connecting NT and C with its positive direction from left to right.
	y	The line connecting (NT), and fifth metatarsal base (VMB) and z axis define a plane: y axis is orthogonal to that plane with its positive direction from proximal to distal segment (obtained as product between the two above described lines).
	x	Product between axis y and z.
	Origin	Midpoint between NT and C.
Forefoot	z	Parallel to the line connecting IMH and VMH with its positive direction from left to right.
	y	The line connecting VMH and IIT and the z axis define a plane: y is orthogonal to the plane with its positive direction upward (obtained as product between the two above described lines).
	x	Product between y and z.
	Origin	Midpoint between IMH e VMH.
Foot	z	Parallel to the line connecting IMH e VMH with its positive direction from left to right.
	y	CA, IMH and VMH define a plane; the line connecting IIT and CA belong to a plane perpendicular to the previous one; z axis is parallel to the line intersection between the two planes with its positive direction forward.
	x	Product between axis y and z.
	Origin	CA.

Table 2.5: Anatomical bone embedded frames [101].

tion of the sustentaculum talii and the peroneal tubercle and the vertical projection of calcaneus;

- midfoot: the area between the anterior reference line of the hindfoot and the line connecting the vertical projection of the first and fifth metatarsal head;
- forefoot: the area between the anterior reference line of the midfoot and the end of the anterior border of the footprint. The plantar surface was compartmentalized so that sensors did not overlap across segments.

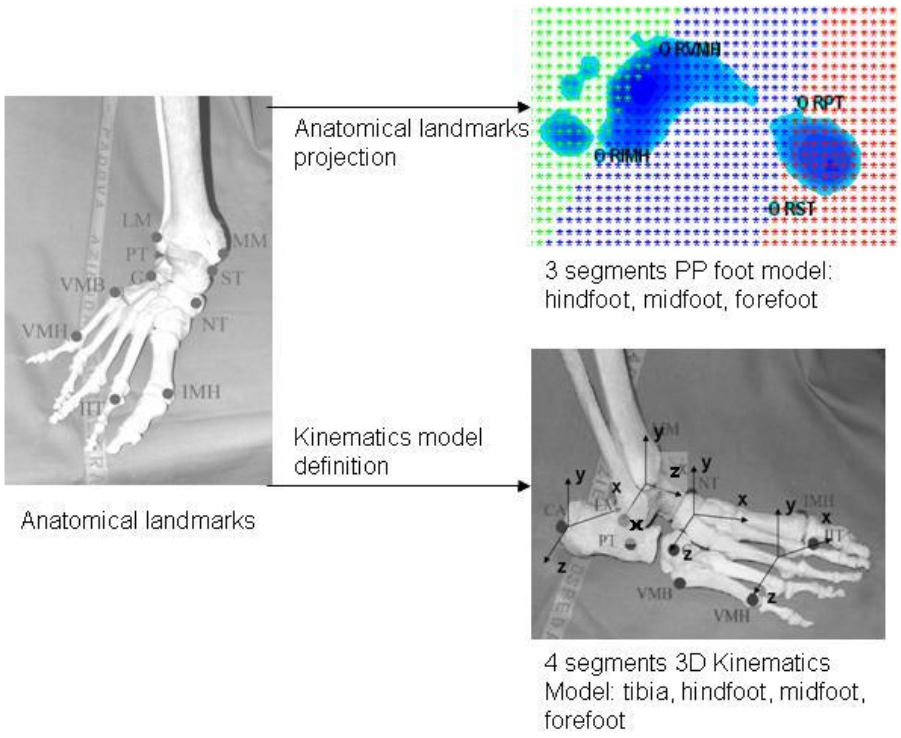

Figure 2.11: Details of the four segment 3D kinematics model and three segment kinetics and plantar pressure model [101, 104].

Local sub-segments vertical ground reaction forces were computed as the summation of the forces measured by each sensor of the pressure platform belonging to the same foot subareas as in [112]. The anterior-posterior and medio-lateral forces, were calculated assuming they were distributed proportionally to the vertical force. This assumption had been previously performed in Winter et al. [117] and Uccioli et al. [112], and lead to successful results. The computational details of this methodology can be found in [104, 112].

Ground reaction forces were then normalized to body weight.

2.4 Tissue characterization of heel pad and metatarsal pad in diabetic subjects

From an experimental point of view, one among the possibilities to quantify biomechanical variables is represented by in-vivo measurement of foot tissues properties. The plantar pad has the role of absorbing impacts during gait thus an accurate study of the plantar tissue in diabetic patients is needed for an accurate prediction of sites at high risk of ulceration.

In the last ten years several approaches and methods to characterize the plantar soft tissue in diabetic patients have been used and several different parameters have been measured. The most common setup is the use of ultrasound probe, often couppled with other methods like indentation system [48, 123], optical pedobarograph [5], or transducer with linear variable displacement [65, 111]. Ultrasonography is a non-invasive technique and it is ideal for direct and dynamic measurements of the plantar pad because it allows an accurate evaluation of the layers (the different structures in the layers - skin, microchambers, macrochambers and bone - have different reflective properties) with real-time continuous imaging [99]. For these reasons it can be easily used for patients.

The thickness of the metatarsal and heel pad have been often measured in different conditions: static unloaded, loaded or weight bearing, in dynamic conditions with different loading profiles or during normal walking.

The characterization of the plantar pad tissue in diabetic patients has commonly been made through the evaluation of the thickness of the pad, the stiffness and the stress-strain curve. In particular, "dynamic" elastic module, energy dissipation ratio and compressibility index from the curve have almost always been calculated.

The evaluation of the thickness of the pad generally demonstrated that in the case of diabetic subjects it is thinner than the healthy subjects one and that the thickness is inversely related to the loss of foot sole sensation and peak pressures. Nevertheless, it has been demonstrated that the unloaded heel pad is not significantly thinner in the diabetic subjects [65, 64, 111] with respect to controls.

The strain of diabetic heel pad is significantly different from that of healthy subjects; in diabetic subjects the microchambers show a higher strain and the

microchambers a decreased one, if compared with those of the healthy's. The resultant overall Young's modulus is larger for the diabetics [64]. As regards to the stiffness, it is significantly increased in the pad under the metatarsal heads. Meanwhile under the heel it displays a distinct behaviour between the micro and macrochamber layer: there is a significantly greater stiffness of macrochambers and lower of the microchambers layer [64]. Finally diabetic subjects have significantly higher energy dissipated (or energy dissipation ratio) in their heel and metatarsal pad. When FE simulation has been applied, it was possible to evaluate internal stresses (tension and compressions) at the heel and the results indicated increasing values for diabetic subjects, in particular proportionally with growth in tissue stiffness [48, 53].

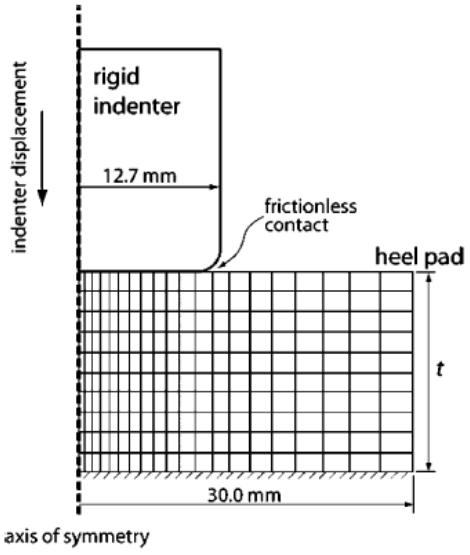

Figure 2.12: The axisymmetric finite-element model of the heel pad and indenter to obtain heel-specific material properties [48].

These non invasive methods provide useful plantar tissue's mechanical properties parameters which can be fed into the simulation to form a patient-specific, anatomically accurate computer model of the foot which allows simulations of consequences of unloading footwear or surgical procedures [53].

2.5 Finite element models of the foot

2.5.1 Finite element method [44]

FE models have been used more and more in many biomechanical investigations with great success due to their ability of modelling structures with irregular geometry and complex material properties, and the ease of simulating complicated boundary and loading conditions in both static and dynamic analyses.

The FE analysis technique is a numerical method to obtain solutions to the differential equations that approximately describe a physical problem. The criterion for modelling is that a complicated problem can be sub-divided into a series of smaller problems in which the differential equations can be solved. By assembling the results of each sub-problem, the behaviour of the entire problem is determined. The sub-divisions are small regions called elements and the solution is calculated in terms of discrete values of primary field variables at nodes (e.g. displacements in 3D). The collection of all the elements and nodes is called the mesh. The number of unknown primary field variables at a node is the degree of freedom at that node.

In order to reduce the computational cost, it is necessary to reduce the number of degrees of freedom to a finite number. This reduction is called discretization: the result is a discrete model, a simplified version of the original physical problem and the solution is also approximated. The number of elements per unit of length, area, or mesh is referred to as the mesh density. The greater it is, the more accurate the results but the greater the computational cost.

The accuracy of the results also depends on the type of elements adopted to create the mesh. Elements can have dimensionality of one, two or three in space. The shape of each element is defined by the position of the nodes. There are several types of elements available to discretize the geometry of interest. Most of them have very simple geometry. For 1-dimension they are usually straight lines or curved segments, for a 2-dimensional (2D) model triangular or quadrilateral elements, for 3D models the most common shapes are tetrahedric, pentahedric or hexahedric.

Many of the FE problems involve finding an approximate (finite element) solution for the displacements, deformations, stresses, forces, in a solid body that is subjected to some history of loading. The exact solution of such a problem requires that both force and moment equilibrium be maintained at all times over any arbitrary volume of the body. The displacement FE method is based

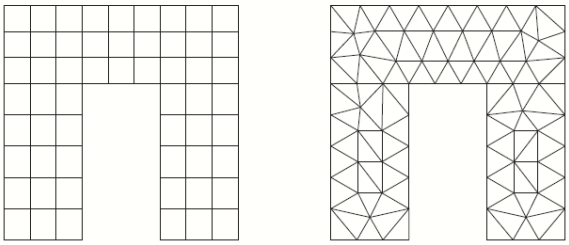

Figure 2.13: Two meshes with different element shapes [44].

on approximating this equilibrium requirement by replacing it with a weaker requirement, that equilibrium must be maintained in an average sense over a finite number of divisions of the volume of the body [44].

Models have always been based on some assumptions which include simplified geometry, limited joint movement, incomplete ligamentous structures, and easy material properties. Early models were based on a simplified or partial foot shape. Simulations were performed under hypothesis of linear material properties, small deformation, and linear boundary conditions, without considering friction.

Recent models have improved in selected aspects by incorporating geometric, material, or boundary nonlinearity (eg, large model deformation, nonlinear material properties, slip/friction contact conditions) [35].

2.5.2 Foot finite element analysis

Several recent models have used the FE method to predict the loading of the foot's components during standing and gait as they relate to foot disorders and therapeutic footwear [7, 22, 31, 29, 35, 37, 36, 47, 54, 52, 76, 88, 96].

The various foot FE models have been developed in order to provide estimates of quantities that cannot be directly measured or to perform simulations that would be onerous or dangerous for human subjects [27].

Each model has been built for a specific purpose thus the simplification level, the properties of the materials, the modeled components were chosen by each author according to the specific aim. Two main categories of foot FE models have been developed: 2D FE models and 3D. Another distinction can be done within 3D models since many of them represent only a part of the foot while others consider the foot as a whole.

2D models of the foot

In the nineties, the first studies that considered the FE analysis of the foot adopted the 2D modelling technique.

A very simple but surprising FE model of the foot was developed by Patil in 1993 [90] and used to study the bones regions of high stresses during three simulated, quasi-static equilibrium positions: mid-stance, heel strike and push off positions. The result of this analysis served as guidance for the following higher level of complexity models.

Moving to more complete models, in 1997 Lemmon et al. decided to overcome the trial-and-error process for the design of foot orthoses and developed a 2D FE model of a slice of the second metatarsal and the underlying soft tissue. They investigated alterations in pressure under metatarsal head as a function of insole thickness and tissue thickness and they demonstrated the reduction of plantar stresses in the simulations with the insole (approximately 2 kPa for each millimeter of thickness of the insole) while the effect of the insole in a foot with reduced tissue resulted in a reduction of the peak pressure by approximately 6 kPa mm^{-1} [76].

Again for insole design purpose but in a different part of the foot, Goske et al. presented a 2D model of a slice of the heel pad in which the bones were unified in a unique structure. Their aim was to study the peak plantar pressures relief produced by different insole materials and shapes [57].

Others examples of 2D models which followed were developed for simulation of surgical intervention like plantar fasciotomy [52, 119]. For this purpose the FE model of medial and lateral plantar longitudinal arches were considered, including ligaments, tendons, cartilage, bones (trabecular and cortical), fat pad and intrinsic muscles.

Obviously in the 2D models the level of simplification and the number of assumptions are high. However they represent a fast and good compromise for some problems limited to a part of the foot or that can be simplified thanks to symmetries or for feasibility studies.

3D models of the foot

The development of geometrically detailed FE foot models has started in late nineties and it has provided new insights into the internal load distribution of the

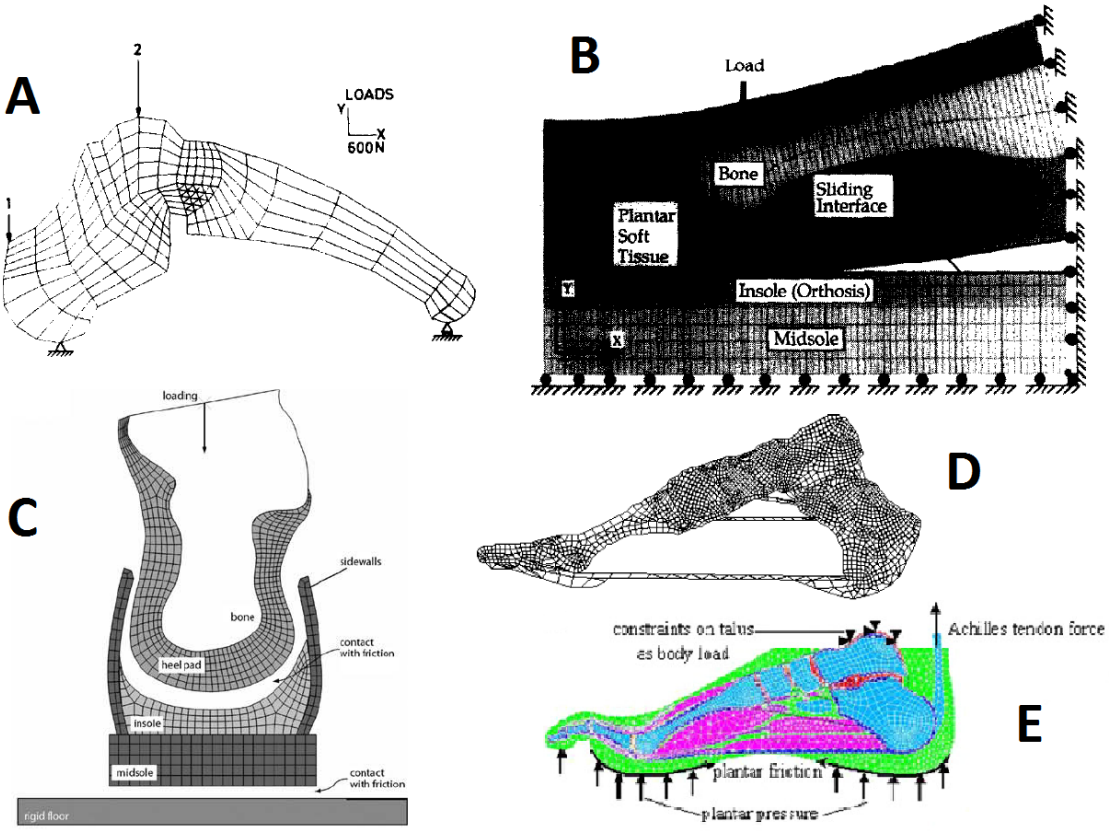

Figure 2.14: 2D FE models of the foot proposed in literature: A) The FE mesh during mid-stance phase [90]; B) The 2D plane strain FE model indicating the locations of bone, plantar soft tissue, insole and midsole materials, the sliding interface, boundary conditions and load [76]; C) Footwear model interacting with the heel to investigate the influence of insole parameters on heel pressure relief [57]; D) The first ray meshed cross-sectional structure of the foot model [52]; E) Anatomical model of skeleton and skin of left foot [119].

foot. Many of them represent only a part of the foot while others that considered the foot as a whole have been developed for the specific aim of assessing the effect of foot orthoses or orthopedic surgery. As stated by Erdemir et al. [48], the 3D FE modeling compensates for the geometry and boundary conditions of the experiment and therefore it is more adequate because it allows the true stress-strain behavior of the heel pad to be predicted.

The model proposed by Chu et al. in 1995 can be considered the first 3D model even if its geometry and FE formulation is very simple. In this work he presented an asymmetric 3D FE model for analysis of the effects of ankle-foot orthosis [38].

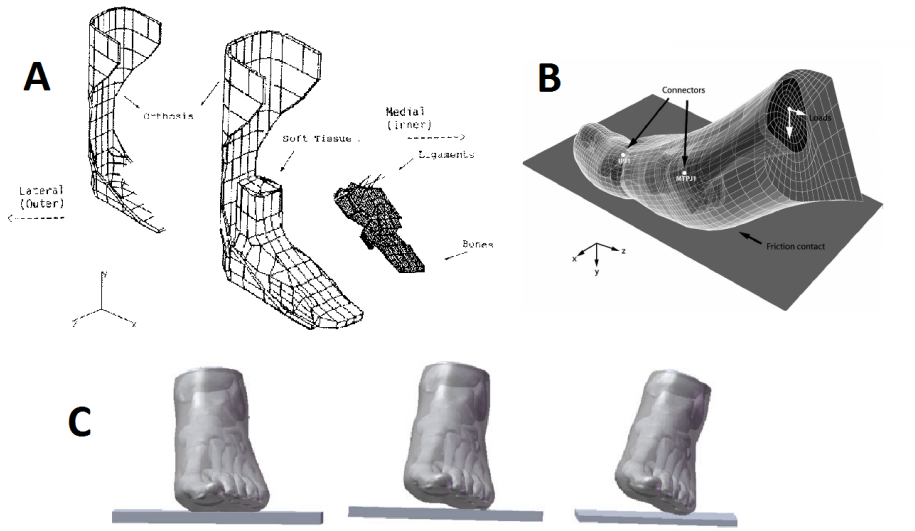

Figure 2.15: 3D FE models of the foot proposed in literature: A) The finite element model of the ankle-foot orthosis system [38]; B) Initial position and loading of the foot for barefoot simulations [22]; C) Different forefoot touchdown conditions [60].

Also Budhabhatti et al. developed a 3D FE model for the evaluation of surgery effect, in this case reducing the complexity by modeling only the first ray of the foot [22].

By considering only the forefoot, Gu et al. developed a 3D FE model to investigate the effect of inversion positions on stress distribution and concentration within the metatarsals [60]. In particular this paper highlighted the importance of the foot position with respect to the ground when positioning the foot relatively to the support in the FE simulations. This aspect is relevant to the development of the 2D and 3D models proposed in the present thesis.

The more important models of healthy feet which have been proposed in recent literature aimed at quantifying the stress distribution by simulating the plantar pressures or the internal stresses and strains.

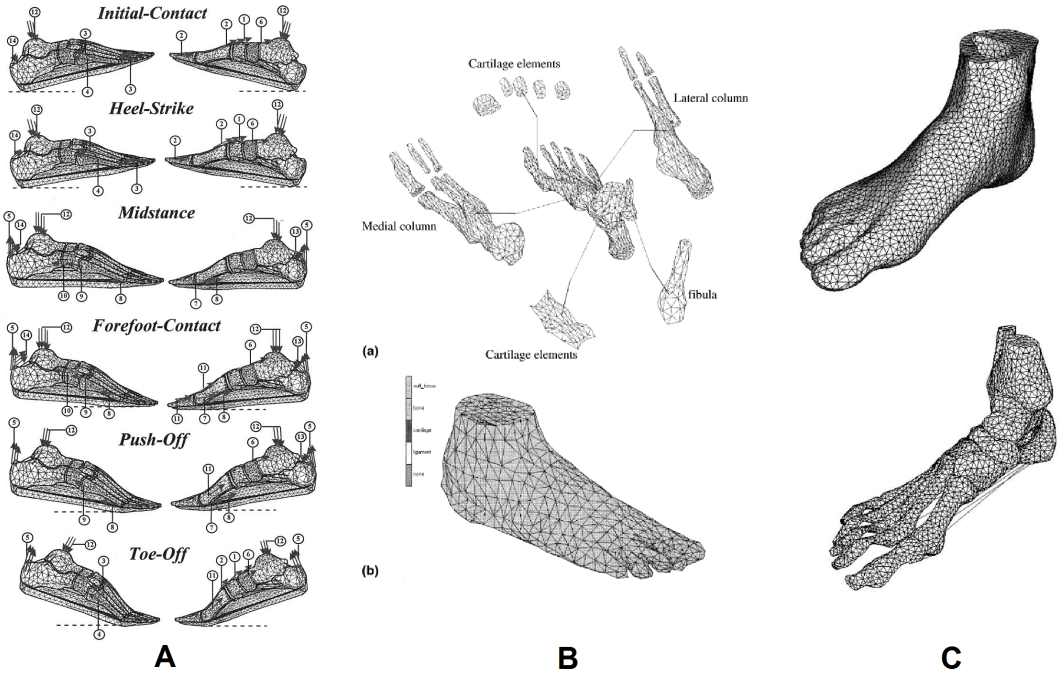

Figure 2.16: 3D FE models of the foot proposed in more recent literature: A) Muscle forces that act on the foot model during the six characteristic subphases of stance [54]; B) Exploded view and complete FE model of the foot [32]; C) The finite element mesh of soft tissues and of bony and ligamentous structures [35].

Gefen et al. [54] developed the first 3D model which incorporated realistic geometry and material properties of both skeletal and soft tissue components of the foot. The peculiarity of this study consists also in the integration of different methods, namely optical contact pressure display and digital fluoroscopy, to move and validate the foot model. Another important add-in of this study with respect to the previous models is that the model simulations were run over a series of six sequential characteristic subphases of the stance. In these configurations they adopted a quasi-static approach by taking into account the inertial forces as muscle forces. The values of forces developed on each of the muscles during the stance phase of gait were taken from the literature. For the validation of the model, the same authors developed new technique for dimensionless characterization of the Foot-Ground Pressure Pattern evolution. This is be based not only on analysis of the model predictions with respect to dynamics of specific feet, but

also allow comparison with statistical data of subjects with different gender/body characteristics [54]. Basically this tool represents a way of assessing the plantar pressure values on 3 subsegments of the pressure map.

The model proposed by Chen WP et al. [32] is the less accurate, with not very detailed geometry and a mesh characterized by a low number of elements. The bones of the five phalanges were modeled to be five integrated parts and the rest of the metatarsals and tarsal bones were modeled with two rigid columns, in order to reduce the complexity of the model. These choices were due to the fact that at that time the computational power of the machines was much lower than now and the FE models needed to be very simple in term of computational complexity. However the authors introduced very important novelties with their model. For example they introduced the possibility of moving the support according to 3D linear and angular displacement of the foot with respect to the ground acquired with a stereophotogrammetric system during gait (only the dorsi-plantarflexion for simplicity). The mesh adopted was tetrahedral. All the elements were assumed to be homogeneous, and the materials were modeled as linear elastic materials and the properties were chosen from previous literature. The main drawbacks of the present model recognized by the authors were the lack of patient specificity (both material properties and the plantar pressures for the validation of the model were derived from literature) and the excessive simplifications on the structures and mesh. The same authors applied the same model to study the effect of total contact insoles on high plantar pressure [31].

The model proposed by Cheung et al. [35] is a highly detailed human foot and ankle model that incorporates realistic geometry of both bony and soft tissue components (in contact with an insole). It was reconstructed from magnetic resonance images, consisting of 28 bony segments, 72 ligaments and the plantar fascia embedded in a volume of encapsulated soft tissue. The structures were meshed with a total of 50,964 tetrahedral elements and the ligaments were defined with tension-only truss elements. All tissues were considered as homogeneous, isotropic, and linearly elastic. A very rigid bottom layer was used to simulate the ground support and to facilitate the application of concentrated ground reaction forces. The foot-insole interface was modelled using contact surfaces with a friction coefficient of 0.6. The insole was properly aligned in a way that permitted an initial foot-ground contact to be established, with minimal induced stress and contact pressure, before loading was applied. The simulations were performed only in balance standing condition, applying to the ground a load of

half-body-weight and an Achilles tendon force of half of the ground-load. The superior surface of the soft tissue, distal tibia, and fibula was fixed throughout the analysis. To validate the model, the plantar pressures were measured for this subject during barefoot standing to calculate the foot's centre of pressure and to compare the plantar pressure distribution predicted by the FE technique. The authors demonstrated that the custom-molded shape is more important in reducing peak plantar pressure than the stiffness of the insole material.

Only two years later, the same authors improved their model adding 9 extrinsic muscle applied at their corresponding tendon insertions according to the lines of action of the muscle tendons. They also prescribed inclination of the ground support relative to the ankle joint as kinematics boundary conditions for the quasi-static FE simulations of the walking foot during heel-strike, midstance and push-off phases of gait. The authors adopted this model for several studies on structural and material parameters of the foot structures also with respect to the design of footwear [33].

The FE model developed by Chen WM et al. [29] had the purpose to predict both the foot 3D, internal, plantar soft-tissue deformation and stress. Its principal novelty with respect to the state of the art was represented by the introduction of an accurate soft tissue model with isotropic, incompressible, hyperelastic second-order polynomial formulation. Furthermore they represented relative articulating movements with surface-to-surface contact elements between adjacent bones. This allows the bones to slide over one another without friction and transmitting only compression forces. The validation of the model was performed through subject-specific acquired plantar pressures and showed good predictions. The preliminary internal stress analysis indicates that stress distribution within the plantar soft-tissue was dramatically influenced by bony prominences due to stress concentration [29].

In Natali et al. [86] the contribution toward the improvement of the existing 3D FE foot models is represented by definition of an appropriate hyperelastic constitutive model of adipose tissues and plantar fascia. This was performed considering that their mechanical behaviour is a determinant factor in affecting the paths of the plantar pressure. However no cartilage elements, nor tendons or ligament, with the exception of the plantar fascia, were added to the model.

All these models and the others not directly mentioned have contributed to the understanding of biomechanic behaviour and performance of foot supports and increased the knowledge of the internal structure of the foot, in special condition

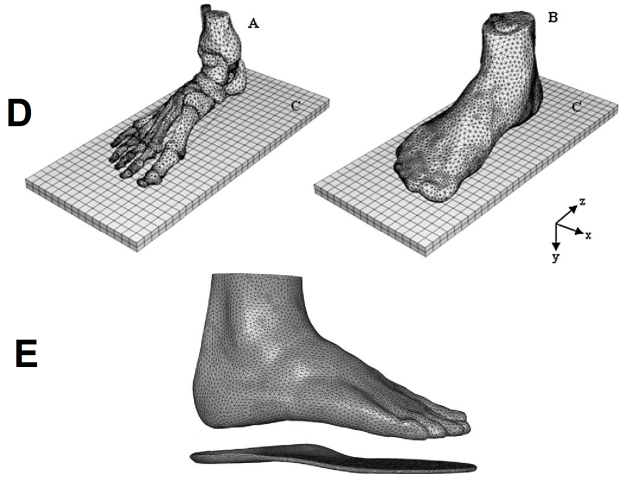

Figure 2.17: More 3D FE models of the foot proposed in recent literature: D) FE model of the skeletal structures of the human foot inclusive of the ligaments and fascia (A), enveloped by a homogenous mass of soft-tissue under the skin (B), standing on the metal plate (C), i.e. ground [29]; E) FE of foot and insole adopted for the analysis [86].

or with respect to specific diseases. The challenge for the future is to continue to decrease the number of simplifications in order to obtain detailed specific-subject models which allows to achieve the best matching between reality and simulations.

FE models of the diabetic foot

The state of the art of diabetic FE foot model can account for just a few models.

The first is the one of Patil et al. which used a 2D model developed according to a lateral X-ray image in order to study internal stress distributions in normal and neuropathic feet [91]. The level of detail of the model was a bit higher than their previous model [90] because they included more muscles. In this case the diabetic pathology was represented in the model by simulating paralysis in muscles. No specific soft tissue material properties were used or diabetic foot geometry and loads. However the results demonstrate that both the shape of the foot and the type of muscle paralysis contribute to the development of high stresses in different regions of the foot. The authors concluded that in the development of more appropriate models of the foot, an extension to 3D models is perhaps more adequate than the introduction of soft tissue. Nevertheless, it is

expected that in quasi-static analyses the effect of soft tissue is only noticeable on the plantar pressures between foot and ground [91]. Thereafter the same authors developed a 3D model of both a normal and a diabetic foot. They couple two 2D arch models previously developed to create a 3D foot and extended to this FE model the methodology and the results of the previous work [67].

In a subsequent study [110], the same models were adapted by the authors themselves by introducing three sets of foot sole soft-tissue properties, namely isotropic with healthy hardness value, diabetic isotropic with higher hardness value and diabetic anisotropic. The values for these properties were calculated as Young modulus from the measures taken with a durometer on 36 diabetic feet and 18 healthy feet in ten standard foot sole areas. The foot models were simulated with standard loads, muscle forces and inclination of the foot sole to the ground while for the material properties decreasing foot sole soft-tissue thicknesses in the forefoot region were applied. The corresponding stresses were calculated. They found that even if the hardness of the foot sole areas in diabetic subjects are higher than those of control subjects, in diabetics, there is a non-uniform variation in hardness in different foot sole areas (anisotropic condition), and this is found to cause higher stresses in the foot sole soft tissues compared with isotropic conditions [110].

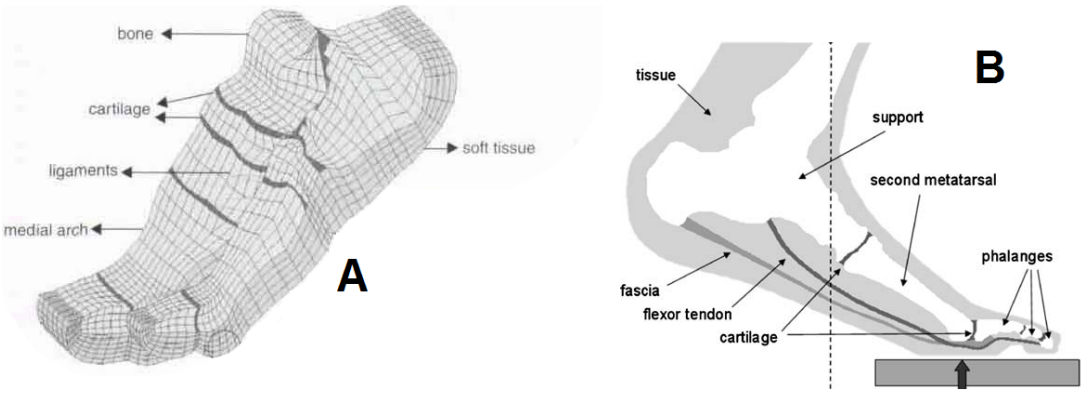

Figure 2.18: FE models of the diabetic foot: A) FE mesh in the 3D 2-arch model of foot in pushoff phase [110]; B) Segmentation for the most complex model considered for analysis [7].

Actis et al. developed patient-specific mathematical models of the second and third rays of the foot for both healthy and diabetic feet [7]. The purpose of this paper was to determine the pressure distribution in the metatarsal head region in the push-off position, both barefoot and with shoe and total contact

insert. They hypothesized and demonstrate that the least complex model to sufficiently well simulate the pressure distribution under the metatarsal heads includes the bony structure segmented as toe, metatarsal and support (with linear material properties), cartilage between the bones, plantar fascia and soft tissue (with nonlinear material properties). The diabetic pathology has been taken into account in the foot geometry construction using data from spiral X-ray computed tomography in two different load cases. The soft tissue material properties were also diabetic specific as they were obtained using an indentor fitted with an ultrasound probe and a load cell. The pressure distribution was measured for each subject using an F-scan system and used to both load the FE model and validate it. The fit of forefoot plantar pressures estimated using the FE models and those explicitly tested were good as evidenced by high Pearson correlations (r = 0.70-0.98) and small bias and dispersion. They reported patient-specific examples and the results of the simulations with shoe [7].

A very recent study which adopted the model database of Physiome project, aimed at developing a subject-specific foot model with anisotropic tissues, exploring the influence of mechanical stiffening on contact pressure and internal stresses and correlate the stress distribution with the plantar sensory nerve branches for different stages of the gait cycle [50]. In particular they developed a free-form deformation method to adapt a generic foot model made of a set of high-order 3D parameterized FE meshes suitable for mechanics to the captured subject foot shape. Then they applied the subject-specific foot kinematic and kinetic to simulate the model behavior during gait. For the kinematic they adopted the foot marker system reported by Leardini et al. [70]. Following this protocol it was possible to group the foot into the forefoot, midfoot and rear-foot to capture the main foot articulations and to prescribe the plantar and dorsiflexion of the first metatarsal. The kinematic data were acquired during the kinematic thus the data are synchronized. For the material properties the authors adapted a microstructurally based constitutive law, the 'pole-zero' law, for passive tissues because it was shown to be numerically stable by allowing for strain limits in each direction without the need for large exponents [50].

As stated above, they also simulated increase in soft tissue stiffening of 1.5, 2 and 2.5 times. They solved the model using quasi-static analysis on three instants of the stance phase of gait, namely the heel strike, the midstance and the toe-off. These stages were chosen to cover the range of foot contact over the sole. For the validation, they adopted foot pressure measurements which were collected with

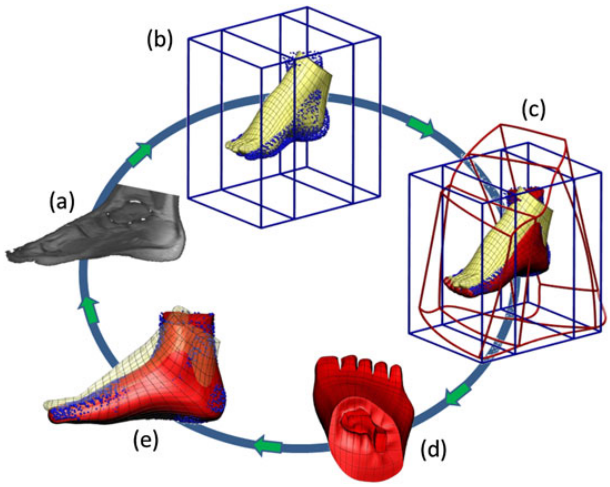

Figure 2.19: 3D FE model developed by Fernandez et al. [50]: (a) T1-weighted MR of the lower limb used to generate subject target data; (b) original Visible Human Male foot embedded in host-mesh with target MR data in blue; (c) deformed host used to morph the Visible Human Male foot (yellow) to subject-specific profile (red); (d) customised internal bone shapes; and (e) new subject-specific foot overlayed with target data and original foot mesh.

E-med foot platform. These were acquired on a separate occasion because the platform was located in a different gait lab. They synchronized and aligned these data with the ground reaction forces in post-processing and they accounted for any differences by averaging three trials. A key outcome from this study is that internal stresses can be up to 1.6 times the surface pressures and increase at a higher rate than surface plantar pressures with increase in tissue stiffness. Hence, injuries in the pathologic foot may initiate in the deep tissue structures and not be detected at the surface in the gait lab or when making clinical evaluation [50].

In general the aims of the researchers is mainly to understand the mechanical etiology of diabetic foot ulcers and the effects of plantar cushioning, to test the efficacies of various types of insoles used in therapeutic footwear or to simulate surgical interventions for unloading the hyper-pressure areas. There are still several topics related to diabetic foot biomechanics that need to be deeply investigated. Even if it has been demonstrated that high plantar stresses are a high risk factor for plantar ulceration [28, 43, 56], a universally accepted level of plantar foot pressure has not been found [11]. Furthermore ulcers developed also under site where there is not peak plantar pressure. There is evidence that mechanical stress concentration in deep tissue and plantar shear stresses play a dominant role in priming ulceration in diabetic foot [11, 121].

2.5.3 Workflow of the development of an FE model of the foot

The workflow reported in the literature for the development of a foot FE model can be summarize in figure 2.20.

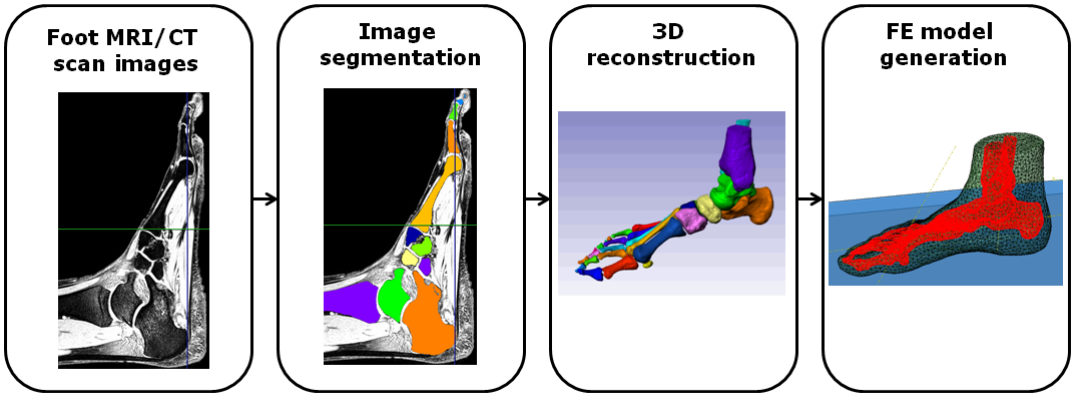

Figure 2.20: Workflow of the development of an FE model of the foot.

This process, from the images to the model, is commonly called *reverse engineering*. In the following paragraphs a detailed description of each stage of the procedure has been reported.

Foot MRI/CT scan images

The foot geometry is usually based on Computer Tomography (CT) or Magnetic Resonance Imaging (MRI).

The acquisition protocol must provide for the foot position in a non weight-bearing condition in order to allow the segmentation of the uncompressed soft tissues. Sometimes ankle-foot orthosis are used to keep the foot in position. Some studies included also a plantar pressure registration device while acquiring the CT or MRI images. This gave the authors the possibility to better lock the foot and correlate the soft tissues deformations to the plantar pressure values [88, 94].

The CT provides 2D and 3D cross-sectional images of an object from flat X-rays images. This allows a detailed morphological reconstruction of the various anatomical structures of the foot, including bones, cartilages, and a bulk soft tissue boundary. The CT images are high-contrast resolution and can distinguish between tissues that differ in physical density by less than 1%. For this reason

the geometry reconstruction is more automated than the MRI as thresholds and confidence connecting region growing techniques can be used for the segmentation.

Several studies in the literature adopted CT [7, 32, 29, 67, 86], even if this is an invasive technique as it is based on X-rays and it does not allow the identification of ligament and tendons insertions. Sometimes a surface laser scan can be used for a better reconstruction of the skin surface [86]. The MRI is based on the property of the water molecules in tissues to get aligned to large magnetic field to produce net average magnetic moment vector which is detected as MR signal. The modern MRI scanner devices have complex libraries of pulse sequences, each of which is optimized to provide image contrast based on the chemical sensitivity of the tissue of interest. In order to obtain the best images matching the requirement for a good segmentation and geometry reconstruction, it is possible to change different parameters. The two basic parameters of image acquisition are the echo time (TE) and the repetition time (TR). Changing the values of TE and TR, a sequence can be called T1-weighted or T2-weighted. On a T2-weighted scan, water- and fluid-containing tissues are bright and fat-containing tissues are dark. The reverse happens for T1-weighted images. Other parameters to consider are the distance between the slices and the slice thickness: the minor distance and the less thick, the more accurate can be the reconstructed geometry.

Obviously the MRI is non invasive but the cost is higher than the one for the CT exam. The main advantage of the MRI technique is the more detailed images, which allow to investigate all the foot structures, even the soft tissues structure and layers [22, 35, 50, 54, 60, 95]. However MRI images are more difficult to be segmented as same gray level can correspond to different tissues, that instead can only be differentiated by the texture of the image. In this case a more user-dependent segmentation has to be performed.

Image segmentation and 3D reconstruction [77]

Often, most of the image-to-model generation process is spent on segmentation. The segmentation is the process of identifying whose object each pixel of an image belongs to.

The images acquisition provides the image volume Greyscale data that can be also called the Background data and can be modified and filtered in order to facilitate and improve the segmentation. The segmentation of background data produces one or more volumes (binary volumes) that are called Masks. A mask contains a binary component (0 or 1) for each pixel of the image, where a value

of 1 means that the pixel belongs to the object the mask is representing (inside) whereas a value of 0 means that the pixel does not belong to the object (outside). These describe how an object fills the space. Each object of interest should be represented by a mask. These masks can be worked on, modified and filtered until you are satisfied with them and decide that they should be converted into a mesh.

Usually in commercial softwares there are several segmentation tools taken from the traditional image processing as for example threshold, confidence connection region growing, binary operators and so on. These facilitate and accelerate the process.

Therefore a typical process outline from scan to volume mesh, would include (see figure 2.21):

- Background data preparation and filtering (noise removal, resampling, cropping);
- Segmentation;
- Mask filtering;
- Surface extraction/mesh generation.

The software more used in the literature for the segmentation is MIMICS. It is specially developed for medical image processing. It should assure highly accurate 3D model of patients' anatomy when used for segmentation of a large range of medical images, coming from CT, MRI, micro CT, Ultrasound and so on. Another software that provides a solution for the conversion of 3D images into CAD, Rapid Prototyped and FE models with increasing success is Simpleware ScanIP. This is a core image processing platform with optional bolt-on modules for mesh generation and CAD integration. The particularity of this software is the different approach in the image-to-mesh process.

Previous approaches to meshing scanned objects/structures have tried to convert bitmapped data into CAD descriptions in order to mesh them. This method, although feasible for simple cases, becomes intractable for complex or multi-part structures. The method adopted by Simpleware is different as the conversion to a CAD description is bypassed and it meshes directly from bitmapped data. This results in a far more robust and automated approach [122].

For this thesis the Simpleware segmentation (ScanIP) and meshing (ScanFE) software were employed.

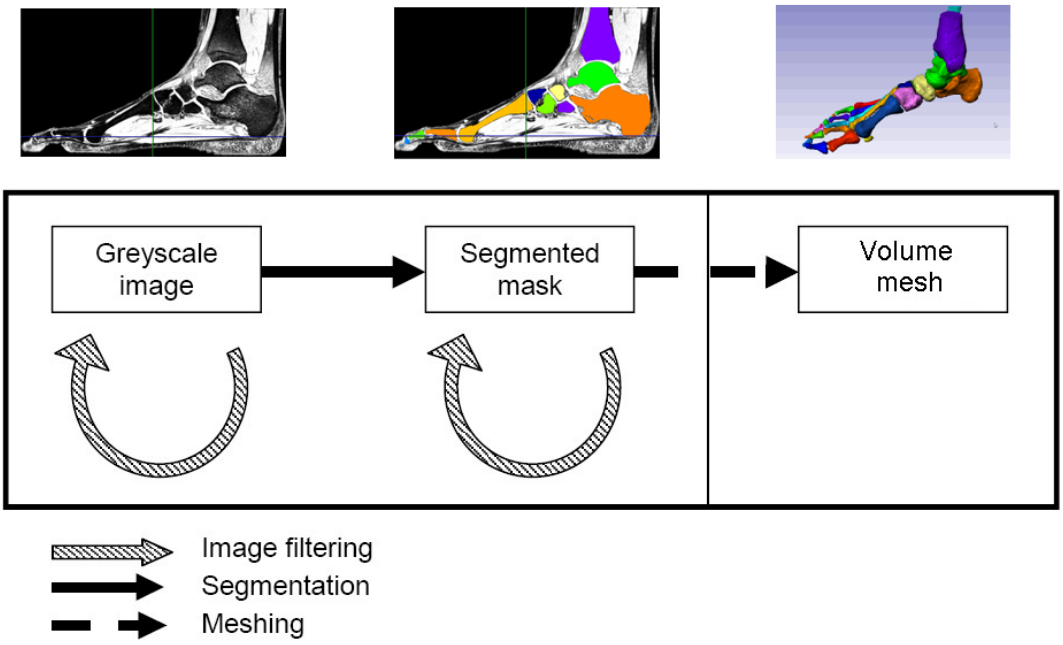

Figure 2.21: Image-to-model process [77].

This step is necessary to obtain clean geometries for adequate discretization.

Various tools exist for smoothing and obtaining triangulated or parametric surfaces. One of the most used in literature is Solidworks that allows to form solid models of each part, but other choices can be Rhinoceros or SALOME.

FE model generation

The FE model generation includes:

- the meshing step,
- the assignment of material properties,
- the assignment of constraints as kinematic boundary constraints, loads, connectors between elements and interaction properties i.e. contact properties.

Meshing: type of elements for the FE models of the foot

The meshing of the FE model can start both from the CAD model, in a more traditional way, and from the segmented images, as reported above. However, the mesh generation includes the setting of the number of elements, the type of

elements (shape) and the element formulation (typically linear or quadratic). The number of element is usually decided according to mesh sensitivity analysis. This is performed to ensure that the mesh density used in the FE model is sufficient to reach the converged numerical results. Mesh refinement process sometimes is carried out in a 2D plane-strain FE model based on a section of the foot. Usually the total strain energy and displacement is adopted as the convergence criteria, with the tolerance level being set as the change of less than 5% [54, 29].

It has been proved that in 2D FE modeling, if there is a choice between triangles and quadrilaterals with similar nodal arrangement, quadrilaterals are always to be preferred. Triangles are quite convenient for mesh generation, mesh transitions and rounding up corners but in finite element analysis with a given number of degree of freedom, 4-noded quadrilateral elements provide better results than 3-noded triangular elements [79].

For what regards the 3D, two types of element shapes are commonly used for mesh generation: tetrahedral and hexahedral. While tetrahedral meshing is highly automated, hexahedral meshing commonly requires user intervention and is labor intensive. Moreover tetrahedral elements that are more versatile to capture the irregularly shapes of the bone structure and the encapsulated soft tissues. As a result, most finite element models of the foot developed to date are built using tetrahedral elements [10, 29, 54, 35, 37, 36]. Nonetheless, hexahedral elements are generally preferred over tetrahedral elements because of their superior performance in terms of convergence rate and accuracy of the solution [109]. Tadepalli et al. examined the relative performance of tetrahedral and hexahedral elements when combined with material and geometric nonlinearities such as material incompressibility, large deformation, and frictional contact, conditions that are common in foot and footwear biomechanics. They proved that hexahedral elements consistently predicted reasonable contact pressures and contact shear stresses while the results from models with linear tetrahedral elements indicated that these elements should only be used under frictionless contact conditions or when the material incompressibility condition can be relaxed and in barefoot conditions results in very poor shear stress predictions [109].

The authors propose to ideally utilize hexahedral meshes for future foot and footwear models. However, given the high complexity of the foot structures and the difficulties in creating an hexahedral mesh for them, the automatic tetrahedral meshing technique results in decreased labor and expedited model development, facilitating mesh generation. Therefore they recognize that quadratic tetrahedral

element formulations can provide a reliable solution albeit with the disadvantage of increased computational cost [109].

Material properties: formulation and parameters for the soft tissues

In foot modeling, 'soft tissue' is considered anything that is not bone or cartilage. In literature regarding whole foot FE models there is not a subdivision between different types of soft tissues. For example in the study of Actis et al. muscles and fat were grouped into a single material type (tissue) with nonlinear elastic properties [7]. Only in a few cases there had been a distinction between skin and internal tissues [59] or 3D segmentation of plantar fascia [30]. In some studies a linear elastic formulation for the soft tissues was adopted [32, 35, 42, 67, 95]. However the non-linear behavior of the material has been demonstrated in several studies (see paragraph 2.4).

A material model which represent the incompressibility of soft tissue is the general hyperelastic material model employing a second-order polynomial strain energy potential. A widely adopted formulation, in particular for 2D FEM models of the foot, is the Ogden's model [48, 57, 59, 63]. The first-order Ogden model describes the strain energy potential (U) in the form of:

$$U = \frac{2\mu}{\alpha^2}(\lambda_1^\alpha + \lambda_2^\alpha + \lambda_3^\alpha - 3) \tag{2.1}$$

where $\lambda_{1,2,3}$ are the deviatoric principal stretches and μ and α are the material properties representing the hyperelastic behavior of the tissue. μ is the initial shear modulus and therefore it is linearly related to initial elastic modulus. The α value is a measure of increase in tangential modulus with increased strain and therefore describes a change in high strain behavior [44].

Other studies prefer the use of the general hyperelastic material model employing a second-order polynomial strain energy potential. This choice is usually made for the 3-D models [29, 60, 76, 37, 36, 33, 95].

The form of the potential is:

$$U = \sum_{i+j=1}^{2} C_{ij}(I_1 - 3)^i(I_2 - 3)^j + \sum_{i=1}^{2} \frac{1}{D_i}(J_{el} - 1)^{2i} \tag{2.2}$$

where U (Nm^{-2}) is the strain energy density, and I_1, I_2, and J_{el} (dimensionless) are the first and second deviatoric strain invariants and elastic volume ratio, respectively. The coefficients C_{ij} describes the shear behavior of the material and

$D_i(m^2N^{-1})$ introduces compressibility [29, 44, 76].

Other formulations have been proposed by Gefen et al. [54] and Natali et al. [86]. The first used an isotropic exponential material with the form[7, 54]:

$$\sigma_S = aexp(b\epsilon) \tag{2.3}$$

whereas σ is the fat pad stress, ϵ is the resulted strain and the constants are $a = 0.006$ and $b = 10.1$ while the second modelled the adipose soft tissues of the foot with a specific isotropic hyperelastic constitutive model defined by the strain energy function:

$$W(I_1, J) = U(J) + W(I_1) \tag{2.4}$$

where the volumetric and the iso-volumetric terms are:

$$U(J) = \frac{K_\nu}{2 + r(r+1)}[(J-1)^2 + J^{-r} + rJ - (r+1)] \tag{2.5}$$

$$W(I_1) = \frac{C_1}{\alpha_1}\{exp[\alpha_1(I_1 - 3)] - 1\} \tag{2.6}$$

The elastic constants of the model K_μ, r, C_1 and α_1 were deduced from the experimental tests, and the mechanical response of the tissue considered as visco-elastic material [86].

In the present thesis particular attention have been paid to the tissue characterization of the plantar pad in diabetic subjects.

In the contest of soft tissue material properties the study of Erdemir et al. should be pointed out [48]. In the literature properties of the heel pads of live subjects have been obtained from indentation testing. Such experimental procedures, however, do not account for the artifacts of boundary conditions and large deformations associated with indentation testing; therefore, they do not represent true stress-strain behavior of the heel pad. In the study of Erdemir et al. a combined methodology of FE modeling and ultrasound imaging to calculate subject-specific properties of heel pads of diabetic subjects in vivo was developed. FE modeling compensates for the geometry and boundary conditions of the experiment and therefore allows the true stress-strain behavior of the heel pad to be predicted [48]. For the identification of the material properties of the heel pad of diabetic and non diabetic control subjects an Ogden material model (equation 2.1) have been adopted. The values of the parameters (μ, α) were reported in

table 3.4 and have been adopted for the 2D heel model studied in this thesis (see chapter 3).

Similarly even though applied to a 3D model, the study of Cheung et al. assessed the effects of soft tissue stiffening on the stress distribution of the plantar surface and bony structures during balanced standing [37]. In this case the encapsulated soft tissue was defined as hyperelastic material with second-order polynomial strain energy potential (equation 2.2). The stress-strain data on the plantar heel pad were adopted from the in vivo ultrasonic measurements [76] to represent the normal soft tissue stiffness. The selected nominal stress values at corresponding nominal strains were multiplied by a factor of 2, 3 and 5 to investigate the biomechanical effect of soft tissue stiffening in different stages of diabetic neuropathy (values of the parameters are reported in figure 4.13). The results showed that a five-fold increase in soft tissue stiffness led to about 35% and 33% increase in the peak plantar pressure at the forefoot and hindfoot regions, respectively [37]. The formulation of the soft tissues reported in this study have been adopted for the 3D model developed in this thesis (see chapter 4).

Another recent study of Gu et al. [59] focused on gaining a better insight into the biomechanical behavior of the soft tissue material properties and their effect on the biomechanical response to loads and contacts stresses. In specific, the authors investigated the heel skin layer through a combined experimental and numerical study. They simulated the hind foot system during heel strike with potential variation of the skin stiffness based on a subject-specific FE model and biomechanical testing. A good agreement between the numerical results and the Novel-emed plantar pressure measurement suggested that the skin properties used were reasonable and accurate and the approach used was a feasible method. They demonstrated that tissue stiffness is quite different after dividing the heel pad into skin and fat pad layers. Even if they did not measure and simulate the specific diabetic skin stiffness, their sensitivity tests demonstrated that an increase in the skin stiffness had a limited effect on the stress and contact pressure of the hind foot bones, but caused a slight increase in the skin stresses, while skin softening caused a decrease in the peak plantar pressure and its distribution pattern changed (figure 2.22) [59].

Boundary constraints

One of the most important points in the simulation of the gait is the choice of

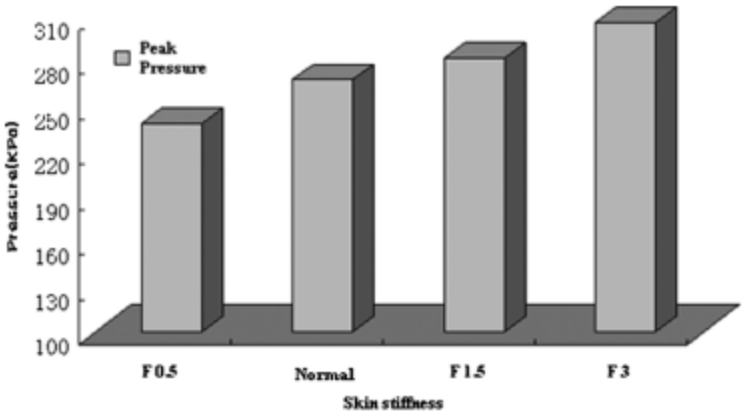

Figure 2.22: Results of the study [59]: Peak plantar pressure value of heel pad with different degrees of skin stiffness.

the boundary conditions. The FE method allows to set complicated loading and boundary conditions in both static and dynamic simulations [34]. The boundary constraints of the FE models include the kinematic boundaries such as fixed nodes or moving parts, connectors between elements or parts of the model, interaction between parts i.e. contacts and loads.

Determining a procedure for initially aligning the foot with respect to the ground and then for moving the foot in the different configurations assumed during the different phases of the gait cycle is a complicated problem, since every subject approaches to the ground in a different way and walks with his specific gait pattern. Therefore, a standardization of the procedure for the boundary condition settings and also a customization of these settings is necessary.

Moreover to study the human foot mechanism and load the foot FE models physiologically, the complex interplay or interrelationship among muscular control, internal joint movement, and plantar loading transfer needs to be considered. The gait analysis technique (paragraph 2.3.1), and in particular some protocols which provide for synchronized acquisitions of kinematic and kinetic, provides the instruments for the quantification of the variables useful in the boundary constraint setting of the FE models [32, 50].

Chapter 3

2D model of the hindfoot

3.1 Introduction

The diabetic foot is determined by the simultaneous presence of both peripheral neuropathy and vasculopathy that alter the biomechanics of the foot with the formation of callosity and ulcerations. The social and economic burden of the diabetic foot can be reduced through a prompt diagnosis and treatment. Finite element (FE) analysis allows characterising and quantifying the loads developed in the different anatomical structures and understanding how these affect foot tissue in dynamic conditions.

In this chapter the creation and validation of two experimentally kinematics-kinetics based bi-dimensional (2D) FE models of the hindfoot of a healthy and a diabetic neuropathic subjects is presented. The models were developed in order to define more efficient subject specific computational model of the hindfoot that accounts for in-vivo kinematics, kinetics and plantar pressure data together with foot magnetic resonance images (MRI) data.

The MRI of one healthy and one neuropathic hindfoot were segmented (Simpleware v.5.0) in order to obtain the geometry and develop the neuropathic subject's foot FE model (2DNSM) and the healthy subject's foot FE model (2DHSM) (Abaqus v.6.12). Six different loading conditions were applied to each model considering different phases of the stance phase of gait (namely: the heel strike, the loading response and the midstance) and either the global vertical ground reaction vector or the hindfoot one. The subject specific kinematic, kinetic and plantar pressure data synchronously acquired during in-vivo gait analysis were used as input for the simulations and for validations purposes. Model validity was established by means of comparison between each subject's peak plantar pressure

experimentally measured and the simulated one by means of evaluating the Root Mean Square Error (RMSE). Both the value and the position of the peak plantar pressure with respect to the plantar surface of the foot were compared.

FE simulations were also run with the kinematics and kinetics data of 20 subjects as input variables (10 healthy and 10 neuropathic subjects). Several simulations were conducted to verify different kinematics and loading conditions for the foot by applying the kinematics and kinetics experimentally measured of the neuropathic subjects to the 2DNSM and of the healthy subjects to the 2DHSM.

3.2 Methods

Two 2D FE models were developed for the hindfoot of both a healthy and a diabetic neuropathic subject. Each subjects' kinematic and kinetic data were extracted from the gait analysis trials.

Simulation tests were performed in two statuses. The first one required the specific biomechanical data of the subjects whose MRI images were used for the creation of the model geometry. The second one instead used the biomechanical data of a set of subjects applied on the specific model of their pathology (healthy subjects on the healthy subject's model and neuropathic subjects on the neuropathic subject's model). Both situations were then tested in two conditions: condition A where simulations used the specific force acting on the hindfoot and condition B where the forces applied were the ones acting on the whole foot. The validation of the models were also performed through the comparison among the simulated and the experimentally measured contact pressures. The peak values and the total distribution of the pressures were compared.

3.2.1 Subjects

The biomechanical analysis of the foot was carried out as in [101, 104] (see paragraph 2.3.4) on 10 healthy (age 58.7±10 years, BMI 24.5±2.6 kg/m^2) and 10 diabetic subjects with neuropathy (age 63.2±6.4 years, BMI 24.3±2.9 kg/m^2). Detailed clinical and demographic characteristics were reported in table 3.1.

Subjects were recruited among the patients attending the outpatient Clinic at the Department of Metabolic Disease of the University of Padova (Italy). Inclusion criteria were: type 1 and 2 diabetic subjects with walking ability, no history of ulcers or neurological disorders (apart from neuropathy), orthopaedic

problems, lower limb surgery, cardiovascular disease. Subjects were classified as neuropathic if they were found to be positive for 3 or more out of a total of 15 specified symptoms [9]. Healthy subjects were recruited among hospital personnel and chosen to be age-, BMI- and gender-matched with the diabetic subjects. All subjects gave written informed consent. The protocol was approved by the local Ethics Committee.

The neurological evaluation included the assessment of symptoms, and signs compatible with peripheral nerve dysfunction. The Michigan Neuropathy Screening Instrument questionnaire was used [49]. Subjects were classified as neuropathic if they were found to be positive for 3 or more out of a total of 15 specified symptoms [9]. The physical examination consisted of: patellar and ankle reflexes, assessment of lower limb muscle strength, sensory testing (pin-prick), touch (10 g Semmens Weinstein monofilament) and vibration perception threshold (128 MHz tuning fork and Biothesiometer), pain sensitivity, electroneurophysiological study, and ankle-to-brachial systolic pressure ratio (Index of Winsor). Cardiovascular autonomic tests were also performed. HbA1c values from the preceding ten years were collected. Each patient had at least one ophthalmologic examination, a urinary albumin-to-creatinine ratio measured, a carotid artery Doppler ultrasound examination, and a 12-leads electrocardiogram in the three months period preceding the study.

All subjects underwent clinical examination of the foot by a single orthopaedic surgeon experienced in foot and ankle conditions [39, 73].

The complete FE model development was performed for one healthy subject and one neuropathic subject (characteristics are reported in table 3.2). The neuropathic subject suffered from diabetes mellitus type 1 for 45 years. He has also developed a retinopathy and a vasculopathy and furthermore he suffered from an hypertensive pathology.

3.2.2 Gait analysis data

Movement analysis was carried out using a 6 cameras stereophotogrammetric system (60-120 Hz, BTS S.r.l, Padova), 2 force plates (FP4060-10, Bertec Corporation, USA, 960 Hz), 2 plantar pressure systems (410 x 410 x 0.5 mm, 0.64 cm2 resolution, 150 Hz, Imagortesi, Piacenza) (instrumentation described in paragraph 2.3.2). The signals coming from all systems were synchronized in post processing as in [101, 104] (see paragraph 2.3.4). A four-segment 3-dimensional (3D) foot kinematic model was adopted as in [101] while a three-segment model

Groups	Healthy Subjects		Neuropathic Subjects	
	n or mean	SD	n or mean	SD
Subjects [n]	10		10	
Sex [n of males]	7		6	
BMI [kg/m^2]	24.9	2.3	24.3	2.9
Hypertensive disease [n]	0		8	
Age [years]	61.2	5.3	63.2	6.4
Peripheral neuropathy [n]	-	-	10	
Diabetic retinopathy [n]	-	-	6	
Microalbuminury [n]	-	-	2	
Vasculopathy [n]	-	-	3	
Vasculopathy (peripheric) [n]	-	-	2	
Vasculopathy (TSA) [n]	-	-	5	
Vasculopathy (coronary) [n]	-	-	1	
Type of diabetes [n]	-	-	type1: 6, type2: 4	
Hb A1c	-	-	7.97	1.28
Years of disease	-	-	28.1	12.5
Cavus foot [n]	6		9	
Flat foot [n]	0		1	
Valgus Hindfoot [n]	3		4	
Varus Hindfoot [n]	0		1	
Hallux valgus [n]	2		4	
Foot deformities [n]	4		5	
Plantar callosity [n]	1		4	

Table 3.1: Demographic and clinical data of the healthy and the neuropathic subjects. n = number of subjects.

Condition	Sex	Age	Weight (kg)	Height (cm)	BMI	Foot size	Type of foot
Healthy subject	F	29	61	174	20.1	40	Dx-Sx normal
Diabetic Neuropathic subject	M	72	79	175	25.8	42.5	Dx-Sx cavus

Table 3.2: Data of diabetic neuropathic and healthy subjects.

for the plantar subarea definition was obtained as in [104]. Thus, for each patient's foot the hindfoot, midfoot, forefoot and tibia subsegments 3D kinematics was calculated together with hindfoot, midfoot, forefoot 3D ground reaction forces and plantar pressure.

The gait analysis protocol was organized in a static acquisition (subject in an upright posture, with feet placed with ankles together, toes pointed 30 degrees apart and the arms along the body [101, 104]) and several walking trials (barefoot and self-selected speed). For the purpose of this study, at each percentage of the stance phase of gait the ground reaction forces (figure 4.6) and the plantar pressures data of either the whole foot or the hindfoot were extracted and the angle between the mediolateral axis of the ankle (through the markers on the malleoli) and the floor was calculated.

3.2.3 FE models

For both the subjects the same reconstruction procedure of foot geometry was performed (see figure 3.1).

Geometry reconstruction

The magnetic resonance images of the foot of an healthy subject (age 28 years, BMI 20.2 kg/m^2) and of a diabetic neuropathic subject (age, 72 years, BMI, 25.1 kg/m^2) were acquired with 1.5T devices (Philips Achieva and Siemens Avanto). The parameters adopted for the acquisitions were reported in table 3.3.

	2DHSM	2DNSM
MR device	Philips Achieva	Siemens Avanto
Sequence type: Multi-Echo Data Image Combination	mFFE	Medic
MR acquisition type:	3D	3D
TR	33.0451	32
TE	9.207	14
Flip angle:	30	30
Spacing between slides:	0.6 mm	0.75 mm
Slice thickness:	1.2 mm	1.5 mm

Table 3.3: Parameters adopted for the MRI acquisitions.

The magnetic resonance images were segmented with Simpleware ScanIP-ScanFE (v.5.0) in order to get a slice of the hindfoot passing through the malleoli.

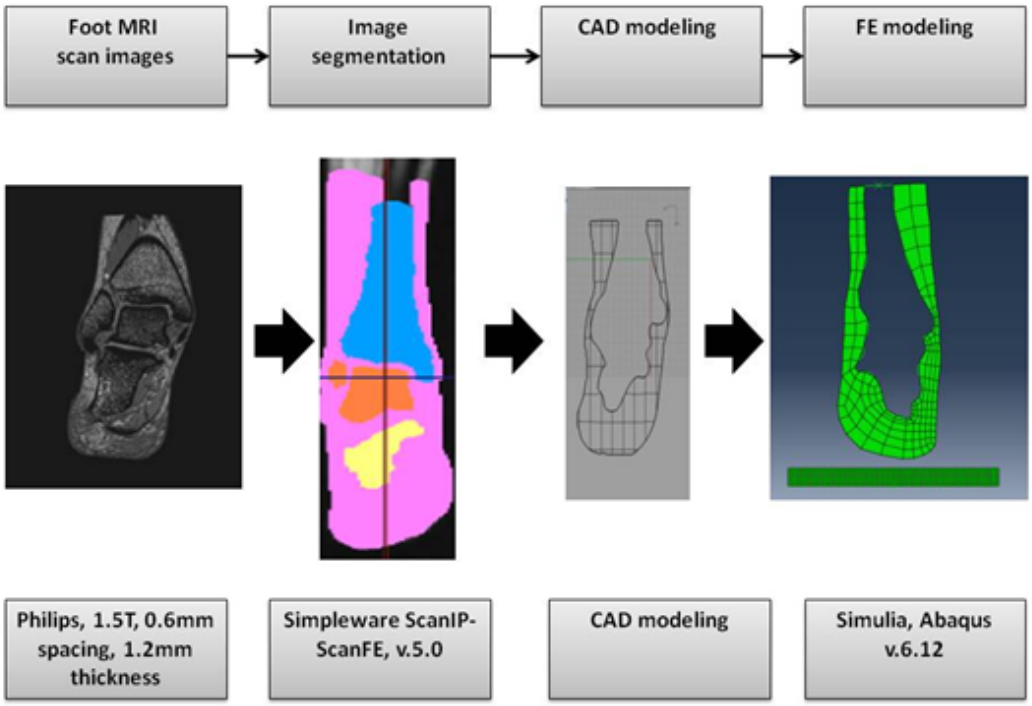

Figure 3.1: Workflow to develop the 2D FE models of the hind foot.

Mesh

The segmented slice was imported into ABAQUS (Simulia, v.6.12) and meshed with quadrilateral elements. The mesh density was set according to the literature [57]. The mean length of the elements sides was 4 mm. An horizontal rectangular element was drawn in ABAQUS under the heel slice to simulate the ground support (see figure 3.2). This part was meshed with 8 mm side quadratic elements with the aim to obtain a contact pressures values comparable with the experimental ones (according to plantar pressure system sensors dimension).

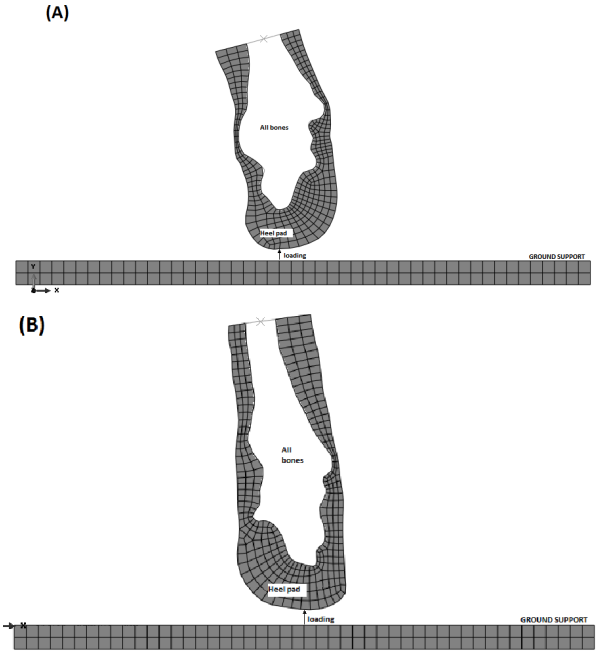

Figure 3.2: Plane strain finite element models of the heel. (A) Model of the hindfoot of the healthy subject. (B) Model of the hindfoot of the neuropathic subject.

Materials properties

The heel pad was represented by a homogeneous isotropic soft tissue model with an hyperelastic material formulation in first order Ogden form and coefficients from [48] (see table 3.4). Both the floor and the bones were modelled as homogeneous isotropic linear elastic materials (see table 3.4) [14, 54, 29].

Part	Material Formulation	Material Parameters		References
Bones	homogeneous, isotropic, linear elastic	E=7300 MPa	ν= 0.3	[54]
Plate (Alluminium 6061)	homogeneous, isotropic, linear elastic	E=68900 MPa	ν= 0.3	[14]
Healthy Heel pad	homogeneous, isotropic, hyperelastic	$\mu = 0.01645$	$\alpha = 6.82$	[48]
Neuropathic Heel pad	homogeneous, isotropic, hyperelastic	$\mu = 0.01688$	$\alpha = 7.02$	[48]

Table 3.4: Material properties for the model parts.

Boundary conditions, contacts and loads

The foot-floor interface was modelled using contact surfaces with a coefficient of friction of 0.6 [37]. The bones were tied to the soft tissues. During the simulation, the superior surfaces of the bones and soft-tissues were completely fixed to simulate the effects of constraints from superior-lying tissues [29]. The correct position of the foot with respect to the floor was set up matching the FE model angle between the floor and the mediolateral axis of the ankle (the axis passing through the prominences of the malleoli) to the experimental one obtained from the kinematic data in the corresponding instant of the stance. The loading conditions were set according to the ground reaction force registered with the force plate during gait.

3.2.4 Numerical simulations and validation method

The FE software ABAQUS (Simulia, v.6.12) was used to perform the numerical stress analyses (figure 3.2). Healthy subject's data were applied on the 2DHSM, while for the neuropathic subjects the 2DNSM was used.

Three instants of the stance phase of gait were chosen to perform the simulations [54]: the initial contact of the heel (1% of the stance), the loading response (first peak of the hindfoot vertical force) and the midstance (minimum height of the markers of the foot from the floor). For each of the abovementioned subphases and for each subject, the model was adapted by changing its geometric positioning relatively to the floor. Thus for each subject the following simulations were run: three simulations corresponding to the 3 sub-phases of the stance phase of gait with the heel vertical force and three with the whole foot vertical force, a simulation with the generic static force (half of the body weight) and one with

the specific static force (% of the body weight calculated from the pressure map).

The models validity was assessed by comparing the results of the simulations (the contact pressures) with their subject and instant-specific plantar pressure experimental data. The latter were extracted from the instant-specific pressure map, which was realigned according to the ankle mediolateral axis. The row at the hindfoot where the peak occurs was chosen.

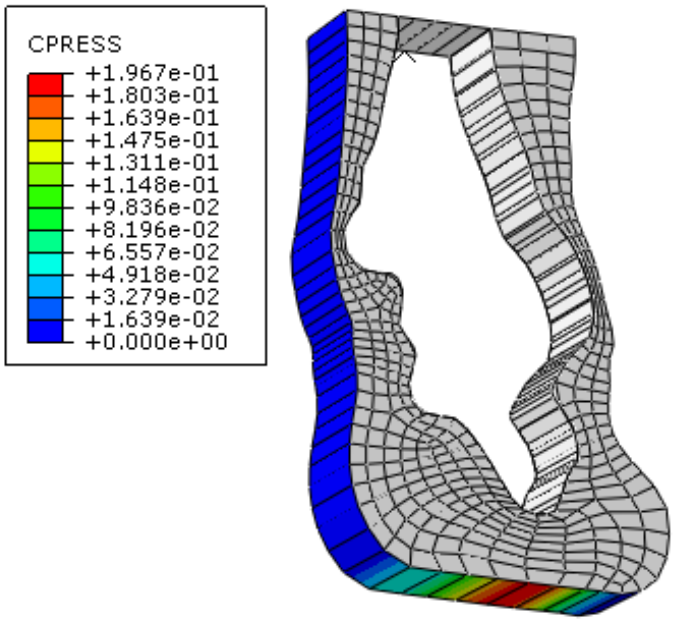

Figure 3.3: Extrusion of the slice of the hindfoot after the simulation (as example). The legend on the left shows the values of the pressures developed under the heel model during the simulation.

The simulations performed by applying the subject specific gait analysis data (one healthy and one neuropathic) to the same subject specific geometry will be presented separately and named "custom models". The results of the other simulations have been reported grouping them according to subject characteristics, and they have been called "healthy subjects" simulations and "neuropathic subjects" simulations. The contact pressure data were extracted from Abaqus and reordered in a vector according to their position on the floor mesh.

3.3 Results

The peak pressure values were adopted to perform the comparison between experimental and simulated data in agreement with [57]. Nevertheless, no spatial

information were considered with this method, thus in order to take into account the distribution of the plantar pressures over the entire contact surface, the comparison of the data have also been performed through the Root Mean Square Error in percentage of the experimental peak value (RMSE%).

3.3.1 Validation with the subject specific data

The results of the simulated custom models (the 2DHSM and the 2DNSM) were reported in figure 3.4 and 3.5. The simulations have been performed by applying the specific hindfoot vertical ground reaction vector (condition A) or the whole foot vertical ground reaction vector (condition B).

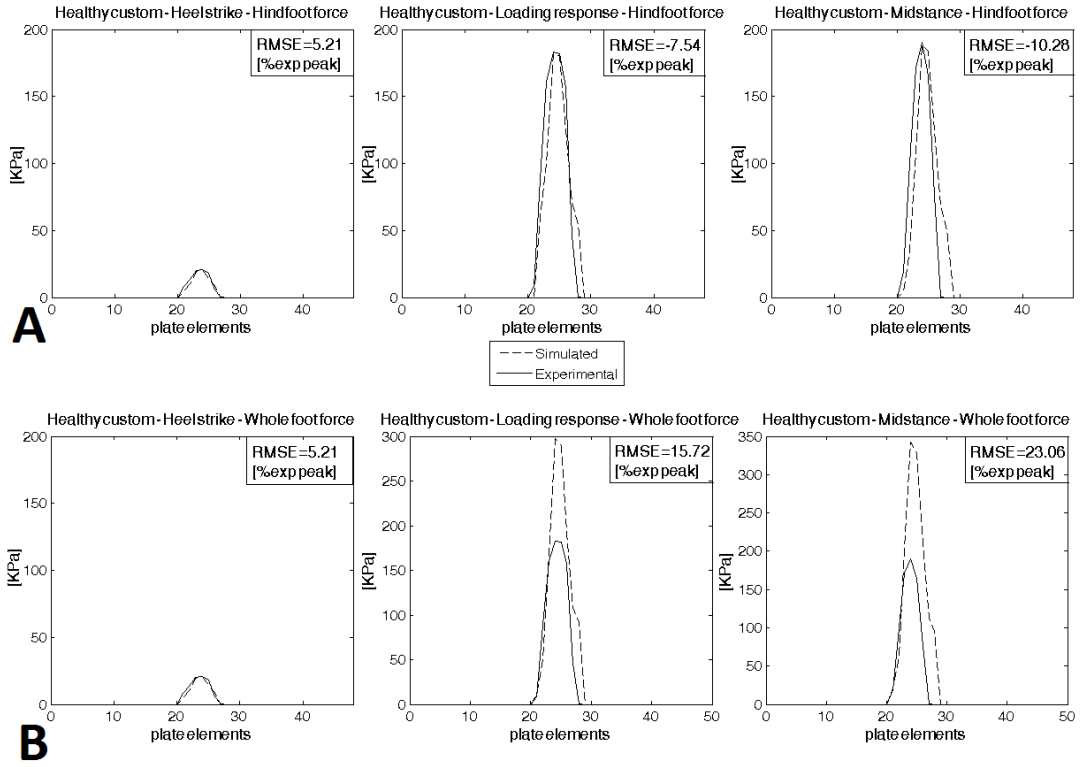

Figure 3.4: Healthy custom model: simulated over experimental pressure line on the three instants of the stance phase of gait. (A) Condition A, (B) Condition B. Minus sign in RMSE% indicates that the simulations underestimated the pressure while no sign indicate that overestimated the experimental one.

The RMSE% values of the static simulation performed by considering half of the body weight in the healthy and neuropathic custom models were respectively 11.8 and 6.3. If a force proportional to the pressures were applied to the model,

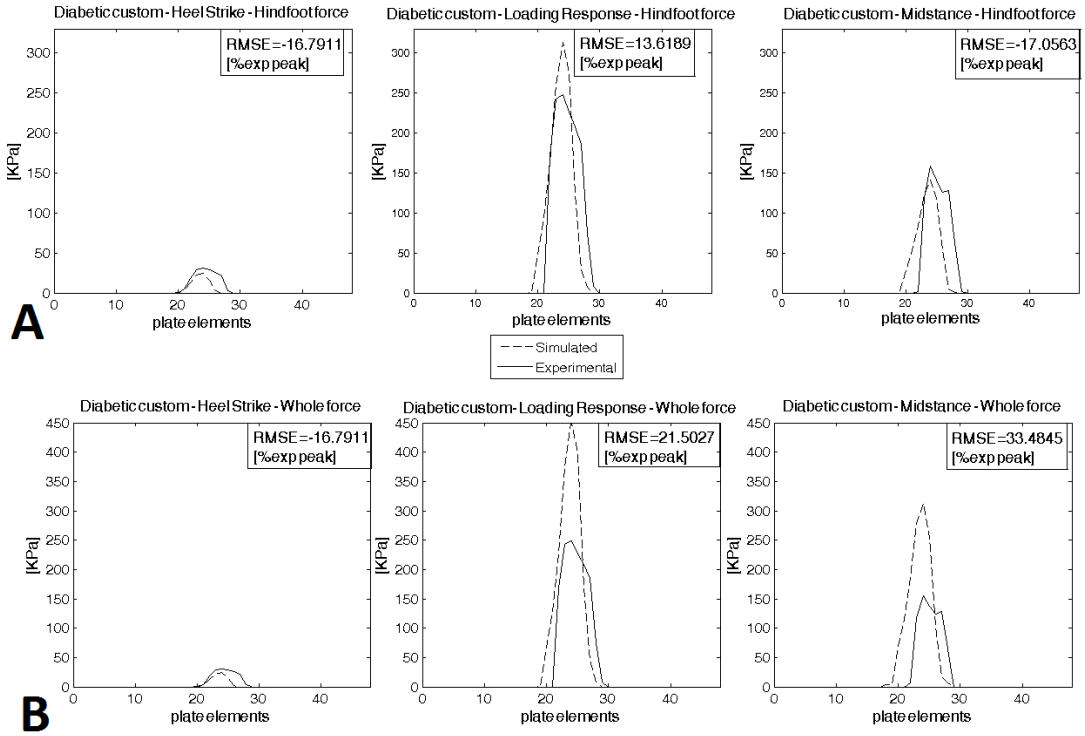

Figure 3.5: Neuropathic custom model: simulated over experimental pressure line on the three instants of the stance phase of gait. (A) Condition A, (B) Condition B. Minus sign in RMSE% indicates that the simulations underestimated the pressure while no sign indicate that overestimated the experimental one.

the RMSE% became respectively 16.4 and 8.9. The differences between the peaks (in percentage of the experimental peak) resulted for the healthy subject in the simulation with half BW equal to -30.1%, while in the case of applying the specific static force resulted equal to -4.7%. In the case of the neuropathic subject the percentage differences resulted respectively 8.15% and 37.8%.

Thereafter, in the simulations performed in condition A, it was shown a better agreement between the experimental and the simulated data then in condition B. In condition A the healthy custom model underestimated the contact pressure distributions by 4.2% but the prediction of the peaks values resulted more accurate (error 1.1% of the experimental peak). In the case of the simulations in condition B, the pressure distributions were overestimated by 14.7% and the peaks by 48.23%. The neuropathic custom model in condition A underestimated the contact pressure distributions by 6.74% (peaks by 30.9%) while in condition B it overestimated them by an average percentage of 12.73% (peaks 69.4%).

3.3.2 Healthy subjects and neuropathic subjects simulations

When considering the simulations performed on all the subjects, subdivided in healthy and neuropathic group, the data obtained from the gait analysis (experimental loads and plantar pressures) used for the simulations were reported in table 3.5 (mean and standard deviation values within each group have been reported).

The results of the simulations have been compared by means of T-tests on the peaks of the plantar pressures (figure 3.6 and table 3.6).

Also in the non-custom models the pressures simulated in condition B were statistically different from the experimental ones for every group and in every tested instant ($p< 10^{-7}$) of the stance phase of gait with the exception of the heel strike when the ground reaction force of the whole foot corresponds to the one of the hindfoot. As a result the RMSE% increases in condition B. When considering the simulations in static condition, in both cases (static with specific force and static with half of body weight) the differences between the experimental and the simulated data were not significant. However the RMSE% did not decrease (values were reported in table 3.6).

Moreover, a brief description of the ability of the model in detecting the differences among the two groups of subjects can be found in figure 3.7 When loads altered by the presence of a pathology, as occurs in the case of diabetic neuropathy,

Force	Healthy subjects		Neuropathic subjects	
[% of body weight]	mean	sd	mean	sd
heel strike - hindfoot	4.93%	0.88%	5.24%	1.20%
loading response - hindfoot	62.73%	7.77%	74.18%	10.12%
midstance - hindfoot	39.23%	7.89%	37.44%	14.64%
Static load - Half of Body weight	50.00%	0.00%	50.00%	0.00%
heel strike - whole foot	4.93%	0.88%	5.24%	1.20%
loading response - whole foot	85.05%	13.15%	93.76%	13.74%
midstance - whole foot	90.86%	7.87%	87.15%	8.09%
Peak plantar pressures	**Healthy subjects**		**Neuropathic subjects**	
[% of body weight]	mean	sd	mean	sd
static	31.44%	5.83%	28.06%	7.18%
heel strike	3.28%	1.22%	3.28%	0.61%
loading response	27.82%	3.90%	28.05%	5.33%
midstance	24.22%	4.30%	19.69%	5.32%

Table 3.5: Experimental loads and plantar pressures (only peaks were reported) used for the simulations and validations: healthy group and neuropathic group.

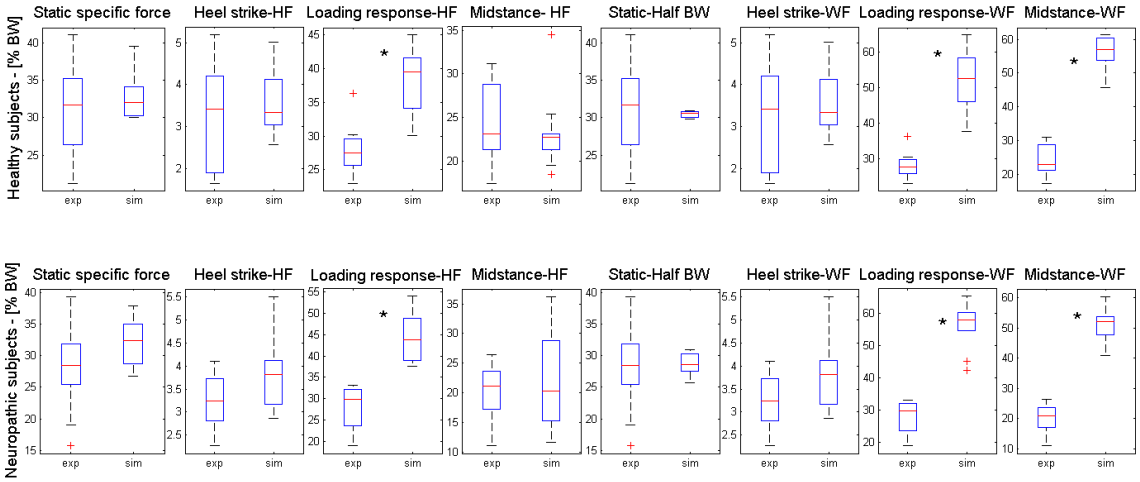

Figure 3.6: Results of the simulations performed in condition A (Hindfoot force - HF) and in condition B (Whole foot force - WF): boxplot of the experimental (exp) and simulated (sim) contact pressures in the groups of subjects (healthy subjects and neuropathic subjects). BW=body weight.

Force [% body weight]	**Healthy subjects**			**Neuropathic subjects**		
	T-test	**PP error%**	**RMSE%**	**T-test**	**PP error%**	**RMSE%**
Static specific force	0.59	14.76	15.86	0.12	33.96	13.88
Heel strike - HF	0.65	30.96	14.75	0.09	27.93	11.83
Loading response- HF	0.00*	42.25	14.28	0.00*	56.63	17.45
Midstance - HF	0.63	15.57	11.01	0.51	26.07	13.56
Static - half of BW	0.61	14.91	12.88	0.78	24.60	12.52
Heel strike - WF	0.65	30.96	14.75	0.09	27.93	11.83
Loading response- WF	0.00*	92.94	23.23	0.00*	97.45	24.40
Midstance- WF	0.00*	137.13	31.44	0.00*	184.45	45.17

Table 3.6: Results of the simulations performed in condition A (Hindfoot force - HF) and in condition B (Whole foot force - WF)comparison between experimental and simulated contact pressures. PP=peak pressure. BW=body weight. Specific force=% of the body weight calculated from the pressure map. RMSE%= root mean square error between the entire simulated and experimental pressure curve, in percentage of the peak experimental pressure: the reported value represents the mean value among all the subject of the same group. * statistical significance ($p<0.05$)

were used as input in the neuropathic model, the plantar pressures resulting from the simulations were high and significantly different from the corresponding ones on the healthy feet in agreement with the literature [8, 56, 69].

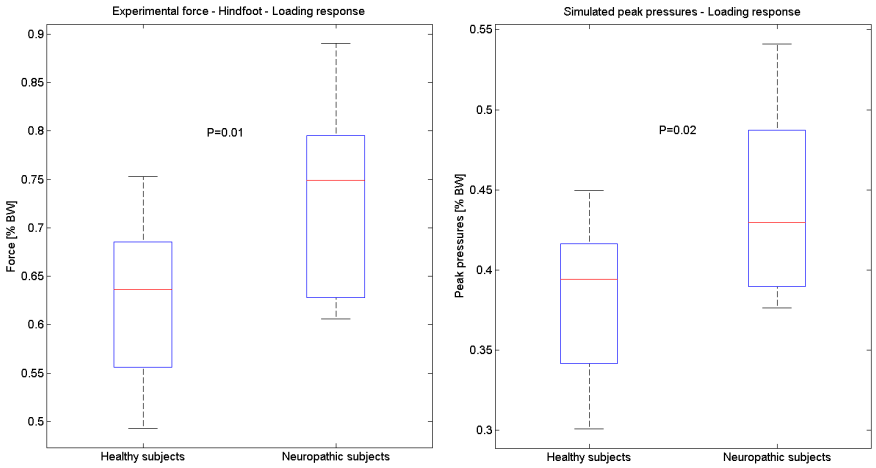

Figure 3.7: (left) Experimental ground reaction forces at the hindfoot during loading response. These forces were adopted to load the models. (right) Simulated peak pressures obtained when the models were loaded with the forces on the (left).

The model simulated with the specific load of the hindfoot displayed in every case better results than the model ran with the forces registered under the whole foot. In summary, the simulations which used the hindfoot specific ground reaction forces as loads shown an average RMSE% of pressure distributions for both the healthy and the neuropathic foot models of around 13% for all the subjects.

3.4 Discussion

The principal novelty of the present study should be considered the development of a subject specific FE model of the neuropathic foot whose subject specificity can be found in term of foot geometry (obtained from MRI), kinematics and kinetics experimentally measured data.

The state of the art of the simulations of the foot FE models mainly reported simulations performed in static standing condition applying the load of half of a body weight [119] as input to run the simulation process. Some others performed their simulation by applying the load of the midstance or other phases of the stance phase of gait by considering as input the vertical force calculated as mean value among multiple subject or trials or as the sum of the pressures registered

during one single phase of the stance [57, 47]. Only in the work of Gefen et al. a model of a healthy foot simulating six gait sub-phases can be found. In that case the loading conditions of each phase were taken from previous literature and the geometric positioning was calculated from fluoroscopic dynamic acquisition of the subject's foot [54].

The validation process was performed through the comparison between the peak plantar pressures experimentally measured and the simulated ones. Some papers adopted the experimental peak values of works already previously published [96] while others integrated pressure over the contact area of the subject whose foot geometry and weight was used to create and simulate the model [57]. In general, none of the proposed models adopted, for the validation, the plantar pressure distribution acquired synchronously to the loads adopted for the simulation.

Several 2D and 3D foot FE models were reported in the literature [7, 22, 31, 29, 35, 37, 36, 47, 54, 52, 76, 88, 96] but just a few of them considered the diabetic foot pathology [7, 91, 110, 50].

The FE model developed herein allowed the customization of the results of the simulations both in the healthy and the diabetic neuropathic foot cases. The kinematic and kinetic (the position of the foot and the loads) used to run the simulations were specific of each subject's hindfoot in the specific instants of the stance phase of gait. Furthermore, the plantar pressures used to validate the model were subject, space and time matched with the data used for the simulations. Since the main problems in the diabetic foot are due to changes in the biomechanics [113], the latter cannot be ignored in the simulation process.

In the present contribution it has been demonstrated that foot positioning in the FE simulation has a great influence on the simulated stress distributions and that there is a better agreement between the predicted pressures and the experimental one if the angles between the foot and the floor are set before applying the loads [60]. In the model proposed herein the foot position has been set according to the angles between the foot axes and the floor during gait in each subject specific kinematic acquisition. A similar procedure can be found in Gefen et al., however they adopted the specific anteroposterior position of the foot in a specific gait sub-phase captured from a fluoroscopy and the synchronized pressures used for the model validation [54]. In that case the procedure was invasive, since X-rays had to be used in continuous mode, and furthermore no synchronized ground reaction force plates were used. In the approach proposed

herein, only double tape mounted skin markers were stitched to the patients, as currently done in movement analysis trials. Of course it can be argue that the precision in the estimate of the kinematics was affected by skin artefact differently than in fluoroscopic conditions.

The majority of the FE models of the foot reported in literature simulated the static loading condition, the midstance or only one critical instant of the stance phase of gait. This is highly limiting because it has been demonstrated that the alterations occur over the entire stance phase of gait [61, 97, 98, 104, 112]. Thus, the heel model validity should be tested on several instants of the heel contact, as can be found in the study of Gefen et al. [54].

The FE models developed herein succeeding in simulating the experimental plantar pressures distribution unless a RMSE% of 13%. These results cannot be compared with the literature unless if we consider that within different conditions from barefoot standing, the model overestimated the contact pressures by a 25% as reported by Goske et al. [57]. Nevertheless, there is a better agreement between the experimental and the simulated data when the forces on the hindfoot were applied, instead of the whole foot ground reaction force (mean RMSE% of 13% versus mean RMSE% of 25%). The custom healthy and neuropathic models resulted in a RMSE% respectively of 7.7% and 15.8% when the hindfoot force was applied. The higher error found in the neuropathic foot model can be due to the soft tissues material formulations, since they were adopted from previous literature [48] and not specifically measured for the patient under study. Several studies implemented a method to measure the plantar pad material properties through indentation tests or ultrasound probe tests. A useful instrument which replicate the loads under the foot at in-vivo registered rates is the Soft Tissue Response Imaging Device [89]. The results on diabetic subjects' soft tissues obtained from this instrument could be used for further improvement of the model developed herein.

Nevertheless, the model developed in this study did not consider horizontal shear forces; given their importance of these forces in the ulceration process, they should be included in the future work. However these issues should be considered beyond the scope of the current contribution it can be concluded that completely custom models with subject specific biomechanical data from gait analysis provided a better adherence to the plantar pressures measured in vivo during gait. Thus, it could be inferred that internal stresses resulting from those type of models can be considered more representative of the real behaviour of the

heel pad.

Even under the restrictive assumptions of 2D representation, which is clearly inadequate for a complete model of the complex mechanics of the foot and of the foot-floor interaction, it is nevertheless possible to run simulations that provide useful informations towards a better understanding of the mechanism of plantar ulcer formation and may provide new insight into planning preventive treatment by including pressure relief insoles in the simulation. Moreover the 2D model proposed herein serve to guide the development of a 3D diabetic foot model.

In conclusion, our research indicated that using the subject specific in-vivo measured biomechanical data for the simulation of the finite element foot model can provide more realistic results on the soft tissue plantar pad pressure distributions and deformations.

Chapter 4

3D model of the foot

4.1 Introduction

Three-dimensional (3D) patient specific finite element (FE) models of the foot allow to characterise and quantify the loads developed in the different anatomical structures of the foot and to understand how these affect foot tissue in dynamic conditions. This knowledge is crucial in understanding the aetiology of diabetic foot and allows identifying the mechanisms priming ulceration.

Although its potential clinical impact, this modelling approach is currently not available in a clinical context.

The aim of this thesis with respect to 3D FE modelling was to advance in this direction. As stated in the previous chapter, FE modelling of the foot, and in some cases footwear, has been explored by a number of groups [6, 22, 31, 29, 36, 47, 54, 57, 120]. The state of the art of the foot FE models reported simulation performed in static standing condition applying the load of half of a body weight [119] as input to run the simulation process. Some others performed their simulation by applying the load of the midstance or other phases of the stance of gait by considering as input the vertical force calculated as mean value among multiple subject or trials or as the sum of the recorded plantar pressures. In particular the work of Gefen et al. reported a model of a healthy foot simulating six gait sub-phases. In that case the loading conditions of each phase were taken from previous literature and the geometric positioning was calculated from fluoroscopic dynamic acquisition of the subject's foot [54].

The aim of the present chapter was to advance in this direction. Therefore a subject specific 3D FE model of both a neuropathic and a healthy foot whose subject specificity can be found in term of foot geometry (obtained from Magnetic

Resonance Images - MRI), kinematics and kinetics experimentally measured data has been developed. The same procedure applied for the development of the 2D FE models previously described was adopted (see chapter 3).

Each subjects' kinematic and kinetic data were extracted from the gait analysis trials while their foot geometry was obtained from MRI images. Replicating what performed with the 2D models, simulation tests were performed in two different conditions. State A required the specific biomechanical data of the subjects whose MRI images were used for the creation of the model geometry. State B applied the biomechanical data of 10 neuropathic and 10 healthy subjects as input to run the FE simulations (healthy subjects' data as input to the healthy subject's model - 3DHSM - and neuropathic subjects' data as input to the neuropathic subject's model - 3DNSM).

The models validity was assessed through comparison between each subject simulated contact pressure and the experimentally measured one. The peak values and the total distribution of the pressures were compared for this purpose.

The same procedure was repeated for both the models (paragraph 2.5.3), in the following paragraphs the details in common between the two models have been reported, focusing in particular on the differences between neuropathic's foot model and the healthy one.

4.2 Methods

4.2.1 Subjects

State A

Two subjects, one healthy (age 28 years, BMI 20.2 kg/m^2) and one diabetic with peripheral neuropathy (age 72 years, BMI 25.1 kg/m^2) were recruited for the FE model development (see table 3.2 for the clinical and demographic characteristics). Written informed consent was obtained from both subjects. The protocol was approved by the local Ethics Committee of the University Clinic, of the Hospital of Padova, Italy.

State B

The biomechanical analysis of the foot was carried out as in [101, 104] (see paragraph 2.3.4) on 10 healthy (age 58.7±10 years, BMI 24.5±2.6 kg/m^2) and 10

diabetic subjects with neuropathy (age 63.2±6.4 years, BMI 24.3±2.9 kg/m^2). Details about the recruitment, the neurological examination, the clinical and demographic characteristics of the subjects of the study were reported at paragraph 3.2.1.

4.2.2 Gait analysis data

The gait analysis was carried out with the instrumentation presented at paragraph 2.3.2 and according to the protocol described at paragraph 2.3.4 and in [101, 104]. This provided synchronized kinematic, kinetic and plantar pressure data. Following this protocol it was also possible to divide the foot into 3 subsegments, namely the forefoot, midfoot and rear-foot(figure 4.1).

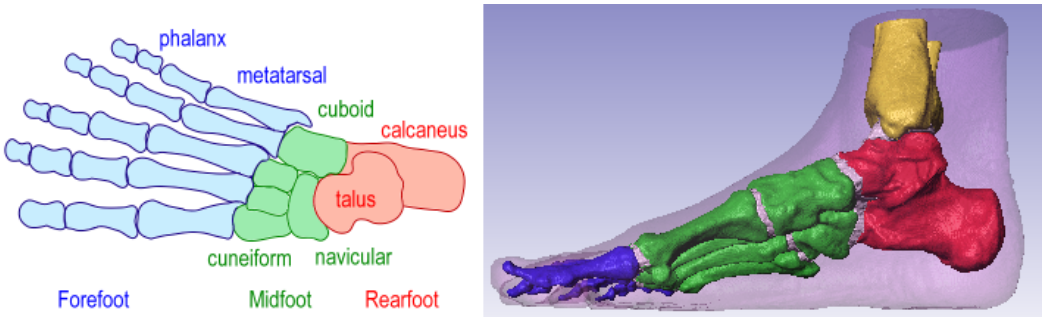

Figure 4.1: Foot bones divided in three foot subsegments as in [104].[2]

The motion analysis acquisitions were organized in a static trial (subject in an upright posture, with feet placed with ankles together, toes pointed 30 degrees apart and the arms along the body [101, 102, 104]) and several gait analysis sessions. The latters were performed by the patients walking at a self-selected speed along a walkway. At least three gait cycles of each limb were recorded for each patient.

For each trial, both full foot and subsegments angular displacements, ground reaction forces and plantar pressure curves were plotted over one stance phase of gait.

State A

In order to cover the range of foot contact over the ground, four instants of the stance phase of gait (red arrows in figure 4.3), when critical loads occurred (as suggested in [54]) were chosen for the FE simulations of 3DHSM and 3DNSM:

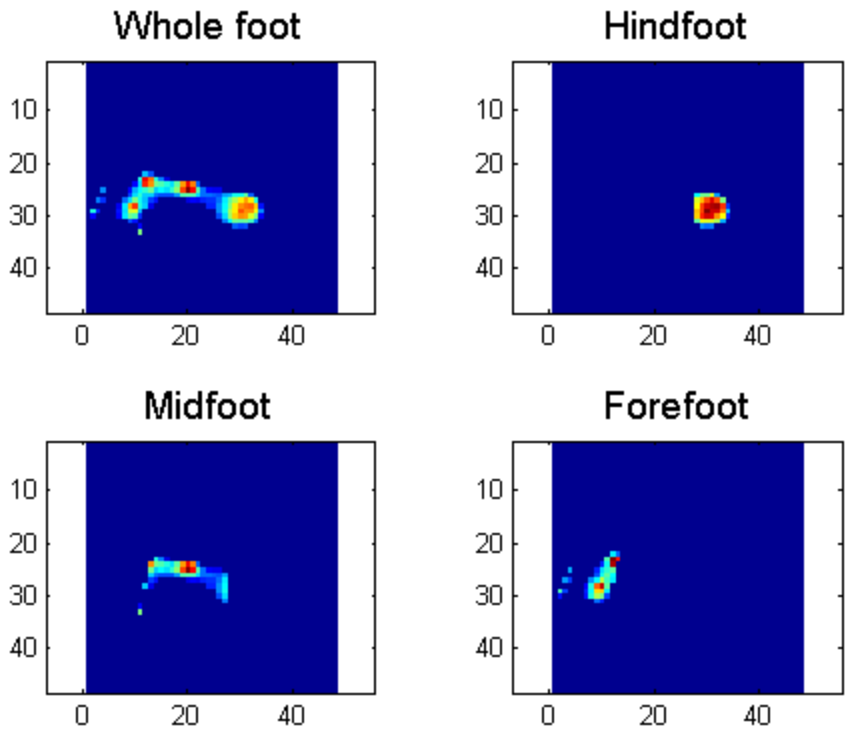

Figure 4.2: Example of foot plantar pressures subarea subdivision. This was performed for the experimental data as well as for the simulated contact pressures.

- the heel strike (the 1% of the stance),
- the loading response (first peak of the hindfoot vertical force),
- midstance (minimum height of the markers of the foot from the floor),
- push off (peak of the forefoot vertical force).

The definitions of these instants were reported at paragraph 2.3.1.

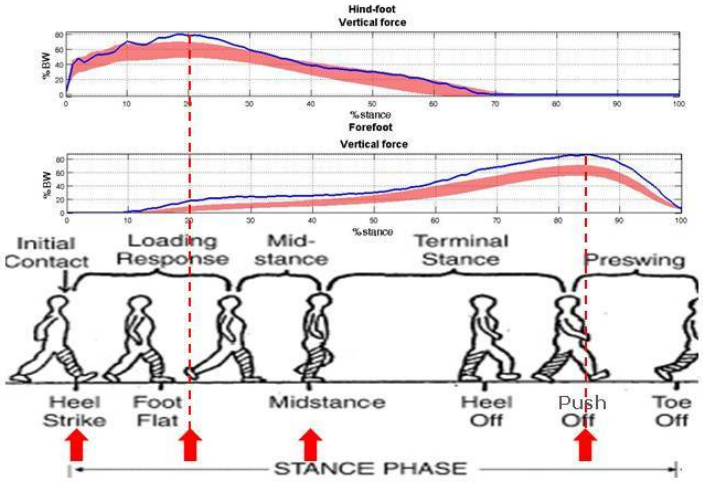

Figure 4.3: Instants of the stance phase identification. Gait cycle figure from [41].

At this stage of the model development, only the whole foot vertical ground reaction force and 3D angular position of the whole foot relative to the global reference system were needed. However for the validation process the plantar pressures of the subsegments were used. For the healthy subjects and the neuropathic subject these data were extracted in each of the instants cited above.

This process gave the possibility of simulating and validating the models with subject- trial and gait sub-phases specific data.

In figures 4.5, 4.6 and 4.7 were reported, over the normative bands, the gait analysis data of the diabetic neuropathic subject recruited for the FE model implementation. Only the right foot data and only one selected trial were reported as the FE model was developed by mean of the right foot geometry and simulated considering one single trial. These data were normalized on the stance phase of gait and on the weight of the subject in order to allow a comparison with the normative bands. However the non-normalized data were extracted to perform the FE model simulations.

As described at paragraph 2.3.3, the neuropathic subjects exhibit altered joint kinematic and altered plantar loads either in vertical or in tangential direction.

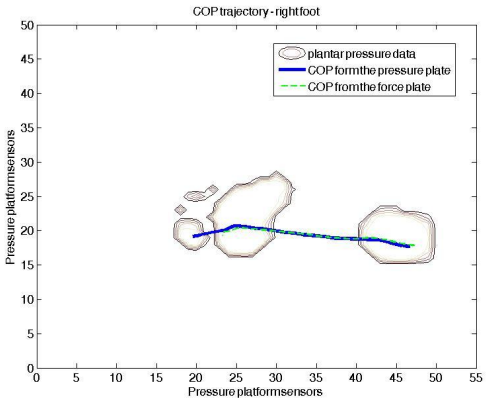

Figure 4.4: Centre of pressure (COP) trajectory of neuropathic subject during one trial.

State B

For the 10 healthy and the 10 diabetic subjects the kinematic-kinetic-plantar pressures data relative to the midstance phase of gait were extracted. In particular the mediolateral inclination with respect to the global reference system was calculated. This was performed in order to allow the FE model position to be adjusted according to the subject specific foot position.

4.2.3 FE models

For both subjects the same procedure of foot geometry reconstruction was performed (see figure 4.8).

Geometry reconstruction

The MRI of the foot of the healthy and the neuropathic subjects were acquired with 1.5 T devices (Philips Achieva and Siemens Avanto). The parameters adopted for the acquisitions were reported in table 4.1.

The multi-fast-field-echo (mFFE) sequence was used, which is basically a gradient echo sequence with multiple echo acquisitions resulting from reversed read out gradients. The multiple echoes were then superimposed onto the first image

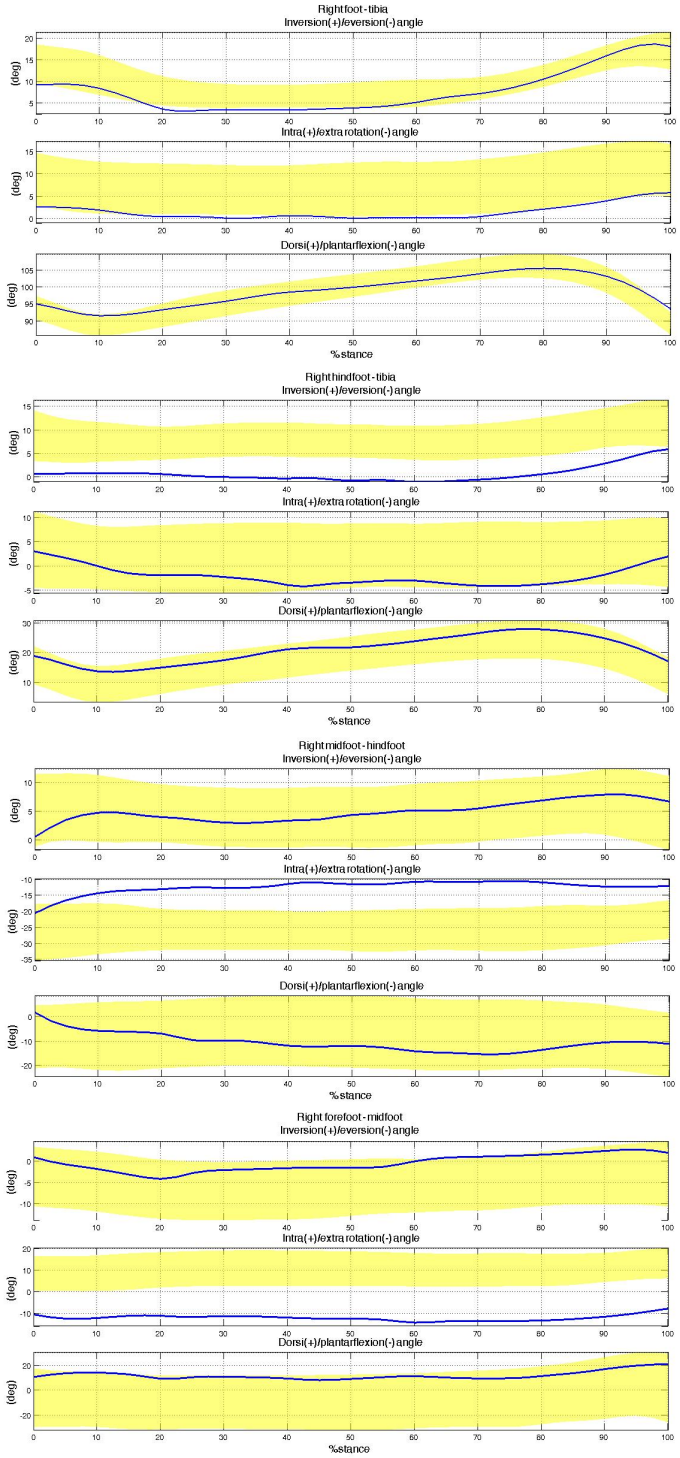

Figure 4.5: From the top: inversion-eversion, intra-extra rotation, dorsi-plantarflexion joint angles between whole foot and tibia, hindfoot and tibia, midfoot and hindfoot, forefoot and midfoot of neuropathic subject during one trial.

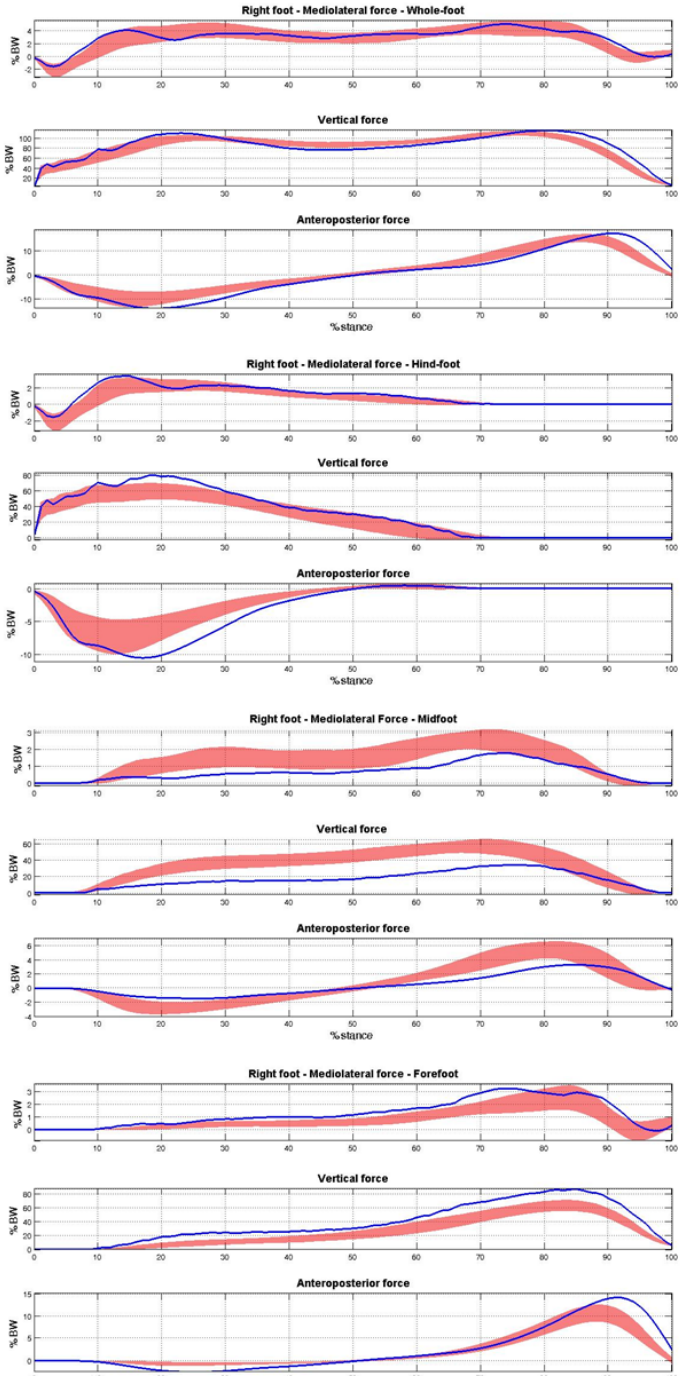

Figure 4.6: Neuropathic subject's ground reaction forces in the three directions: whole foot (upper left) and hindfoot (upper right), midfoot (bottom left) and forefoot (bottom right) components of the ground reaction vector evaluated according to [104].

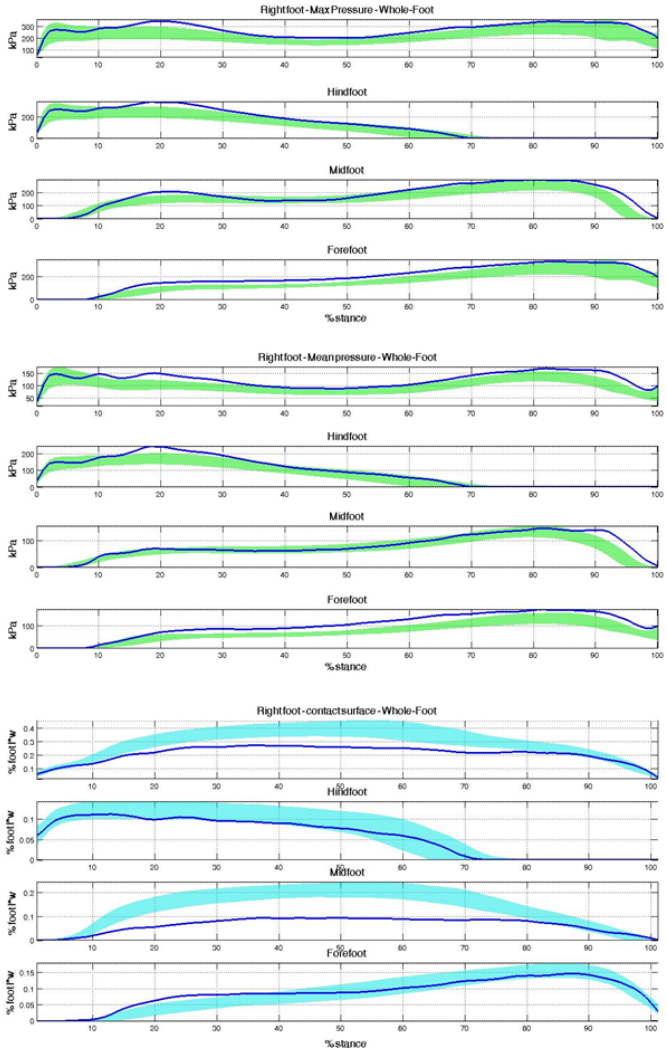

Figure 4.7: Neuropathic subject's peak plantar pressures (top), mean plantar pressures (middle) and contact surfaces (bottom): whole foot (first) and hindfoot (second), midfoot (third) and forefoot (forth) components evaluated according to [104]

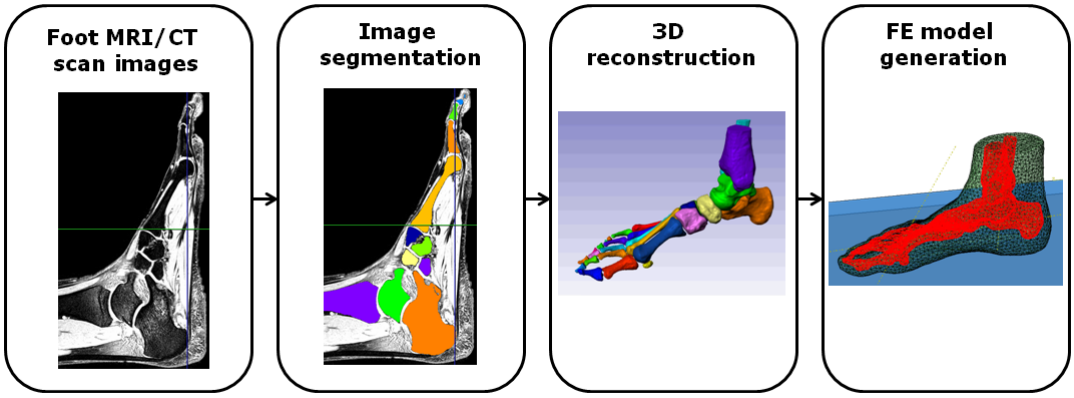

Figure 4.8: Workflow of the development of an FE model of the foot.

	Healthy subject	Neuropathic subject
MR device	Philips Achieva	Siemens Avanto
Sequence type: Multi-Echo Data Image Combination	mFFE	Medic
MR acquisition type:	3D	3D
TR	33.0451	32
TE	9.207	14
Flip angle:	30	30
Spacing between slides:	0.6 mm	0.75 mm
Slice thickness:	1.2 mm	1.5 mm

Table 4.1: Parameters adopted for the MRI acquisitions.

with the shortest echo time, which results in a predominantly T2 weighted final image (see paragraph 2.5.3 for details).

The right feet were acquired in a completely unload condition. Some padding was used around the ankle and the dorsum of the foot in order to lock the movements. The gray-scale-images was filtered with Gaussian filter and segmented with the software Simpleware - ScanIP (v.5.0) (described at paragraph 2.5.3) into 30 bones and the foot skin (as contour of the homogenous mass of foot soft-tissues) (figure 4.9).

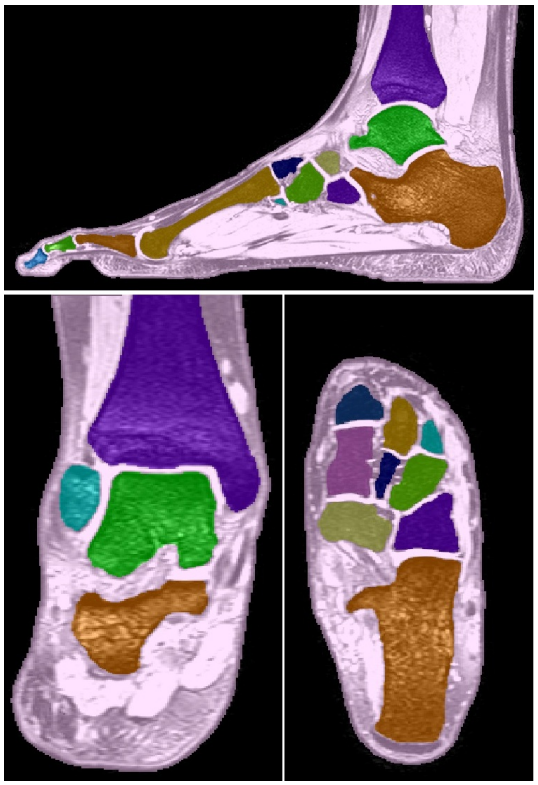

Figure 4.9: Image segmentation with Simpleware (v.5.0). All the bones, the cartilages and the soft tissues (skin, muscles, fat, ligaments) were segmented in a separate mask.

To decrease the model degrees of freedom, the phalanges of each toe were fused. This was performed by considering the work of Actis et al. were they demonstrated that the fusion of the interphalangeal joints has little effect on model results [7]. The sesamoid bones were also considered to be fused to the head of the first metatarsal. This assumption is realistic when toe flexion/extension angles, and hence sesamoid motions, are small [94]. Also the bones belonging to each foot subsegment were fused together, namely: the metatarsals and the

sesamoids into the forefoot, the navicular, the cuboid and the cuneiform into the midfoot and the astragalus and the calcaneus into the hindfoot. The phalanges were kept separate in order to allow their dorsiflexion during the push-off phase. This choice derived from the fact that even if the model includes all 30 bones, motion analysis cannot capture the intricate movement of individual foot bones. In fact, skin artefact error is likely to be larger than the movements of the smaller phalanges bones.

The space between the bones was segmented as cartilage. The bones and cartilage surfaces were Gaussian filtered with a factor of 0.5 as well as the skin mask in order to obtain more realistic surfaces.

The insertions of plantar fascia, Achilles tendon and 4 other ligaments (short plantar ligaments: tendon flexor digitorum, calcaneocuboid ligament, calcaneonavicular ligament, tibio-navicular ligament) were marked on the images as described by Gray [58]. These ligaments were chosen to obtain a correct foot arch support, according to the description of Bourdiol [20]. In particular the plantar fascia have been demonstrated to be always the greatest contributor to arch stability (figure 4.10) [66].

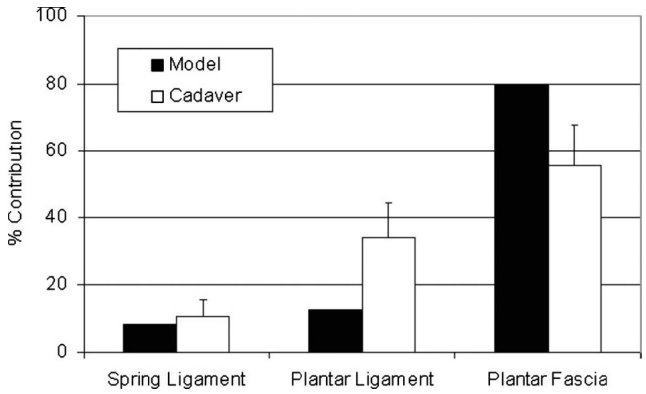

Figure 4.10: Comparison between computational model and experimental cadaver determination of relative contribution of each of the three plantar structures to arch stiffness [66].

For what regards the contact surfaces between the different masks, ScanIP software allows to choose the contact pairs and the node sets that can be exported after the mesh generation process.

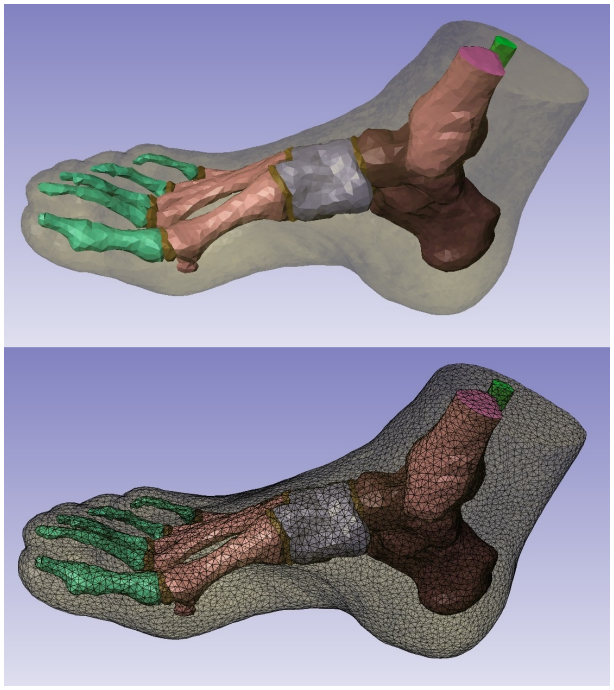

Figure 4.11: 3D reconstruction of the 3DNSM segmented images and mesh generated.

Mesh

As described at paragraph 2.5.3, the mesh was generated directly from the bitmapped data. For this purpose the ScanFE module of Simpleware software was called from the ScanIP work directory. Knowing the advantages and disadvantages of the several continuum FE topology and formulations used to discretize the foot model 3D structure (see paragraph 2.5.3), the foot geometrical complexity do not allows the use of hexahedral elements that usually provide higher accuracy with less computational cost [10].

The mesh algorithm adopted was the Simpleware-FE-Free which created tetrahedral elements. The minimum and maximum edge length was respectively 6 mm and 8 mm in order to obtain a mesh with size of element comparable with those of the plantar pressure mats and a number of elements (34800 for the 3DHSM and 84386 for the 3DNSM) similar to those developed in literature [29, 37]. The target maximum error for the mesh generation process was set to 0.4 mm, which is smaller than the MRI resolution, thus acceptable. The densification of the mesh in the critical areas was allowed. The generated mesh was then imported into the FE software Abaqus-CAE. In order to get the same global reference system position in the FE simulations as in the gait analysis data, the model was

rotated so that the X axis was the mediolateral axis of the foot, the Y axis was the vertical axis of the foot and the Z axis was the anteroposterior axis of the foot (figure 4.12).

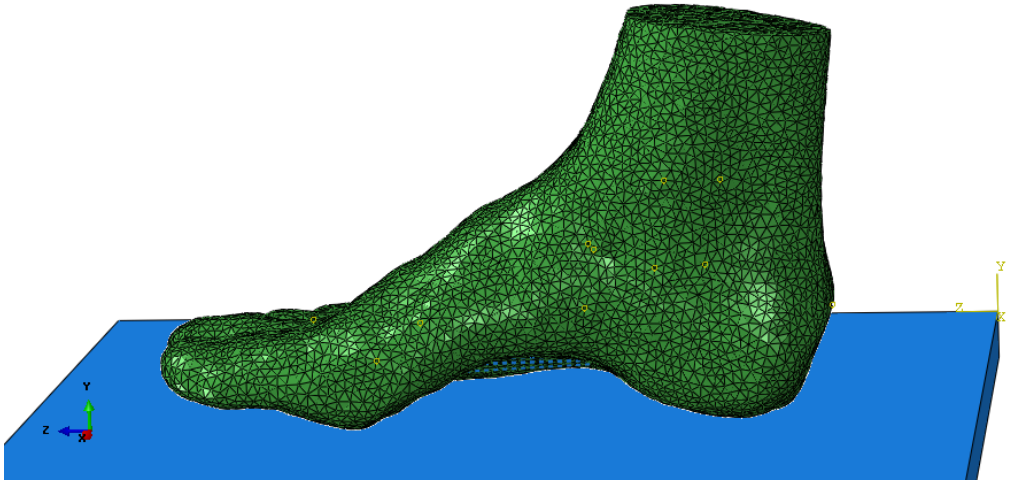

Figure 4.12: 3DNSM in the Abaqus-CAE visualization. In yellow the global reference system of the model coincident with that of the gait analysis acquisitions.

A 3D horizontal plate was drawn in Abaqus to simulate the ground support and the foot-floor contact during stance. In previous literature the authors indicated that the difference between the simulated and the experimental results may be caused by the difference in the resolution between the pressure sensors and the mesh. This because the FE analysis provides solutions of nodal contact pressure rather than an average pressure calculated from nodal force per element's surface area [37]. For this reason the plate in the model developed herein was meshed with hexahedral elements with 8 mm edges. The dimension agreed with the size of the sensors of the plantar pressure devices. This allowed a correct comparison between the simulated and the experimental stress data in the validation process. For the same reason a foot mesh densification was not considered as the output results were taken from the plate nodes.

Materials properties

Material properties of different tissues were obtained from the literature (table 4.2 and figure 4.13).

Bones, ligaments, and plantar fascia were assumed to behave in a linear isotropic behaviour.

As regards the bones, it was demonstrated that in the case of quasi-static loading (and probably in vivo loading) both cortical and trabecular bones behave similarly in a linear elastic fashion by approximation [67].

Component	E	ν
Plate [14]	68900 MPa	0.3
Bones [54]	7300 MPa	0.3
Cartilage [29]	1.01 MPa	0.4
Plantar fascia [29, 37]	350 MPa	-
Tendons - ligaments [29, 37]	250 MPa	-

Table 4.2: Parameters for the homogeneous, isotropic, linear elastic materials.

The plantar soft-tissue was represented as a continuum and its nonlinear material behaviour was modelled using an isotropic, incompressible, hyperelastic second-order polynomial formulation as described at paragraph 2.5.3 (equation 2.2) (figure 4.14). In figure 4.13 are reported the coefficients that have been used for the 3DHSM ("Normal" column). For the 3DNSM the increased stiffness values were adopted (F2, F3 and F5) for a preliminary parametrical study on the effect of tissue stiffening on the pressures maps. Then, for all the other simulations, the N2 value was adopted in the 3DNSM, as in [50].

Coefficients	Normal	$F2$	$F3$	$F5$
C_{10}	0.08556	0.17113	0.25669	0.42782
C_{01}	−0.05841	−0.11683	−0.17524	−0.29207
C_{20}	0.03900	0.07800	0.11700	0.19499
C_{11}	−0.02319	−0.04638	−0.06957	−0.11594
C_{02}	0.00851	0.01702	0.02553	0.04256
D_1	3.65273	1.82636	1.21758	0.73055
D_2	0.00000	0.00000	0.00000	0.00000

Units are $\mathrm{N\,mm^{-2}}$ for C_{ij} and $\mathrm{mm^2\,N^{-1}}$ for D_i. Values for these coefficients for the encapsulated soft tissue were calculated by ABAQUS based on uniaxial stress–strain data in Fig. 2. $F2$, $F3$ and $F5$ correspond to simulations of two, three and five times the stiffness of normal tissue.

Figure 4.13: Coefficients of the hyperelastic material model used for the soft tissues [37].

Boundary conditions, contacts and loads

Meshes for the bones and the soft-tissue components shared the same nodes however surface-to-surface "tie" pairs were created to avoid the elements to sep-

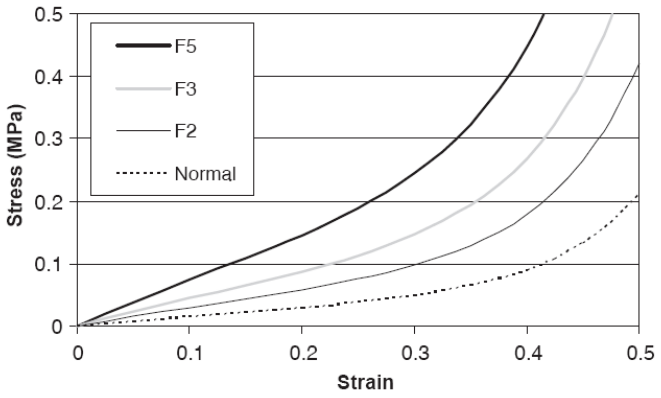

Figure 4.14: Nonlinear stress-strain response of soft tissue adopted for the FE model [37].

arate while moving. A tie pair was created also between bones and cartilage so that they can transmit compression forces. During simulations, the superior surfaces of the tibia, fibula and soft-tissue were fully fixed to simulate the effects of constraints from superior-lying tissues. Contact surface-to-surface was defined between the deformable plantar soft tissues and the rigid plate, with a coefficient of friction of 0.6, which is the value reported in the literature for in vivo skin ground frictional properties [29]. This contact description restricted contact surfaces to penetrate each other by allowing deformation and also sliding [22].

The passive soft-tissue stabilizers of the foot skeleton, the ligaments previously cited and the plantar fascia, were inserted into the model as axial connector elements (2-node cables) with a "no compression" option, in accordance to their physiological function (figure 4.15). This would allow these elements to resist tension-producing forces when stabilizing the foot skeleton. Five 2-node cable elements connecting the plantar side of each of the five metatarsal heads and the calcaneus were created to represent the plantar aponeurosis. Four 2-node cable elements connecting the plantar side of the cuboid and the calcaneus were created to simulate the short plantar ligaments [31].

In previous literature the ground support was properly aligned such that an initial foot- ground contact was established with minimal induced stress before the application of the loading conditions [37]. In other cases adjustments to the orientation of the whole model was conducted by an optimization protocol that minimized the difference between the model predicted and experimentally measured pressures [22]. For the present thesis, the foot was positioned relatively

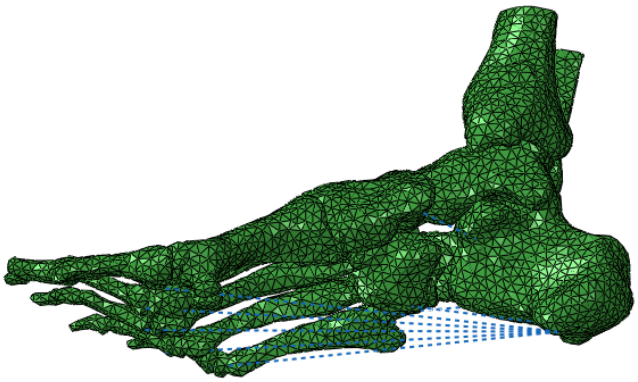

Figure 4.15: Passive soft-tissue stabilizers of the foot skeleton (blue - axial connector elements).

to the plate according to the position acquired with the stereophotogrammetric system following this procedure:

- the same anatomical landmark adopted for the gait analysis protocol were identified on the skin surface of the FE model.
- the reference system of the foot was created in Abaqus with the same rules adopted in the gait analysis protocol [102] and the 3D angles relatively to the global reference system were calculated.
- the FE foot was rotated and aligned to the midstance position calculated with the stereophotogrammetric data.

FE analysis was performed in Abaqus (Simulia, v.6.12).

The complete FE model which includes the metal plate representing the ground is shown in figure 4.12.

Simulations

Abaqus CAE/pre-processor was used to set up the FE model for the simulations. The latter was adapted by altering its loading characteristics and its geometric positioning [54] for each of the investigated subphases (see paragraph 4.2.2) (State A) or for each subject (State B).

In the first step of each simulation the FE foot model was rotated and the subject- and instant- specific position registered during experimental gait was matched. In the second step of each simulation the plate was moved to get in

contact with the foot [32]. Then, in the third step, the vertical ground reaction force was applied to the FE plate according to the loads registered during gait analysis. The point of application was constrained to allow movement in the vector direction only. In the midstance simulations the gastrocnemius-soleus muscle force acting through the Achilles tendon was applied by a force vectors acting on the insertion point detected from the MRI. In accordance with previous literature, the muscle load in static or midstance was set as 50% of the force acting on the foot during standing [37]. For the other instants of simulation, a fixed position of the ankle joint was kept.

All the steps of the simulations were performed with non-linear geometrical analysis.

Data output and validation method

The FE model simulation was then ran by adopting the synchronized kinetics and kinematics as input data and it was successfully solved using Abaqus (Simulia, v.6.12) on a quad-core computer with parallelization on multiple processors and taking about 1 hour to solve for each position. The Abaqus CAE/post-processor was used to report results from FE calculations. The model outcome measures of interest were the contact stresses at foot-supporting interface and the von Mises stresses in bony structures and soft tissues. Plantar fascia total force was also exported. The contact pressures measured at the nodes of the plate was used for the experimental validation of the model.

4.3 Results

Two geometrical accurate 3D FE model of the healthy and neuropathic subject's foot and ankle complex were developed. The models were able to predict both the plantar pressure distribution and the internal stresses/strains within bones and soft tissues of the ankle and foot under various loading and supporting conditions.

The adopted kinematic protocol provided the tools to assess the validity of the developed models with an anatomically based approach because it allowed the definition of foot subsegments (described at paragraph 2.3.4). The areas of comparison between the simulated and the experimental data were taken according to the real foot subsegments. This methodology should be considered more accurate than what currently done in the literature by comparing the whole foot

peak pressure values [10, 32, 37, 86, 96].

4.3.1 State A: validation with the experimental subject specific plantar pressures

In order to evaluate the foot and ankle 3DHSM and 3DNSM validity, in figures 4.16 the similarity between the stress distribution pattern of the simulation and the experimental data can be observed.

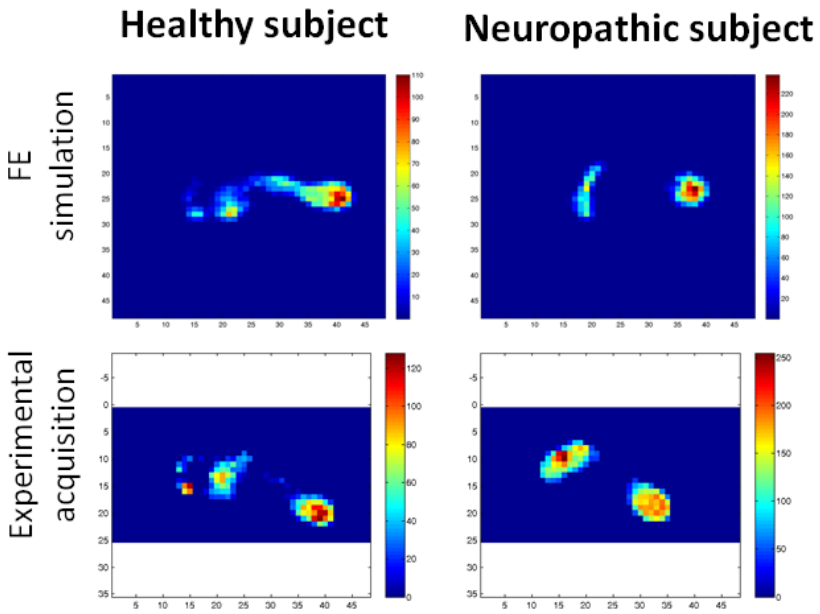

Figure 4.16: Plantar pressure maps of the static trials: simulated and experimental.

Initially, the data relative to the static acquisitions were investigated. The 3DHSM and the 3DNSM loaded with their subject-specific static standing vertical forces underestimated the experimental peak plantar pressure respectively of 13.9% and 6.3%. These values were calculated as difference between the simulated and the experimental peak pressures in percentage of the experimental ones.

The comparison between the experimental and simulated data within the different sub-phases of the stance phase of gait showed that there was a good agreement in the overall patterns of predicted and measured plantar pressure distributions during heel strike, loading response, midstance and push off phases

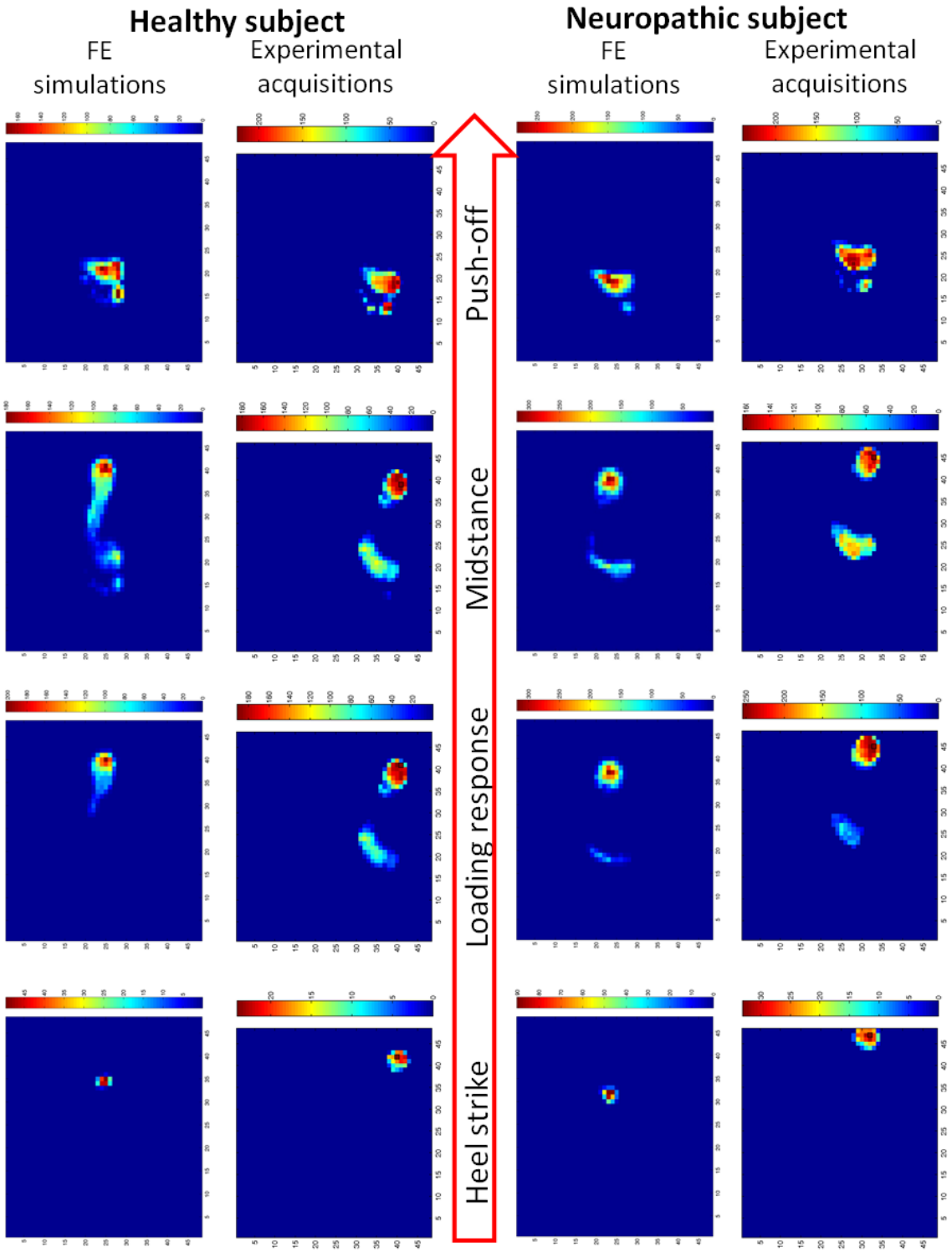

Figure 4.17: Plantar pressure maps of the stance subphases: simulations of the 3DHSM and the 3DNSM with the specific kinematic and kinetic experimental data.

although both models overestimated contact pressures and contact area under the lateral mid foot.

Healthy subject model

The FE 3DHSM predicted maximum contact plantar pressure values at the whole foot were 110.15 KPA, 49.71 KPa, 201.65 KPa, 180.18 KPa and 170.35 KPa for the static standing, heel strike, loading response, midstance and push off respectively. The obtained experimental results were compared with the FE results for each case. Experimental peak pressures of 128 KPa, 24 KPa, 192 KPa, 185 KPa and 225 KPa were measured for the foot plantar area in static and in each instant of the stance phase cited above, respectively.

From the heel strike to the midstance, the peak pressure values occurred at the heel as the position of the foot or the loads act through the hindfoot. During the push off, the forefoot pushed toward the ground to provide the progression of the leg, thus the peak pressure occurred in this area both in the experimental acquisitions and the FE simulations.

The values of the maximum and mean plantar pressures on each foot subarea were reported in figure 4.18 and table 4.3.

		Mean pressure [KPa]			
		Whole foot	**Hindfoot**	**Midfoot**	**Forefoot**
HS	exp	13.77	13.77	0	0
HS	sim	12.39	12.39	0	0
LR	exp	39.68	51.26	9.9	0
LR	sim	66.65	93.42	22.24	48.17
MS	exp	32.97	58.5	24.17	18.55
MS	sim	74.13	102	23.63	59.98
PO	exp	47.47	0	14.64	50.66
PO	sim	93.88	0	0	93.88

Table 4.3: State A - 3DHSM: mean plantar pressures on the whole foot and the three foot subareas. HS= heel strike, LR=loading response, MS=midstance, PO=push-off, exp=experimental, sim=simulated.

The FE predicted contact areas were 12.8 cm^2, 64 cm^2, 155.5 cm^2 and 79.3 cm^2 for the four instants in the same order as reported above, compared to 16 cm^2, 77.4 cm^2, 78.1 cm^2 and 53.8 cm^2 obtained from the experimental measurements. In the midstance and push-off the contact surface was overestimated by the FE model.

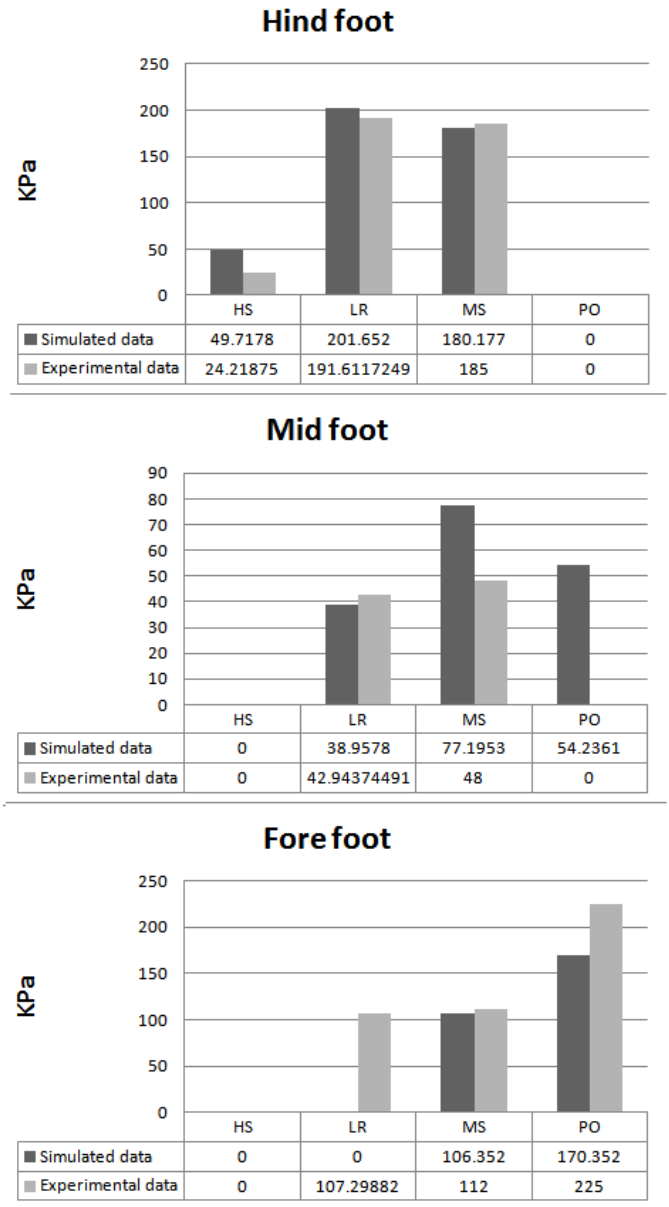

Figure 4.18: State A - 3DHSM: peak plantar pressures on the three foot subareas. HS= heel strike, LR=loading response, MS=midstance, PO=push-off.

Neuropathic subject model

The FE 3DNSM on the whole foot predicted maximum contact plantar pressure values were 238.77 KPa, 90.27 KPa, 319.34 KPa, 202.77 KPa and 330.65 KPa for the static standing, heel strike, loading response, midstance and push off respectively.

The experimental peak pressures for the foot plantar area were 255 KPa, 33 KPa, 255 KPa, 163 KPa and 241 KPa, measured in the static standing, heel strike, loading response, midstance and push off respectively. The FE 3DNSM always largely overestimated the peak pressure values.

The values of the maximum and mean plantar pressures on each subarea are reported in figure 4.19 and table 4.4.

		Mean pressure [KPa]			
		Whole foot	**Hindfoot**	**Midfoot**	**Forefoot**
HS	exp	24.71	24.71	0.00	0.00
HS	sim	18.99	18.99	0.00	0.00
LR	exp	58.56	84.15	12.63	25.89
LR	sim	99.90	159.04	1.48	42.81
MS	exp	43.80	54.47	26.45	35.42
MS	sim	78.55	92.33	53.42	79.12
PO	exp	83.47	0.00	58.07	99.23
PO	sim	123.75	0.00	120.11	125.84

Table 4.4: State A - 3DNSM: mean plantar pressures on the whole foot and the three foot subareas. HS= heel strike, LR=loading response, MS=midstance, PO=push-off, exp=experimental, sim=simulated.

The FE predicted contact areas were 15.4 cm^2, 71.7 cm^2, 69.1 cm^2 and 51.8 cm^2 for the heel strike, loading response, midstance and push-off respectively, compared to 19.2 cm^2, 62.1 cm^2, 69.1 cm^2 and 49.3 cm^2 obtained from the experimental measurements. With the exception of the midstance, for the 3DNSM the error in the contact surface prediction was below the 20% of the experimental value.

4.3.2 State A: Internal stresses

The FE analysis has the benefit of quantifying the overall deformation, stress and strain distributions of a structure to be analyzed.

Peak stress level calculated from the internal plantar soft-tissues and from

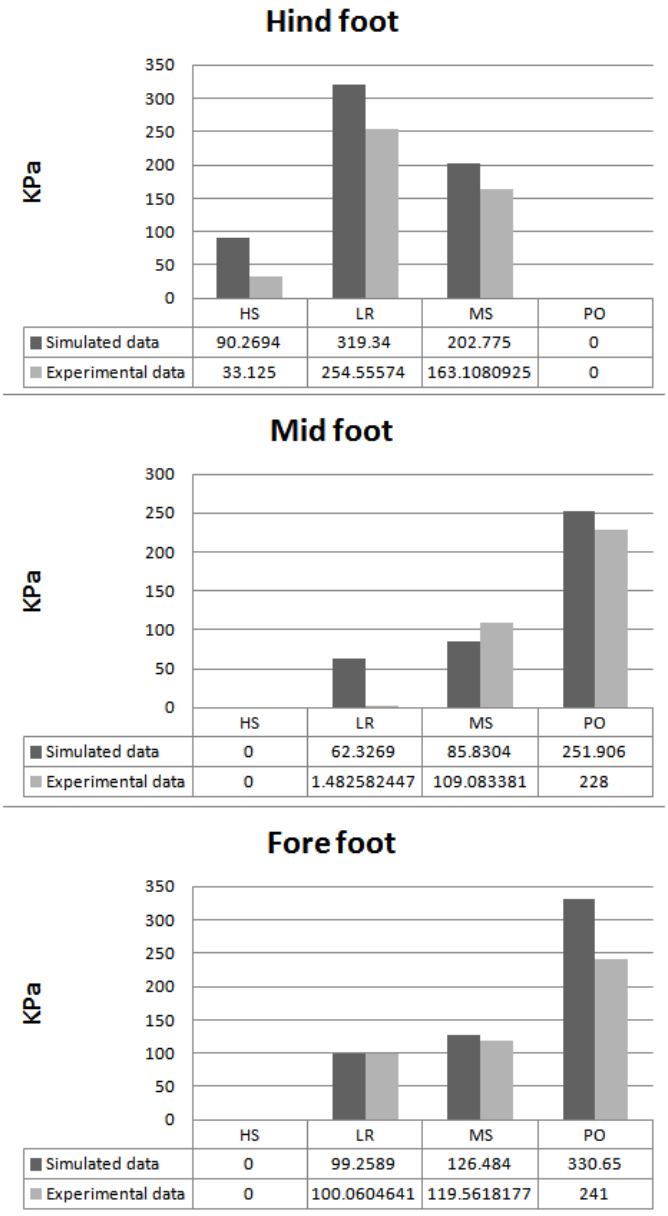

Figure 4.19: State A - 3DNSM: peak plantar pressures on the three foot subareas. HS= heel strike, LR=loading response, MS=midstance, PO=push-off.

the bones was expressed in terms of von Mises stress, which was previously used as a parameter related to the strength of biological tissues of bone and plantar soft-tissue [29].

The stress distributions of the plantar pad at the midstance are shown in figure 4.20 for 3DNSM. The peak values relative to each simulated instant and for both the 3DHSM and the 3DNSM were reported in figure 4.21.

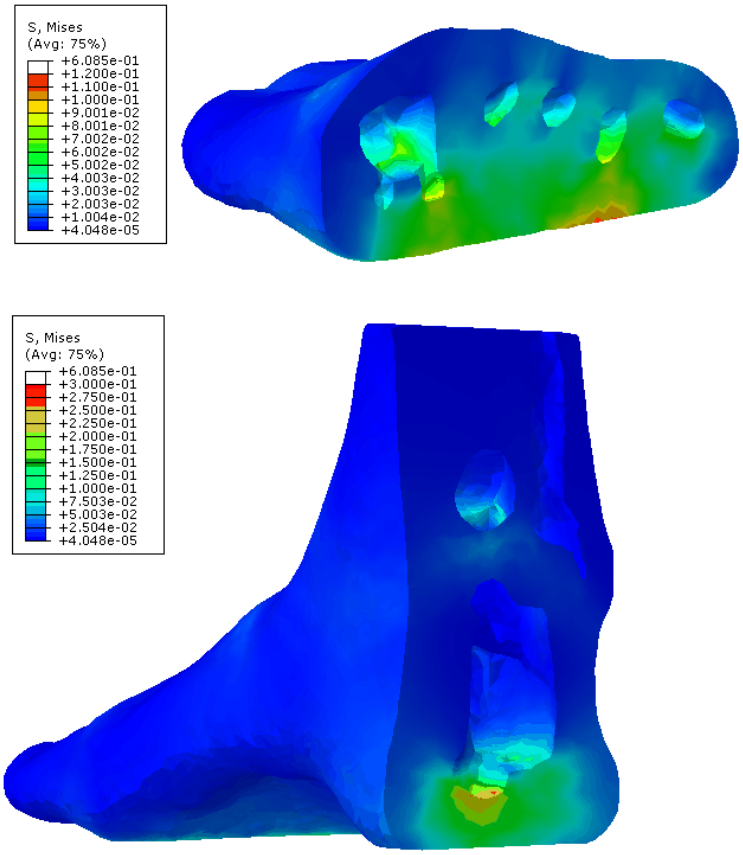

Figure 4.20: Von Mises stresses in the soft tissues during simulated midstance: metatarsal heads section (top) and heel section (bottom).

In correspondence of the bone structure, peak of stress were present at the metatarsal and talus bones. The insertion points of the fascia (insertions of the five connector elements) at the phalanges connection region and plantar aspect of the calcaneus, experienced large stress due to the generated fascia plantar tension (figure 4.22).

Plantar fascia tensions were reported at paragraph 4.3.5.

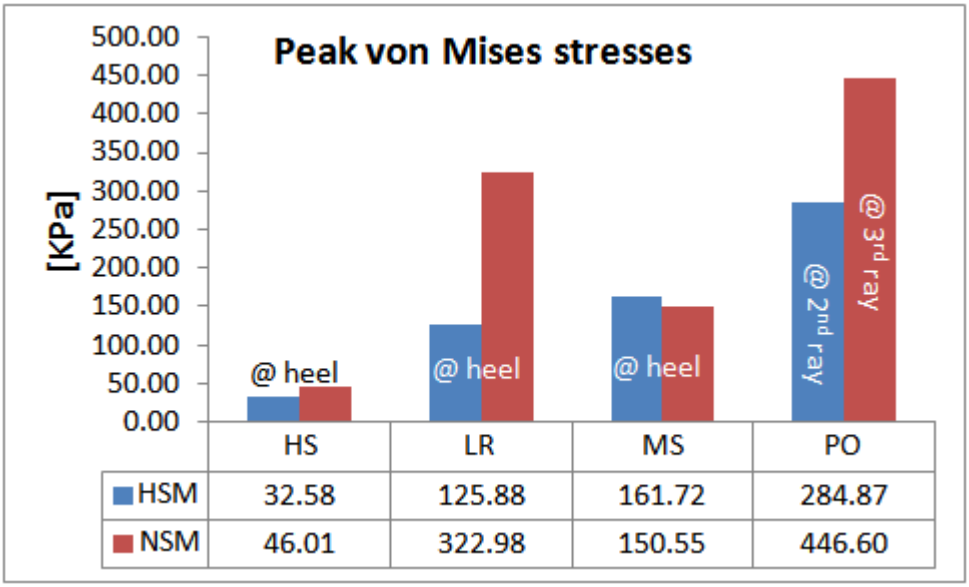

	HS	LR	MS	PO
HSM	32.58	125.88	161.72	284.87
NSM	46.01	322.98	150.55	446.60

Figure 4.21: Peak von Mises stresses occurring in the four instants of simulation of the 3DHSM and the 3DNSM. HS=heel strike, LR=loading response, MS= midstance, PO=push-off. The locations where the peak occurred were the heel bone-soft tissue interface (@heel) and the connection between the metatarsal heads and the phalanx (@1st -5th ray).

4.3.3 State A: Effect of stiffness

For the 3DNSM the effect of different soft tissue stiffness was tested. The formulations adopted for the soft tissue materials were reported at paragraph 2.5.3. Four conditions were tested according to [37]: normal (N) and stiffened by factor 2 (N2), 3 (N3) and 5 (N5).

The tests were performed under the identical loading condition and foot position relatively to the ground. The midstance configuration was chosen because allowed the evaluation of both the heel pad and metatarsals pad behaviour under compression.

Figure 4.23 shows the effects of soft tissue stiffness on the peak plantar pressure. It can be noticed that increasing the stiffness, the areas where pressures increase were under the heel and the metatarsal heads, concentrating under the bony prominences. Simultaneously the pressures decreased around them, signifying a decrease in the contact surface area (figure 4.24), thus a lower possibility of spreading the loads.

Maximum pressures of 443.3KPa and 277.8KPa were predicted at the hindfoot and at forefoot, respectively, with soft tissue stiffness of 5 times the normal values.

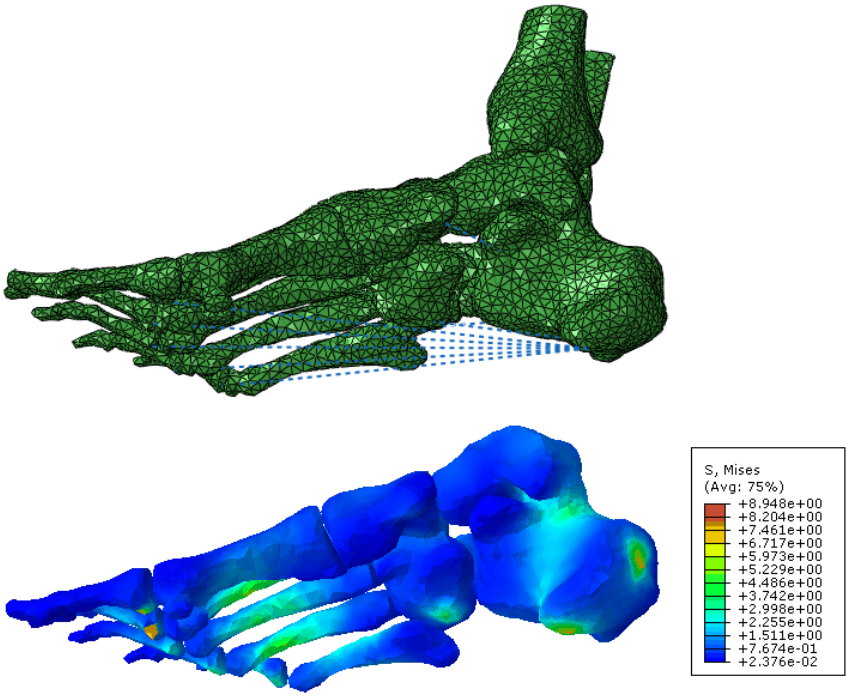

Figure 4.22: Von Mises stresses at the bones during simulated midstance: unloaded foot with fascia connectors visible (top) and loaded foot coloured according to von Mises values (bottom).

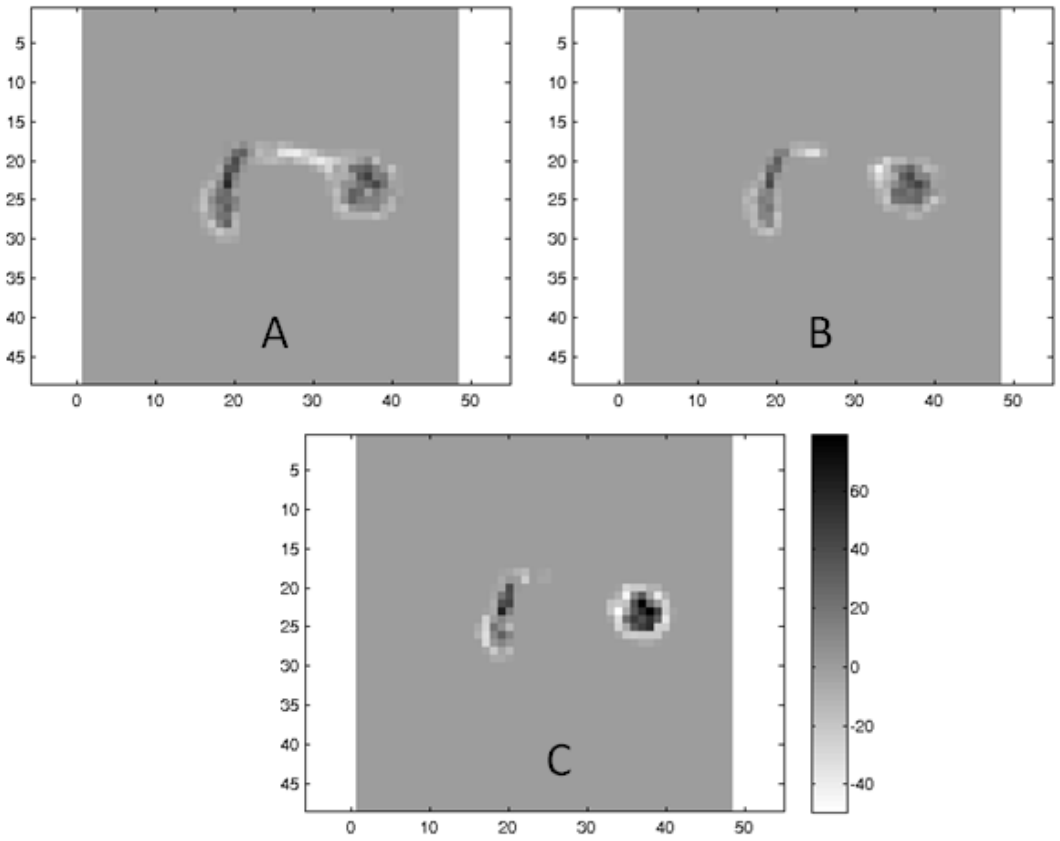

Figure 4.23: Effect of the increasing in soft tissue stiffness. Black colour indicates an increased plantar pressure value when increased stiffness parameters were used. White colour indicates a decreased pressure value. A) pressure values obtained with stiffness N2 vs pressure values obtained with stiffness N. B) N3 vs N2. C) N5 vs N3.

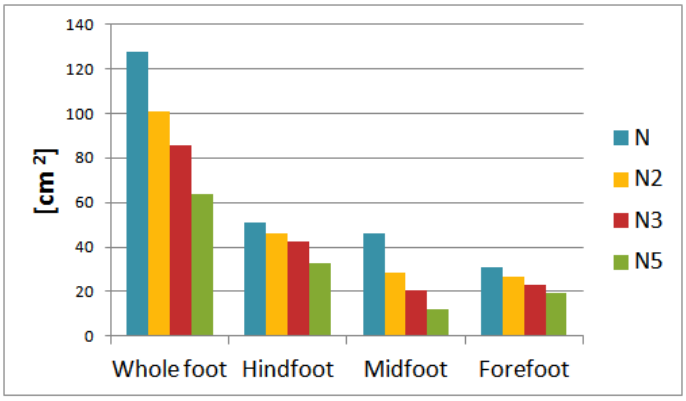

Figure 4.24: Contact surfaces in the foot subareas with increasing soft tissue stiffness.

These were the 56% and the 139% of the pressure values obtained at the same areas simulating the midstance with normal soft tissue properties.

Looking at the internal stresses at the plantar soft tissues, in particular at the von Mises parameter, the maximum values were always reached at the plantar bony prominence of the calcaneus. The relation between the peak values and the stiffness appeared to be inversely proportional, while the mean stress increased (figure 4.25).

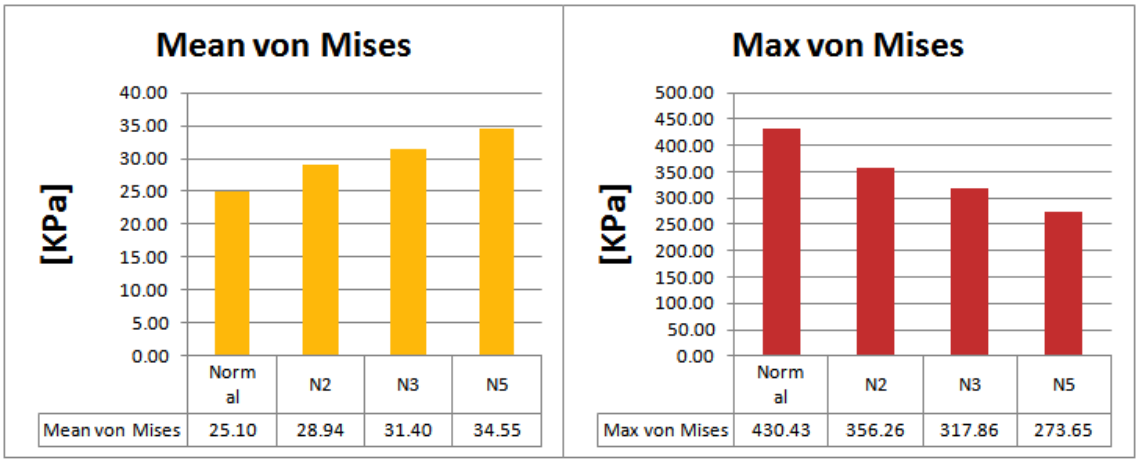

Figure 4.25: Mean and maximum von Mises internal stresses values at the plantar soft tissues for the 4 degrees of stiffness.

4.3.4 State A: Effect of the Achilles tendon

The effect of the force applied at the posterior calcaneus to simulate the Achilles tendon (AT) was tested in the midstance phase. Relatively to the condition when the load through the plate alone was applied to the foot, the contact pressure under the metatarsal heads and the phalanges increased with the load application at the calcaneus, reducing consequently the load-bearing at the hindfoot.

The predicted peak pressures at the hindfoot were 226.2 KPa without AT and 202.8KPa with AT force while an increase of 16.5% and 20% occurred at the midfoot and forefoot respectively if the AT force was applied. The same situation was registered in correspondence of the contact surfaces, if we considered that they decreased at the hindfoot (9.7%) and increased at the forefoot (17.2%) with the load of the AT.

In figure 4.26 are reported the contact pressure maps of the two conditions and in figure 4.27 can be found the difference between the two.

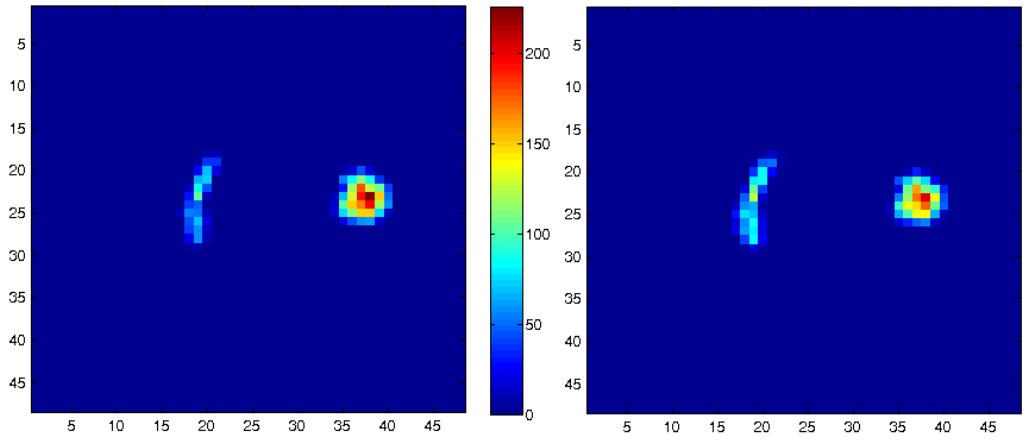

Figure 4.26: Pressure maps of the simulations without (left) and with (right) Achilles tendon force applied to the posterior calcaneus.

4.3.5 State A: Plantar fascia tensile force

The forces exerted by the plantar fascia (the five connectors) in the 3DHSM and 3DNSM during the static and the midstance simulations were investigated in order to verify the assumptions behind the model development process and to compare the obtained values with those presented in literature.

For both the 3DHSM and the 3DNSM the predicted tensile forces on the plantar fascia in static and midstance loading conditions showed decreasing values from the medial to the lateral region. In 3DHSM, the values ranged from 72.7 N in the 1^{st} ray to 8.6 N in the 5^{th} ray, while under the midstance loading condition, the values of the force ranged between 121.2 and 14.2 N (figure 4.28). The 3DNSM values were reported in figure 4.29.

The total tensile forces in the plantar fascia of the 3DHSM and the 3DNSM was 268.8 N and 119.8 N, respectively, in the midstance and 162.5 N and 78.9 N in the static.

4.3.6 State B: Healthy subjects results

The results of the FE simulations ran with the data of the 10 healthy subjects as input with respect to the midstance phase of gait were reported in the following

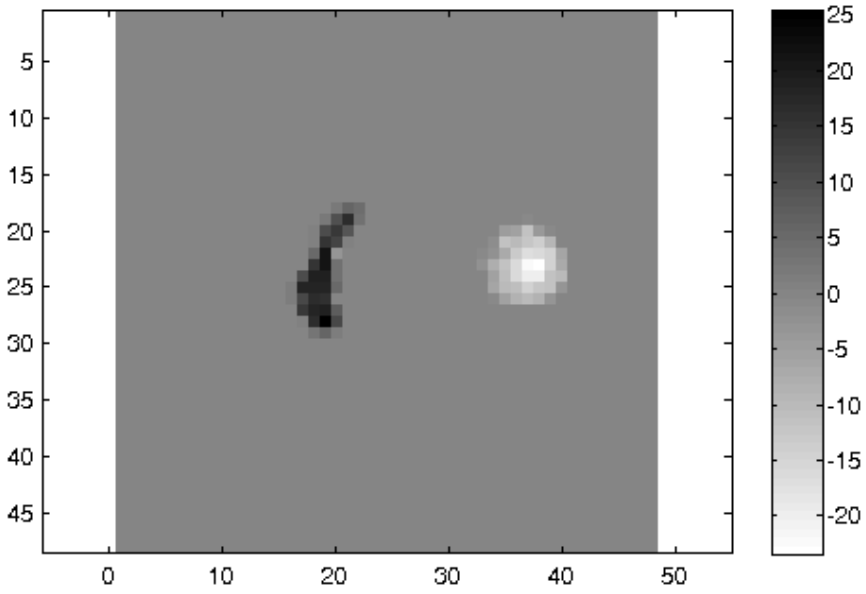

Figure 4.27: Difference between the pressure maps predicted without AT and with AT. Black indicates an increase in the pressure values if AT force was applied while white indicates a decrease.

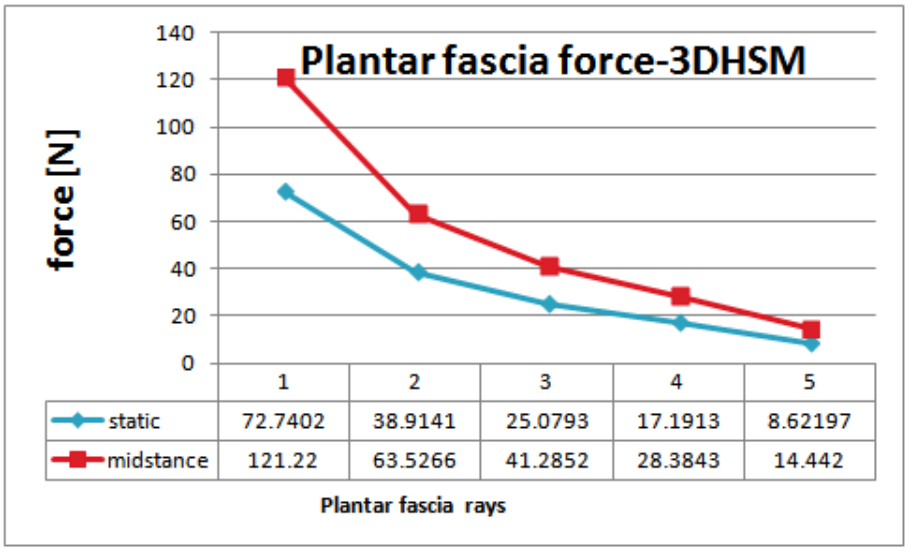

Figure 4.28: Plantar fascia forces in the 3DHSM generated during static and midstance simulations. Numbers from 1 to 5 correspond to the plantar fascia rays.

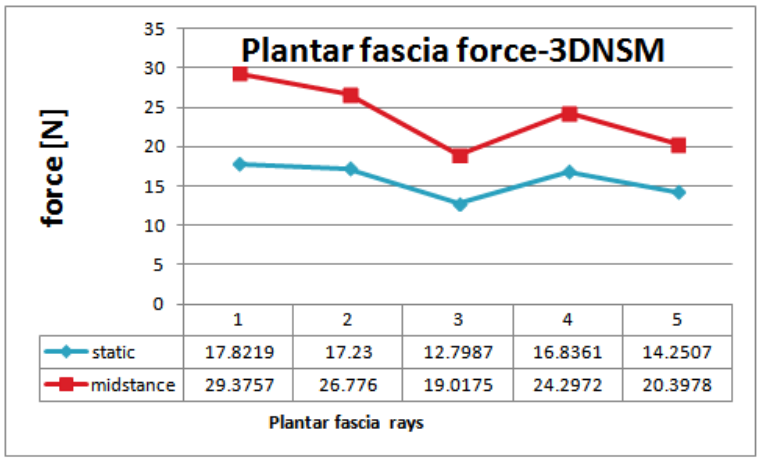

Figure 4.29: Plantar fascia forces in the 3DNSM generated during static and midstance simulations. Numbers from 1 to 5 correspond to the plantar fascia rays.

figures (4.30 and 4.31). The experimental values were also shown in figures 4.32 and 4.33. The peak and mean pressures and the contact surfaces were expressed respectively in percentage of the body weight and of the foot length.

In the following figures (4.34 and 4.35) the differences between the simulated and the experimental values were expressed in term of percentage of the simulated value. The positive values indicated an overestimation of the simulation with respect to the experimental values, while the negative values indicate an underestimation.

4.3.7 State B: Diabetic neuropathic subjects results

The results of the FE simulations ran with the data of the 10 neuropathic subjects as input with respect to the midstance phase of gait were reported in the following figures (4.36 and 4.37). The experimental values were also shown in figures 4.38 and 4.39. The peak and mean pressures and the contact surfaces were expressed respectively in percentage of the body weight and of the foot length.

In the following figures (4.40 and 4.41) the differences between the simulated and the experimental values were expressed in term of percentage of the simulated value. The positive values indicated an overestimation of the simulation with respect to the experimental values, while the negative values indicated an underestimation.

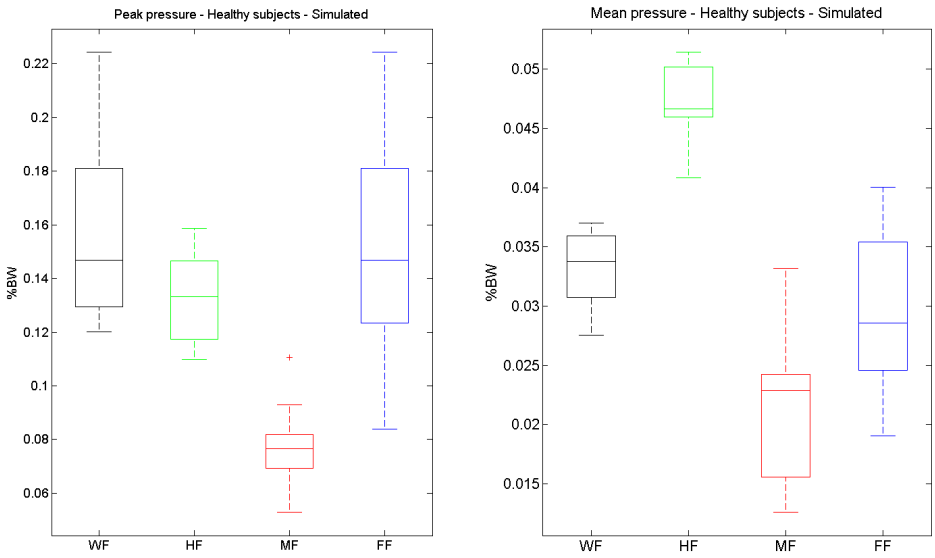

Figure 4.30: Healthy subjects' simulated peak and mean plantar pressures in the whole foot (WF-black) and in each foot subarea: hindfoot (HF-green), midfoot (MF-red) and forefoot (FF-blue). The values are expressed in percentage of the body weight (%BW).

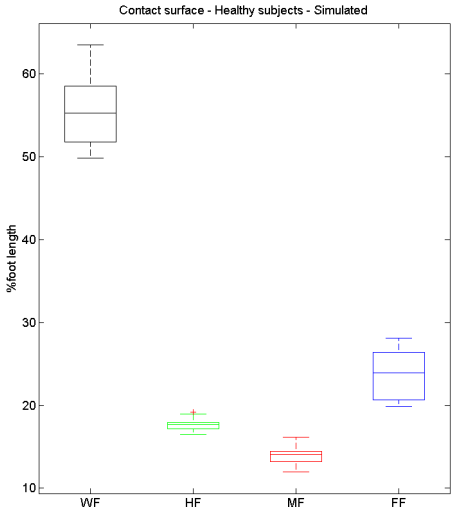

Figure 4.31: Healthy subjects' simulated contact surface in the whole foot (WF-black) and in each foot subarea: hindfoot (HF-green), midfoot (MF-red) and forefoot (FF-blue). The values are expressed in percentage of the foot length.

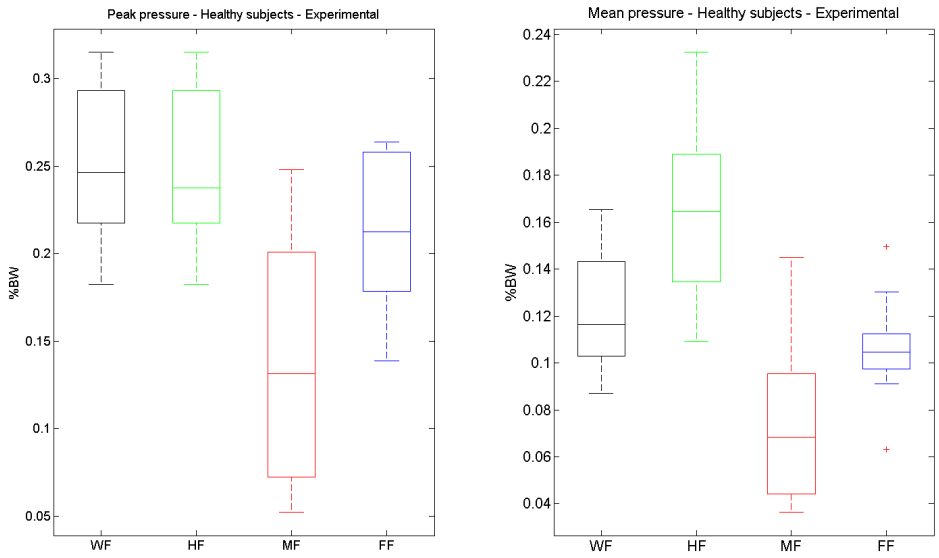

Figure 4.32: Healthy subjects' experimental peak and mean plantar pressures in the whole foot (WF-black) and in each foot subarea: hindfoot (HF-green), midfoot (MF-red) and forefoot (FF-blue). The values are expressed in percentage of the body weight (%BW).

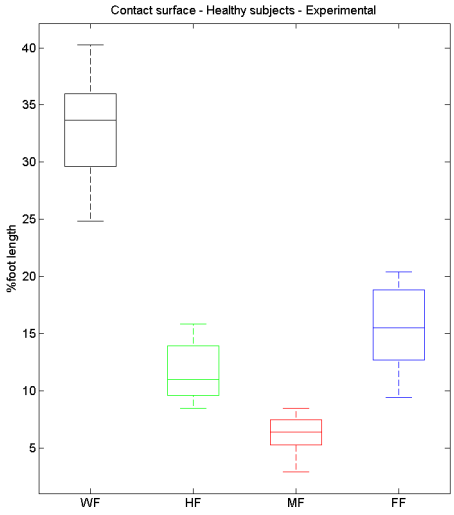

Figure 4.33: Healthy subjects' experimental contact surface in the whole foot (WF-black) and in each foot subarea: hindfoot (HF-green), midfoot (MF-red) and forefoot (FF-blue). The values are expressed in percentage of the foot length.

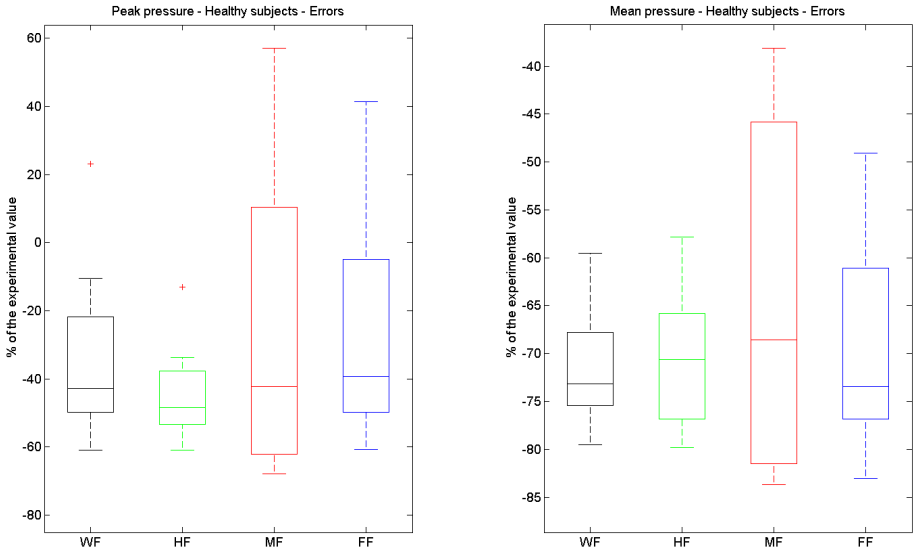

Figure 4.34: Healthy subjects' errors (difference between the simulated and the experimental values) for peak and mean pressures in the whole foot (WF-black) and in each foot subarea: hindfoot (HF-green), midfoot (MF-red) and forefoot (FF-blue). The values are expressed in percentage of the experimental value.

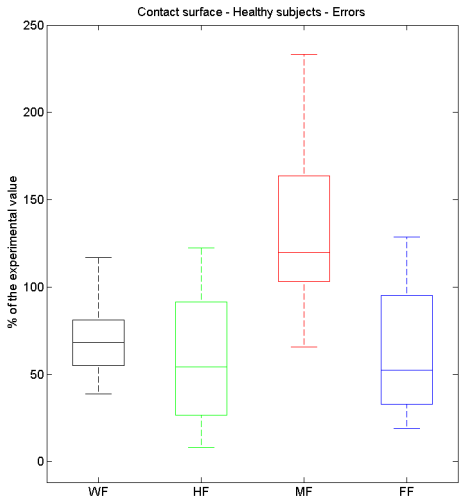

Figure 4.35: Healthy subjects' errors (difference between the simulated and the experimental values) for contact surfaces in the whole foot (WF-black) and in each foot subarea: hindfoot (HF-green), midfoot (MF-red) and forefoot (FF-blue). The values are expressed in percentage of the experimental value.

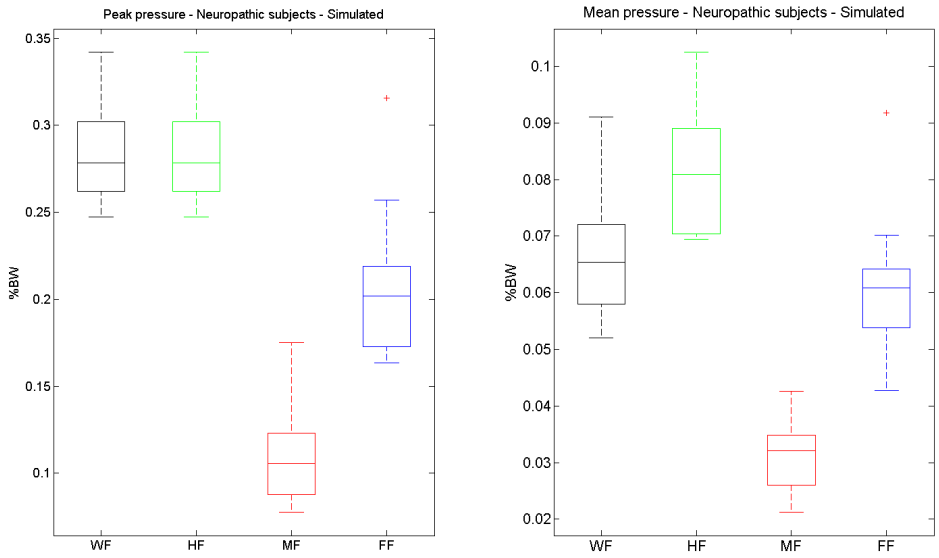

Figure 4.36: Neuropathic subjects' simulated peak and mean plantar pressures in the whole foot (WF-black) and in each foot subarea: hindfoot (HF-green), midfoot (MF-red) and forefoot (FF-blue). The values are expressed in percentage of the body weight (%BW).

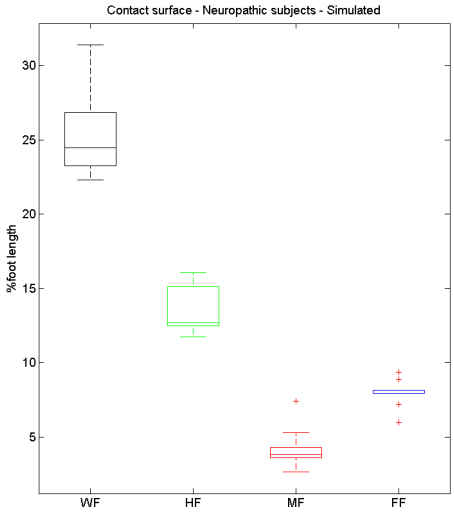

Figure 4.37: Neuropathic subjects' simulated contact surface in the whole foot (WF-black) and in each foot subarea: hindfoot (HF-green), midfoot (MF-red) and forefoot (FF-blue). The values are expressed in percentage of the foot length.

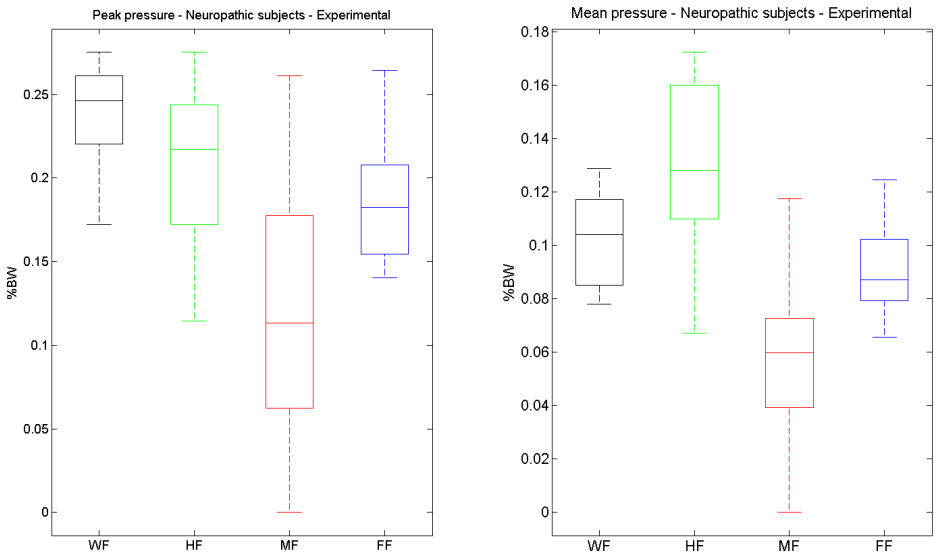

Figure 4.38: Neuropathic subjects' experimental peak and mean plantar pressures in the whole foot (WF-black) and in each foot subarea: hindfoot (HF-green), midfoot (MF-red) and forefoot (FF-blue). The values are expressed in percentage of the body weight (%BW).

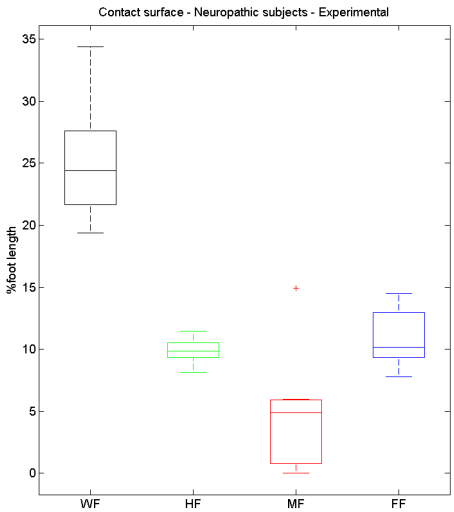

Figure 4.39: Neuropathic subjects' experimental contact surface in the whole foot (WF-black) and in each foot subarea: hindfoot (HF-green), midfoot (MF-red) and forefoot (FF-blue). The values are expressed in percentage of the foot length.

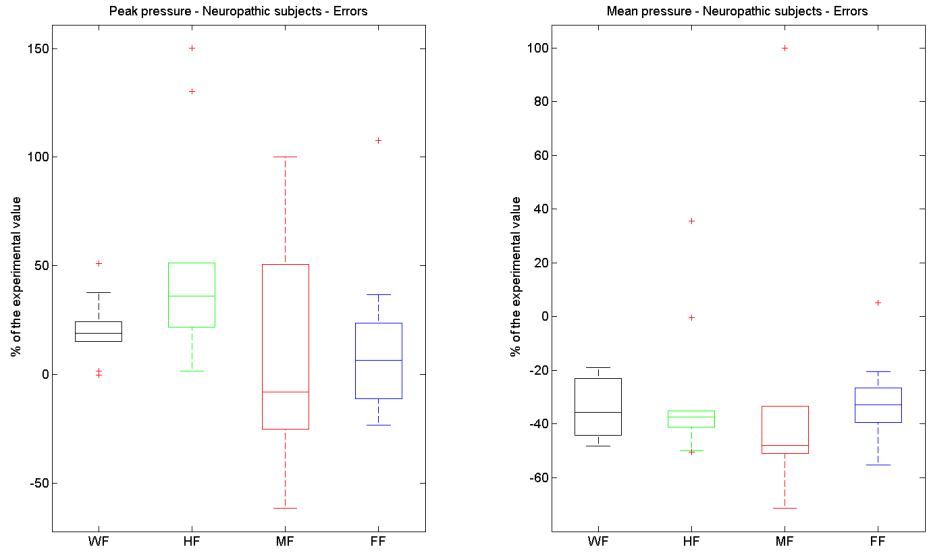

Figure 4.40: Neuropathic subjects' errors (difference between the simulated and the experimental values) for peak and mean pressures in the whole foot (WF-black) and in each foot subarea: hindfoot (HF-green), midfoot (MF-red) and forefoot (FF-blue). The values are expressed in percentage of the experimental value.

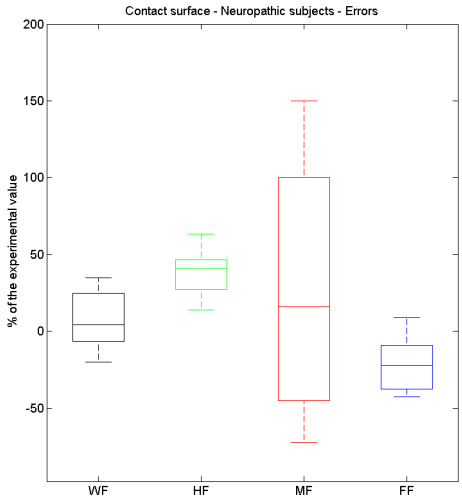

Figure 4.41: Neuropathic subjects' errors (difference between the simulated and the experimental values) for contact surfaces in the whole foot (WF-black) and in each foot subarea: hindfoot (HF-green), midfoot (MF-red) and forefoot (FF-blue). The values are expressed in percentage of the experimental value.

4.3.8 State B: Comparison between healthy and neuropathic subjects' results

The comparison between the simulated results of the healthy subjects and the ones of the neuropathic subjects was performed in order to assess the ability of the model of highlighting the differences between the two groups of subjects (figures 4.42 and 4.43).

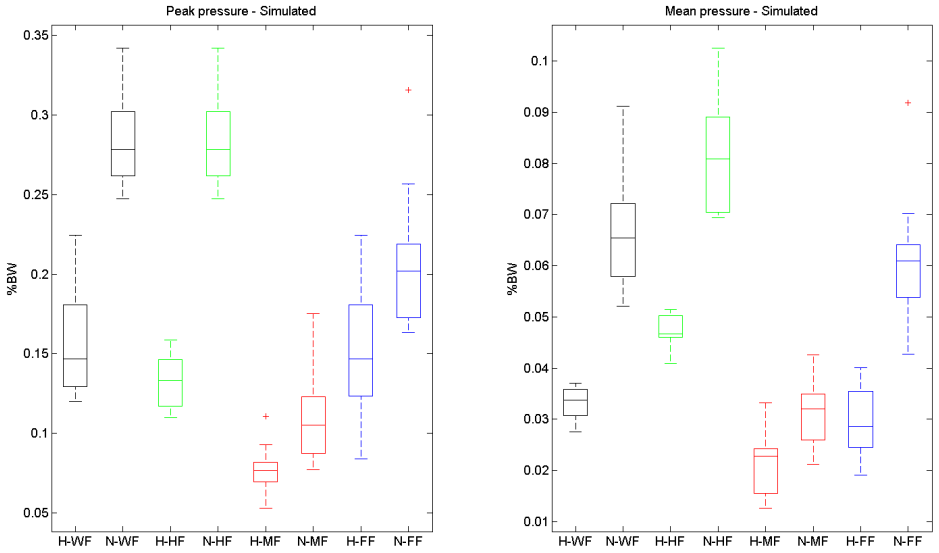

Figure 4.42: Simulated data of the healthy subjects (H) and the neuropathic subjects (N) for the peak and the mean pressures in the whole foot (WF-black) and in each foot subarea: hindfoot (HF-green), midfoot (MF-red) and forefoot (FF-blue). The values are expressed in percentage of the body weight of each subject (%BW).

These simulated results highlighted increased pressures in the neuropathic subjects both in the peak and the mean values, while very low contact surfaces were found for these subjects.

4.4 Discussion

In this chapter, two 3D anatomical FE models of both a healthy subject's foot and a neuropathic subject's one were established, based on MRI. These models were driven by the same subjects' kinematic-kinetic data acquired during gait

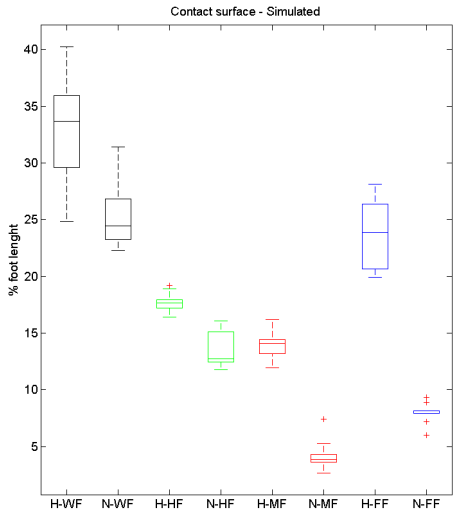

Figure 4.43: Simulated data of the healthy subjects (H) and the neuropathic subjects (N) for contact surfaces in the whole foot (WF-black) and in each foot subarea: hindfoot (HF-green), midfoot (MF-red) and forefoot (FF-blue). The values are expressed in percentage of the foot length.

(State A) in order to customize the results of the simulations. The plantar pressure data registered synchronously with the kinematic-kinetic data were adopted as gold standard for the validation of the models. Then simulations were driven for the two models by adopting the kinematic-kinetic data of 10 healthy and 10 neuropathic subjects during gait as input (State B), in order to obtain their plantar pressures as output.

The peculiarity of this study consisted mainly in the integration of different methods, namely the FE method and the gait analysis. The latter was performed by means of a protocol that allows integrated kinematic-kinetic and plantar pressure assessment. this procedure was adopted either to move or validate a healthy and a neuropathic foot model. Whole foot subject specific FE models of the healthy and the neuropathic foot whose subject specificity can be found in term of foot geometry (obtained from MRI), were developed and the boundary constraints were derived from kinematics and kinetics experimentally measured data with a protocol for the assessment of 3D foot kinematics, kinetics and plantar pressures. The results demonstrated that plantar pressures and internal stresses during gait can be obtained using a realistic 3D model, by combining these two techniques, gait analysis and FE modeling, not only for the healthy foot assess-

ment, but also for the diabetic neuropathic foot modeling.

The validation of the FE foot model is a very important issue and should be carried out to assess the reliability of model prediction. For what regards the results of State A, the comparison showed that there was a reasonable agreement in the overall patterns of predicted and measured plantar pressure distribution during heel strike, loading response, midstance and push off phases although the model overestimated contact pressure and contact area under the lateral midfoot as in [96]. For the 3DNSM, the simulated peak plantar pressures were higher than pressures measured during gait. Nevertheless, for the 3DHSM the simulations overestimated the overall peak pressures in the first half of the stance while it underestimated the peak pressures in the midstance and push-off instants, as Petre et al. highlighted in their paper [94]. This was noticed also by Fernandez et al.: the peak average values for heel strike and midstance from the pressure platform were lower than the model predictions [50]. However the model predictions of contact pressures and contact surfaces were within the range of the experimental pressure taken from the same subjects.

For the 3DHSM the results (180.2 KPa for the whole foot in midstance) were consistent with values reported in literature. Specifically, Chen et al. reported 370-1000 KPa for pressure range [32]; Qiu et al., Cheung et al. and Antunes et al. reported respectively 198 KPa [96], 230 KPa [37] and 131 KPa [10] as FE predicted peak plantar pressures; finally in the simulations of Natali et al. the peak values ranged between 120 KPa and 160 KPa [86]. For the diabetic condition the peak pressure values that can be found in literature are 279 KPa given by Actis et al. [7] and 240 KPa by Fernandez et al. [50] while the 3DNSM developed herein resulted in 202.77 KPa. A good agreement was found also between the peak values at the several instants of the stance phase of gait investigated herein (paragraph 4.3.1) and the ones reported in literature. In Fernandez et al. at heel strike the predicted contact pattern was isolated on the heel with a peak of 675 KPa. At midstance the contact pattern was concentrated along the lateral plantar region with a peak at the heel of 240 KPa. At toe-off the model predicted contact across the ball of the foot with a peak on the third to fourth metatarsals of 319 KPa [50].

Von Mises stress predictions of the two models, 3DHSM and 3DNSM, at midstance were respectively of 162 KPa and 150 KPa. These values were quite low if compared with the results of Gefen et al. (300-600 KPa in the heel pad) [54] and of Yarnitzky et al. (250-400 KPa) [120].

The results of the parametric test on tissue stiffness (paragraph 4.3.3) agreed with those of Cheung et al. and [37] and Fernandez et al. [50] as foot contact area decreased when tissue stiffness was increasing. Nevertheless the results on the 3DNSM simulations did not perfectly agree with the gait experimental data, nor if the minor stiffness coefficients were used, or with the medial or maximum stiffness. This could be due to the soft tissue formulation adopted. Even if several studies were performed on the plantar pad soft tissue stiffness of diabetic foot [48, 53, 65, 64, 99, 111, 123], there is still a lack of formulations obtained from experimental tests which adopt gait-comparable forces and velocities for the actuator of the ultrasound probe. Useful results could be obtained from a recently proposed device composed by an ultrasound probe, a linear variable displacement transducer and a load cell driven vertically by an actuator to contact the plantar surface of the heel. Drive profiles were generated from barefoot walking motion data and the large plate top of this device impact the plantar aspect of the foot as it happens during real gait. Thus more realistic results could be obtained, especially for the diabetic subjects [89].

The State B simulations were performed using the biomechanical data of a set of subjects applied on the model specific of their pathology (healthy subjects on the 3DHSM and neuropathic subjects on the 3DNSM) in the midstance phase of gait. The results of State B for the healthy subjects showed a poor agreement with the data experimentally acquired. The FE 3DHSM simulations performed with the data of the 10 healthy subjects as input underestimated the plantar pressures in all the three foot subareas while it overestimated the contact surfaces everywhere. For what regards the neuropathic subjects' group, the results found better agreement. For instance in the peak pressure values the mean errors of the simulations with respect to the experimental data were below the 20% with the exception of the hindfoot. These results confirmed the need of a subject specific model for each subject since, as stated in several studies [8, 15, 16, 56, 61, 69, 74, 75, 73, 81, 107, 112], the foot morphology have a high influence on foot function in term of kinematics and kinetics as well as in plantar pressure distribution.

In the literature almost every study cited at paragraph 2.5.2 adopted CT or MRI images to reconstruct the model geometry. This allowed taking into account for foot type, bony prominences, foot deformities, soft tissues thickness and so on. Some exceptions were represented by the studies where the aim was focused on one particular parametric problem. For example in the study of Fernandez et al. the developed model had only the healthy subject geometry characteristics. In

contrast with Fernandez et al., the aim of the present thesis was to obtain a high subject specificity thus MRI derived feet geometries were reconstructed for both the healthy and the neuropathic subjects and the foot motion was prescribed in the simulations using motion capture.

A brief comparison was performed between the healthy subjects' and the neuropathic subjects' simulated results, even if the number of subjects in the groups was low and a T-test, with the corresponding normality test, was not reliable. As it would be expected and as it was already widely demonstrated in literature [23, 27, 85, 56, 112], the peak pressures and the mean pressures were higher in the neuropathic subjects with respect to the healthy ones. Nevertheless the neuropathic subject whose foot geometry was reconstructed in the FE 3DNSM has a cavus foot; this type of foot is characterized by plantar pressures concentrated at the hindfoot and forefoot, as no spread of the loads occurs in the midfoot [74]. To prove this, in the neuropathic group the contact surface of the forefoot and especially the midfoot were much lower than the ones of the healthy group.

There were a number of simplifications applied during the development of the foot models that should be considered when interpreting the results.

All current material properties used in these models were selected according to the literature. This may explain why the FE models overestimated the peak pressure values at the hindfoot during the heel strike. In particular a uniform soft tissue mass was used to represent all foot structures except for bones and joint cartilage. A more adequate integration of the internal structures of the plantar soft tissue, such as a formulation which includes the micro- and macro-chambers layers [64] or the skin [59] might help to highlight interactions among different levels more precisely.

Only plantar ligaments and fascia were modelled; straight node-to-node link elements and with no cross-sectional areas were used. This can be indicative of the fact that in the healthy subject the midfoot pressure was not correctly predicted for the midstance phase of gait. It was demonstrated that the plantar fascia plays an important role in maintaining the medial longitudinal arch during weight-bearing [66].

No muscles were added to the bone, cartilage and soft tissues geometry. However to study the human foot mechanism, the complex interplay or interrelationship among muscular control, internal joint movement, and plantar loading transfer needs to be considered [29]. This may explain why in the 3DHSM midfoot the pressure values were overestimated during push-off and in the 3DNSM

the hindfoot and midfoot simulated peak pressures were much higher than the experimental ones. Some models developed in previous studies included the muscle forces and ankle joint loads. The values of the forces were either adopted from literature, adapting them with a trial & error process in order to get the correct plantar pressures [54], or obtained from musculoskeletal models [62, 95]. Adding the muscles forces could be considered as future improvement of the models developed herein.

The fidelity of the model is largely dictated by the number of degrees of freedom. Researchers typically interested in centre of pressure and ground reaction force grouped most bones of the foot into a rigid body [42, 62]. In the current model all 30 bones of the foot were captured with motion analysis techniques. Even if the stereophotogrammetric procedure has errors associated with skin artefact [72] and also it cannot capture the intricate movement of individual foot bones, the movement of the heel, midfoot and forefoot are necessary to describe the key movements of the foot. Therefore in the present study the bones were grouped into forefoot, midfoot, hindfoot and the fixed tibia-fibula, in agreement also with [32, 37, 33, 50], to capture the main foot articulations.

Despite the limitations, the approaches and methods adopted herein can be considered satisfactory.

Chapter 5

Conclusions

Several studies have highlighted that biomechanical factors play a crucial role in the aetiology, treatment and prevention of diabetic foot ulcers. Recent literature on the diabetic foot indicates that mechanical stresses, high plantar pressures or/and high tangential stresses, acting within the soft tissues of the foot can contribute to the formation of neuropathic ulcers. While it is important to study the in-vivo diabetic foot-to-floor interactions during gait, models for simulations of deformations and stresses in the diabetic plantar pad are required to predict high risk areas or to investigate the performance of different insoles design for optimal pressure relief. The FE models allow taking into account the critical aspects of the diabetic foot, namely the movement, the morphology, the tissue properties and the loads.

Existing FE models of the foot or footwear in the literature [6, 13, 22, 24, 31, 36, 47, 48, 54, 57, 67, 76, 120] were developed under certain simplifications and assumptions such as a simplified or partial foot shape, assumptions of linear material properties, infinitesimal deformation and linear boundary conditions without considering friction and slip. Although several 3D foot models were developed recently to study the biomechanical behaviour of the human foot and ankle, to the author knowledge a subject-specific geometrically detailed and realistic customized boundary constraints 3D FE model of the neuropathic foot and ankle has not been reported.

The present thesis aimed at developing 2 different typology of FE models in order to enable the possibility of identifying high risk diabetic subjects for plantar ulcer formation together with the specific plantar area at risk.

First of all, a 2D FE model of the hindfoot was developed and the experimentally acquired in-vivo kinematics and kinetics of an healthy and a diabetic

neuropathic subjects were adopted as input in the simulation process (see chapter 3). The purpose was to define more efficient subject specific computational model of the foot (in this specific case a part of it, namely the hindfoot) that accounts for in-vivo kinematics, kinetics and plantar pressure data together with foot MRI data. Six different loading conditions were applied to the model considering different phases of the stance phase of gait (namely: the heel strike, the loading response and the midstance) and either the global vertical ground reaction vector or the hindfoot one. The subject specific kinematic, kinetic and plantar pressure data synchronously acquired during in-vivo gait analysis were used as input for the simulations and for validation purposes. This procedure was applied both to a neuropathic and to a healthy subjects. Model validity was established by means of comparison between each subject peak plantar pressure experimentally measured and the simulated one by means of evaluating the Root Mean Square Error. Both the value and the position of the peak plantar pressure with respect to the plantar surface of the foot were compared. The 2D FE simulations were run also with the kinematics and kinetics data of 20 subjects as input variables (10 healthy and 10 neuropathic subjects). Again the experimental plantar pressure data were used in order to estimate the validity of the simulated results.

Second a complete foot 3D FE model of the same subjects' feet (chapter 4) was developed. The former was based on subject specific MRI (the same subjects' data of the 2D model) and the FE simulations were driven with the gait analysis data as previously performed for the 2D model. This procedure was applied both to a neuropathic and to an healthy subjects. These FE simulations were driven with the same subjects' kinematic-kinetic data acquired during gait (State A). The plantar pressure data registered synchronously with the kinematic-kinetic data were adopted as gold standard for the validation of the models. As previously performed in the case of the 2D FE models, the data of 20 subjects were used as input variables (10 healthy and 10 neuropathic subjects) for further simulations, and their experimental plantar pressure data were used in order to estimate the validity of the simulated results.

The principal aim of the present thesis was to simulate the biomechanical behaviour of a diabetic neuropathic foot in order to predict the high stresses on its plantar surface. To achieve this, it has been developed a method that apply subject-specific loading and boundary conditions obtained by means of integrated and synchronized kinematic-kinetic data acquired during in-vivo gait analysis.

Compared to the plantar pressure predicted values reported in the literature

the results of the simulations performed within the present thesis shows a good agreement. Moreover the comparison between experimental and simulated plantar pressure laid to satisfactory results in term of RMSE%. The best results were obtained in the case of subject specific subareas ground reaction forces and subjects specific kinematics applied as input to the simulations performed with the model generated with the MRI data of the same subjects. This was true both in the case of the 2D FE model simulations and the 3D FE model ones.

Main limitations of the present approach can be considered the presence of skin artefact which affect the precision of the kinematic data used as input to the FE model simulations. Furthermore the computational formulation of foot subarea kinetics is based on simplified hypothesis [55, 104, 112] which may affect the precision of the plantar pressure estimation output of the FE model simulation. However results of the present contribution showed better agreement between experimental and simulated plantar pressure in the case of specific foot subarea ground reaction forces applied as input than when using the global ground reaction vector.

A detailed discussion of both results and limitations of the models developed herein has been provided in the discussion sections of chapter 3 and 4.

Original Contributions

Three main original contributions were given to the FE foot models development process.

First of all, the kinematic-kinetic boundary constraints were set according to a validated gait analysis protocol for the assessment of 3D kinematic-kinetic-plantar pressures on the foot of healthy and diabetic subjects [101, 104]. This specific gait analysis protocol enabled to establish the validity of the results by comparing the simulated plantar pressures with those experimentally acquired synchronously with the kinematic and loads boundary constraints used in the FE model simulations.

None of the models proposed in the literature adopted this expedient; all of them collected the foot pressure measurements on a separate set of acquisitions. It should be mentioned that every different landing angle of the foot or loading condition produce a different pressure map and the average values (as it is usually done in order to accounted for the differences between the trials [50] are not representative of the gait of the subject.

Moreover the adopted kinematic protocol provides the tools to assess the validity of the developed models with an anatomically based approach because it allows the identification of specific foot subsegments (described at paragraph 2.3.4). The areas of comparison between the simulated and the experimental data are taken according to the real foot subsegments.

In some studies a subdivision of the plantar aspect of the foot was performed according to the footprint shape [67] or to proportions over the foot length [37]. These methods can be considered useful but not accurate in presence of foot deformities. Unfortunately this is the case of diabetic foot subjects (see paragraph 2.2.1). The methodology developed herein resulted also more accurate (mean RMSE% improves from 25% to 13% of the peak experimental value) than when the simulations were run considering the whole foot ground reaction forces and the whole foot peak pressure, as it is currently done in the literature [35, 57, 76, 86].

Finally, thanks to this protocol, the predicted plantar pressures could be subdivided into the three foot sub-areas, allowing the possibility to obtain more information in term of assessment of the foot biomechanical behaviour.

Second, a state-of-the-art neuropathic foot FE model was developed and simulations driven with neuropathic subject specific synchronised kinematics and kinetics. This included in the FE formulation the add-in value of the gait analysis technique.

Last but not less important, the mesh generation was performed through a very recently proposed grid-based meshing approach that is remarkably straightforward, robust, accurate and efficient (paragraphs 2.5.3 and 4.2.3). With this method, the mesh can be generated automatically with image-based accuracy and domain boundaries of the FE model lying exactly on the isosurfaces [122]. Moreover the mesh of the 3D horizontal plate was generated with hexahedral elements of 8 mm edges. This dimension agreed with the size of the sensors of the plantar pressure devices. This choice allowed a correct comparison between the simulated and the experimental stress data in the validation process. This specific choice find agreement with previous literature where some authors indicated that the difference between the simulated and the experimental results could be due to the difference in the resolution between the pressure sensors and the mesh [10, 37]. Thereafter, from a quantitative point of view the FE results lead to higher values than the experimental ones. This difference might be derived from the resolution of the pressure sensors that report an average pressure over a sensor area while the FEA model reports the contact pressure as calculated from a nodal force per

element's surface area [10].

The results of the present study may have significant impact on providing a useful tool for effective evaluation of existing or the development of new offloading techniques at the foot-support interface. Indeed this thesis examined plantar pressure at plantar surface of both a healthy and a neuropathic foot. Some parametric modeling analysis was conducted to highlight potential implications of soft tissue stiffening in the neuropathic foot.

Obviously with more experimental data available, the model could be further refined and validated to produce relevant predictions for clinical applications. However at the present state these models can be a basic tool for possible applications in studying the influence of therapeutic interventions that adopt plantar support for stress redistributions.

Future developments

Further developments are suggested, in order to make the models more realistic, more subject-specific, more reliable and more accurate, thus more suitable for clinical applications.

Among the advantages and potentials of deriving a FE numerical model there is the possibility to estimate also the distribution of the shear stress generated at the interface between foot and plate/insole: As reported in paragraph 2.3.3, it has been demonstrated that in the diabetic foot the tangential forces are high and proven risk factors for ulceration. Thus this is an important variable in order to evaluate the ulceration process and the insole effectiveness in reducing the risk of injury. For these reasons, in the immediate future the predicted shear stresses will be considered, compared with those experimentally acquired and included in the subject-specific neuropathic patient assessment set-up.

As reported in paragraph 4.4, an important improvement of the models can be introduced in term of soft tissues properties mathematical formulation. As reported by Gefen et al. [53], in the future the attending medical staff would be able to perform measurements of the plantar tissue's mechanical properties using ultrasound elastography or a similar non invasive technique, and these data will be fed into the simulation to form a patient-specific, anatomically accurate computer model of the foot. At the present time, the closer improvement can be performed through a new soft tissue formulation by using for instance the device proposed by Parker et al. [89].

Another step forward particularly relevant for the neuropathic model, can be performed separating the soft tissues in internal and skin layer, because tissue stiffness, as shown by Gu et al. [59], is quite different after dividing the heel pad into skin and fat pad layer. Besides in the neuropathic feet the calluses formation and skin dryness and hardness are risk factors for ulcer formation as they increase the peak plantar pressures [8, 53, 56, 69, 115].

For the improvement of the neuropathic model, the presence of vasculopathy should also be considered. To model the mechanical behaviour of diseased soft tissue of the pathologic foot, only macroscale changes in constitutive properties are usually considered. Since it has been demonstrated that the diabetic tissue has significantly morphological changes in the tissue, which may alter mechanical characteristics under loading, Mithraratne et al. investigated the blood flow in major arteries of the pathologic foot where the soft tissue stiffening occurs. Simulation results reveal that a two-fold increase in tissue stiffness leads to about 28% reduction in blood flow to the affected region [80]. In this direction to predict the risk of ulceration a multiscale model is needed, with the introduction of a micro-level of diabetic foot biological-tissue with cells and tissue structures which consider the nutrient flows from the vessels through the extracellular matrix to the cells [105].

Moreover, a macro-level can be added. A musculoskeletal model which includes the muscle forces prediction from the gait analysis derived kinematic-kinetic data, as performed by Qian et al. [95], can be joined with this project. This could provide realistic muscle forces synchronised with the other data which can be used to drive the FE model in the simulations.

With this perspective, potential applications for the FE modeling process and method in the current study can be found in the study of foot deformities and their influence on loading patterns.

Furthermore, in the diabetic foot treatment footwear and orthotic devices can prevent the occurrence and recurrence of foot ulceration by obtaining a different distribution and by limiting the peak values in plantar aspect of the foot. However, when using orthoses or other inserts care must be taken not to increase pressures over another region of the foot [115]. The FE models can be adopted to study the mechanical interaction between foot and insole through the plantar pressure prediction that can be considered in the footwear/orthotic design process. This approach is more efficient than a trial- error approach, limiting the necessity of insole manufacturing, which is time consuming and expensive. The

effects of a change of insole shape, thickness or material stiffness could be easily evaluated by comparing different solutions, leading to the optimized configuration [86].

Bibliography

[1] Imago s.n.c. http://www.imagortesi.com/.

[2] Surface anatomy, NTUPT. http://www.pt.ntu.edu.tw/hmchai/SurfaceAnatomy/.

[3] WHO | world health organization. http://www.who.int/en/.

[4] C. A. Abbott, L. Vileikyte, S. Williamson, A. L. Carrington, and A. J. Boulton. Multicenter study of the incidence of and predictive risk factors for diabetic neuropathic foot ulceration. *Diabetes Care*, 21(7):1071–1075, July 1998.

[5] F. Abouaesha, C. H. M. van Schie, D. G. Armstrong, and A. J. M. Boulton. Plantar soft-tissue thickness predicts high peak plantar pressure in the diabetic foot. *Journal of the American Podiatric Medical Association*, 94(1):39–42, Feb. 2004.

[6] R. L. Actis, L. B. Ventura, D. J. Lott, K. E. Smith, P. K. Commean, M. K. Hastings, and M. J. Mueller. Multi-plug insole design to reduce peak plantar pressure on the diabetic foot during walking. *Medical & Biological Engineering & Computing*, 46:363–371, Feb. 2008.

[7] R. L. Actis, L. B. Ventura, K. E. Smith, P. K. Commean, D. J. Lott, T. K. Pilgram, and M. J. Mueller. Numerical simulation of the plantar pressure distribution in the diabetic foot during the push-off stance. *Medical & Biological Engineering & Computing*, 44(8):653–663, Aug. 2006.

[8] J. H. Ahroni, E. J. Boyko, and R. C. Forsberg. Clinical correlates of plantar pressure among diabetic veterans. *Diabetes care*, 22(6):965–972, June 1999.

[9] American Diabetes Association. Peripheral arterial disease in people with diabetes. *Diabetes Care*, 26(12):3333–3341, Jan. 2003.

[10] J. P. Antunes, G. R. Dias, A. T. Coelho, F. Rebelo, and T. Pereira. Nonlinear 3D foot FEA modelling from CT scan medical images. In *Computational Vision and Medical Imaging Processing*, pages 135–141. Taveres, Jmrs and Jorge, R. M. N., 2011.

[11] D. G. Armstrong, E. J. Peters, K. A. Athanasiou, and L. A. Lavery. Is there a critical level of plantar foot pressure to identify patients at risk for neuropathic foot ulceration? *The Journal of Foot and Ankle Surgery*, 37(4):303–307, Aug. 1998.

[12] E. Atlas, Z. Yizhar, S. Khamis, N. Slomka, S. Hayek, and A. Gefen. Utilization of the foot load monitor for evaluating deep plantar tissue stresses in patients with diabetes: Proof-of-concept studies. *Gait & Posture*, 29(3):377–382, Apr. 2009.

[13] Z. Barani, M. Haghpanahi, and H. Katoozian. Three dimensional stress analysis of diabetic insole: a finite element approach. *Technology and Health Care: Official Journal of the European Society for Engineering and Medicine*, 13(3):185–192, 2005.

[14] Bertec corporation. Force plate user manual. Columbus OH, USA.

[15] J. Bevans. Biomechanics and plantar ulcers in diabetes. *The Foot*, 2(3):166–172, Sept. 1992.

[16] J. Bevans and P. Bowker. Foot structure and function: aetiological risk factors for callus formation in diabetic and non-diabetic subjects. *The Foot*, 9(3):120–127, Sept. 1999.

[17] A. J. Boulton. Diabetic neuropathy: Is pain god's greatest gift to mankind? *Seminars in Vascular Surgery*, 25(2):61–65, June 2012.

[18] A. J. Boulton, L. Vileikyte, G. Ragnarson-Tennvall, and J. Apelqvist. The global burden of diabetic foot disease. *The Lancet*, 366(9498):1719–1724, 2005.

[19] A. J. M. Boulton. Diabetic neuropathy: is pain god's greatest gift to mankind? *Seminars in vascular surgery*, 25(2):61–65, June 2012.

[20] R. J. Bourdiol. *Pied et statique*. Maisonneuve, 1980.

[21] C. K. Bowering. Diabetic foot ulcers. pathophysiology, assessment, and therapy. *Canadian Family Physician*, 47:1007–1016, May 2001.

[22] S. P. Budhabhatti, A. Erdemir, M. Petre, J. Sferra, B. Donley, and P. R. Cavanagh. Finite element modeling of the first ray of the foot: a tool for the design of interventions. *Journal of Biomechanical Engineering*, 129(5):750–756, Oct. 2007.

[23] S. A. Bus, G. D. Valk, R. W. van Deursen, D. G. Armstrong, C. Caravaggi, P. Hlavek, K. Bakker, and P. R. Cavanagh. The effectiveness of footwear and offloading interventions to prevent and heal foot ulcers and reduce plantar pressure in diabetes: a systematic review. *Diabetes/Metabolism Research and Reviews*, 24(S1):S162–S180, May 2008.

[24] D. L. A. Camacho, W. R. Ledoux, E. S. Rohr, B. J. Sangeorzan, and R. P. Ching. A three-dimensional, anatomically detailed foot model: a foundation for a finite element simulation and means of quantifying foot-bone position. *Journal of Rehabilitation Research and Development*, 39(3):401–410, June 2002.

[25] A. Cappello, A. Cappozzo, and P. E. di Prampero. *Bioingegneria della postura e del movimento*. Patron, 2003.

[26] M. C. Carson, M. E. Harrington, N. Thompson, J. J. O'Connor, and T. N. Theologis. Kinematic analysis of a multi-segment foot model for research and clinical applications: a repeatability analysis. *Journal of biomechanics*, 34(10):1299–1307, Oct. 2001.

[27] P. Cavanagh, A. Erdemir, M. Petre, T. Owings, G. Botek, S. Chokhandre, and R. Bafna. Biomechanical factors in diabetic foot disease. *Journal of Foot and Ankle Research*, 1(Suppl 1):K4, 2008.

[28] P. R. Cavanagh, G. G. Simoneau, and J. S. Ulbrecht. Ulceration, unsteadiness, and uncertainty: the biomechanical consequences of diabetes mellitus. *Journal of biomechanics*, 26 Suppl 1:23–40, 1993.

[29] W.-M. Chen, T. Lee, P. V.-S. Lee, J. W. Lee, and S.-J. Lee. Effects of internal stress concentrations in plantar soft-tissue–a preliminary three-dimensional finite element analysis. *Medical Engineering & Physics*, 32(4):324–331, May 2010.

[30] W.-M. Chen, J. Park, S.-B. Park, V. P.-W. Shim, and T. Lee. Role of gastrocnemiussoleus muscle in forefoot force transmission at heel rise a 3D finite element analysis. *Journal of Biomechanics*, 45(10):1783–1789, June 2012.

[31] W.-P. Chen, C.-W. Ju, and F.-T. Tang. Effects of total contact insoles on the plantar stress redistribution: a finite element analysis. *Clinical Biomechanics (Bristol, Avon)*, 18(6):S17–24, July 2003.

[32] W. P. Chen, F. T. Tang, and C. W. Ju. Stress distribution of the foot during mid-stance to push-off in barefoot gait: a 3-d finite element analysis. *Clinical Biomechanics (Bristol, Avon)*, 16(7):614–620, Aug. 2001.

[33] J. T.-M. Cheung and B. M. Nigg. Clinical applications of computational simulation of foot and ankle. *Sport-Orthopdie - Sport-Traumatologie - Sports Orthopaedics and Traumatology*, 23(4):264–271, Jan. 2008.

[34] J. T.-M. Cheung, J. Yu, D. W.-C. Wong, and M. Zhang. Current methods in computer-aided engineering for footwear design. *Footwear Science*, 1(1):31–46, 2009.

[35] J. T.-M. Cheung and M. Zhang. A 3-dimensional finite element model of the human foot and ankle for insole design. *Archives of Physical Medicine and Rehabilitation*, 86(2):353–358, Feb. 2005.

[36] J. T.-M. Cheung and M. Zhang. Parametric design of pressure-relieving foot orthosis using statistics-based finite element method. *Medical Engineering & Physics*, 30(3):269–277, Apr. 2008.

[37] J. T.-M. Cheung, M. Zhang, A. K.-L. Leung, and Y.-B. Fan. Three-dimensional finite element analysis of the foot during standing–a material sensitivity study. *Journal of Biomechanics*, 38(5):1045–1054, May 2005.

[38] T. M. Chu and N. P. Reddy. Stress distribution in the ankle-foot orthosis used to correct pathological gait. *Journal of rehabilitation research and development*, 32(4):349–360, Nov. 1995.

[39] M. S. Cowley, E. J. Boyko, J. B. Shofer, J. H. Ahroni, and W. R. Ledoux. Foot ulcer risk and location in relation to prospective clinical assessment of foot shape and mobility among persons with diabetes. *Diabetes research and clinical practice*, 82(2):226–232, Nov. 2008.

[40] F. Crawford, M. Inkster, J. Kleijnen, and T. Fahey. Predicting foot ulcers in patients with diabetes: a systematic review and meta-analysis. *QJM*, 100(2):65–86, Jan. 2007.

[41] S. Cuccurullo. Gait analysis. http://www.ncbi.nlm.nih.gov, 2004.

[42] X.-Q. Dai, Y. Li, M. Zhang, and J. T.-M. Cheung. Effect of sock on biomechanical responses of foot during walking. *Clinical Biomechanics*, 21(3):314–321, Mar. 2006.

[43] E. D'Ambrogi, L. Giurato, M. A. D'Agostino, C. Giacomozzi, V. Macellari, A. Caselli, and L. Uccioli. Contribution of plantar fascia to the increased forefoot pressures in diabetic patients. *Diabetes Care*, 26(5):1525 –1529, May 2003.

[44] Dassault Systemes. Abaqus theory manual, Simulia Corp., Providence, RI, USA.

[45] R. B. Davis III, S. unpuu, D. Tyburski, and J. R. Gage. A gait analysis data collection and reduction technique. *Human Movement Science*, 10(5):575–587, Oct. 1991.

[46] K. Deschamps, F. Staes, P. Roosen, F. Nobels, K. Desloovere, H. Bruyninckx, and G. A. Matricali. Body of evidence supporting the clinical use of 3D multisegment foot models: a systematic review. *Gait & posture*, 33(3):338–349, Mar. 2011.

[47] A. Erdemir, J. J. Saucerman, D. Lemmon, B. Loppnow, B. Turso, J. S. Ulbrecht, and P. R. Cavanagh. Local plantar pressure relief in therapeutic footwear: design guidelines from finite element models. *Journal of Biomechanics*, 38(9):1798–1806, Sept. 2005.

[48] A. Erdemir, M. L. Viveiros, J. S. Ulbrecht, and P. R. Cavanagh. An inverse finite-element model of heel-pad indentation. *Journal of Biomechanics*, 39(7):1279–1286, 2006.

[49] E. L. Feldman, M. J. Stevens, P. K. Thomas, M. B. Brown, N. Canal, and D. A. Greene. A practical two-step quantitative clinical and electrophysiological assessment for the diagnosis and staging of diabetic neuropathy. *Diabetes care*, 17(11):1281–1289, Nov. 1994.

[50] J. Fernandez, M. Ul Haque, P. Hunter, and K. Mithraratne. Mechanics of the foot part 1: A continuum framework for evaluating soft tissue stiffening in the pathologic foot. *International Journal for Numerical Methods in Biomedical Engineering*, 28(10):1056–1070, 2012.

[51] D. J. Fernando, E. A. Masson, A. Veves, and A. J. Boulton. Relationship of limited joint mobility to abnormal foot pressures and diabetic foot ulceration. *Diabetes care*, 14(1):8–11, Jan. 1991.

[52] A. Gefen. Stress analysis of the standing foot following surgical plantar fascia release. *Journal of Biomechanics*, 35(5):629–637, May 2002.

[53] A. Gefen. Plantar soft tissue loading under the medial metatarsals in the standing diabetic foot. *Medical Engineering & Physics*, 25(6):491–499, July 2003.

[54] A. Gefen, M. Megido-Ravid, Y. Itzchak, and M. Arcan. Biomechanical analysis of the three-dimensional foot structure during gait: a basic tool for clinical applications. *Journal of Biomechanical Engineering*, 122(6):630–639, Dec. 2000.

[55] C. Giacomozzi, V. Macellari, A. Leardini, and M. G. Benedetti. Integrated pressure-force-kinematics measuring system for the characterisation of plantar foot loading during locomotion. *Medical & biological engineering & computing*, 38(2):156–163, Mar. 2000.

[56] C. Giacomozzi and F. Martelli. Peak pressure curve: An effective parameter for early detection of foot functional impairments in diabetic patients. *Gait & Posture*, 23(4):464–470, June 2006.

[57] S. Goske, A. Erdemir, M. Petre, S. Budhabhatti, and P. R. Cavanagh. Reduction of plantar heel pressures: Insole design using finite element analysis. *Journal of Biomechanics*, 39(13):2363–2370, Jan. 2006.

[58] H. Gray. *Anatomy of the human body.* Lea & Febiger, 1918.

[59] Y. Gu, J. Li, X. Ren, M. J. Lake, and Y. Zeng. Heel skin stiffness effect on the hind foot biomechanics during heel strike. *Skin Research and Technology.*, 16(3):291–296, Aug. 2010.

[60] Y. D. Gu, X. J. Ren, J. S. Li, M. J. Lake, Q. Y. Zhang, and Y. J. Zeng. Computer simulation of stress distribution in the metatarsals at different inversion landing angles using the finite element method. *International Orthopaedics*, 34(5):669–676, June 2010.

[61] A. Guiotto, Z. Sawacha, G. Guarneri, G. Cristoferi, A. Avogaro, and C. Cobelli. The role of foot morphology on foot function in diabetic subjects with or without neuropathy. *Gait & posture*, Nov. 2012.

[62] J. P. Halloran, M. Ackermann, A. Erdemir, and A. J. van den Bogert. Concurrent musculoskeletal dynamics and finite element analysis predicts altered gait patterns to reduce foot tissue loading. *Journal of Biomechanics*, 43(14):2810–2815, Oct. 2010.

[63] J. P. Halloran, A. Erdemir, and A. J. van den Bogert. Adaptive surrogate modeling for efficient coupling of musculoskeletal control and tissue deformation models. *Journal of Biomechanical Engineering*, 131(1):011014, Jan. 2009.

[64] C.-C. Hsu, W.-C. Tsai, C.-L. Wang, S.-H. Pao, Y.-W. Shau, and Y.-S. Chuan. Microchambers and macrochambers in heel pads: are they functionally different? *Journal of Applied Physiology*, 102(6):2227 –2231, June 2007.

[65] T. C. Hsu, C. L. Wang, Y. W. Shau, F. T. Tang, K. L. Li, and C. Y. Chen. Altered heelpad mechanical properties in patients with type 2 diabetes mellitus. *Diabetic Medicine*, 17(12):854–859, Dec. 2000.

[66] J. M. Iaquinto and J. S. Wayne. Computational model of the lower leg and foot/ankle complex: application to arch stability. *Journal of Biomechanical Engineering*, 132(2):021009, Feb. 2010.

[67] S. Jacob and M. K. Patil. Stress analysis in three-dimensional foot models of normal and diabetic neuropathy. *Frontiers of Medical and Biological Engineering*, 9(3):211–227, 1999.

[68] J. W. Klaesner, M. K. Hastings, D. Zou, C. Lewis, and M. J. Mueller. Plantar tissue stiffness in patients with diabetes mellitus and peripheral neuropathy. *Archives of Physical Medicine and Rehabilitation*, 83(12):1796–1801, Dec. 2002.

[69] L. A. Lavery, D. G. Armstrong, R. P. Wunderlich, J. Tredwell, and A. J. M. Boulton. Predictive value of foot pressure assessment as part of a population-based diabetes disease management program. *Diabetes care*, 26(4):1069–1073, Apr. 2003.

[70] A. Leardini, M. G. Benedetti, L. Berti, D. Bettinelli, R. Nativo, and S. Giannini. Rear-foot, mid-foot and fore-foot motion during the stance phase of gait. *Gait & posture*, 25(3):453–462, Mar. 2007.

[71] A. Leardini, M. G. Benedetti, F. Catani, L. Simoncini, and S. Giannini. An anatomically based protocol for the description of foot segment kinematics during gait. *Clinical biomechanics (Bristol, Avon)*, 14(8):528–536, Oct. 1999.

[72] A. Leardini, L. Chiari, U. Della Croce, and A. Cappozzo. Human movement analysis using stereophotogrammetry. part 3. soft tissue artifact assessment and compensation. *Gait & posture*, 21(2):212–225, Feb. 2005.

[73] W. R. Ledoux, E. S. Rohr, R. P. Ching, and B. J. Sangeorzan. Effect of foot shape on the three-dimensional position of foot bones. *Journal of Orthopaedic Research: Official Publication of the Orthopaedic Research Society*, 24(12):2176–2186, Dec. 2006.

[74] W. R. Ledoux, J. B. Shofer, J. H. Ahroni, D. G. Smith, B. J. Sangeorzan, and E. J. Boyko. Biomechanical differences among pes cavus, neutrally aligned, and pes planus feet in subjects with diabetes. *Foot & ankle international / American Orthopaedic Foot and Ankle Society [and] Swiss Foot and Ankle Society*, 24(11):845–850, Nov. 2003.

[75] W. R. Ledoux, J. B. Shofer, D. G. Smith, K. Sullivan, S. G. Hayes, M. Assal, and G. E. Reiber. Relationship between foot type, foot deformity, and ulcer occurrence in the high-risk diabetic foot. *Journal of rehabilitation research and development*, 42(5):665–672, Oct. 2005.

[76] D. Lemmon, T. Shiang, A. Hashmi, J. S. Ulbrecht, and P. R. Cavanagh. The effect of insoles in therapeutic footwearA finite element approach. *Journal of Biomechanics*, 30(6):615–620, June 1997.

[77] S. LTD. ScanIP, +FE and +CAD reference guide, 2011.

[78] B. A. MacWilliams, M. Cowley, and D. E. Nicholson. Foot kinematics and kinetics during adolescent gait. *Gait & posture*, 17(3):214–224, June 2003.

[79] A. Malanthara and W. Gerstle. Comparative study of unstructured meshes made of triangles and quadrilaterals. In *In Proceedings of the 6th International Meshing Roundtable*, pages 437–447, 1997.

[80] K. Mithraratne, H. Ho, P. Hunter, and J. Fernandez. Mechanics of the foot part 2: A coupled solidfluid model to investigate blood transport in the pathologic foot. *International Journal for Numerical Methods in Biomedical Engineering*, 28(10):1071–1081, 2012.

[81] E. Morag and P. R. Cavanagh. Structural and functional predictors of regional peak pressures under the foot during walking. *Journal of biomechanics*, 32(4):359–370, Apr. 1999.

[82] M. J. Mueller, J. E. Diamond, A. Delitto, and D. R. Sinacore. Insensitivity, limited joint mobility, and plantar ulcers in patients with diabetes mellitus. *Physical therapy*, 69(6):453–459; discussion 459–462, June 1989.

[83] M. J. Mueller, M. Hastings, P. K. Commean, K. E. Smith, T. K. Pilgram, D. Robertson, and J. Johnson. Forefoot structural predictors of plantar pressures during walking in people with diabetes and peripheral neuropathy. *Journal of biomechanics*, 36(7):1009–1017, July 2003.

[84] M. J. Mueller, D. R. Sinacore, S. Hoogstrate, and L. Daly. Hip and ankle walking strategies: effect on peak plantar pressures and implications for neuropathic ulceration. *Archives of physical medicine and rehabilitation*, 75(11):1196–1200, Nov. 1994.

[85] M. J. Mueller, D. Zou, K. L. Bohnert, L. J. Tuttle, and D. R. Sinacore. Plantar stresses on the neuropathic foot during barefoot walking. *Physical therapy*, 88(11):1375–1384, Nov. 2008.

[86] A. Natali, A. Forestiero, E. Carniel, P. Pavan, and C. Dal Zovo. Investigation of foot plantar pressure: experimental and numerical analysis. *Medical and Biological Engineering and Computing*, 48(12):1167–1174, Dec. 2010.

[87] C. Nester, R. K. Jones, A. Liu, D. Howard, A. Lundberg, A. Arndt, P. Lundgren, A. Stacoff, and P. Wolf. Foot kinematics during walking mea-

sured using bone and surface mounted markers. *Journal of biomechanics*, 40(15):3412–3423, 2007.

[88] M. Oosterwaal, S. Telfer, S. Trholm, S. Carbes, L. W. v. Rhijn, R. Macduff, K. Meijer, and J. Woodburn. Generation of subject-specific, dynamic, multisegment ankle and foot models to improve orthotic design: a feasibility study. *BMC Musculoskeletal Disorders*, 12(1):256, Nov. 2011.

[89] D. Parker, G. Cooper, S. Pearson, D. Howard, G. Crofts, and C. Nester. In vivo measurement of the biomechanical properties of plantar soft tissues under simulated gait conditions. *Journal of Foot and Ankle Research*, 5(Suppl 1):O39, 2012.

[90] K. M. Patil, L. H. Braak, and A. Huson. Stresses in a simplified two dimensional model of a normal foot - a preliminary analysis. *Mechanics Research Communications*, 20(1):1–7, 1993.

[91] K. M. Patil, L. H. Braak, and A. Huson. Analysis of stresses in two-dimensional models of normal and neuropathic feet. *Medical and Biological Engineering and Computing*, 34(4):280–284, July 1996.

[92] S. P. Pendsey. Understanding diabetic foot. *International Journal of Diabetes in Developing Countries*, 30(2):75–79, 2010.

[93] J. Perry. *Gait Analysis: Normal and Pathological Function*. Slack, 1992.

[94] M. Petre, A. Erdemir, and P. R. Cavanagh. An MRI-compatible foot-loading device for assessment of internal tissue deformation. *Journal of biomechanics*, 41(2):470–474, 2008.

[95] Z.-h. Qian, L. Ren, Y. Ding, and L. Ren. A three-dimensional musculoskeletal model of the human foot complex using finite element method. *ISB 2011- Bruxelles*, 2011.

[96] T.-X. Qiu, E.-C. Teo, Y.-B. Yan, and W. Lei. Finite element modeling of a 3D coupled foot-boot model. *Medical Engineering & Physics*, June 2011.

[97] S. Rao, C. Saltzman, and H. J. Yack. Segmental foot mobility in individuals with and without diabetes and neuropathy. *Clinical biomechanics (Bristol, Avon)*, 22(4):464–471, May 2007.

[98] S. Rao, C. L. Saltzman, and H. J. Yack. Relationships between segmental foot mobility and plantar loading in individuals with and without diabetes and neuropathy. *Gait & posture*, 31(2):251–255, Feb. 2010.

[99] K. Rome, R. Campbell, A. Flint, and I. Haslock. Reliability of weight-bearing heel pad thickness measurements by ultrasound. *Clinical Biomechanics*, 13(4-5):374–375, June 1998.

[100] I. C. Sacco and A. C. Amadio. A study of biomechanical parameters in gait analysis and sensitive cronaxie of diabetic neuropathic patients. *Clinical biomechanics (Bristol, Avon)*, 15(3):196–202, Mar. 2000.

[101] Z. Sawacha, G. Cristoferi, G. Guarneri, S. Corazza, G. Don, P. Denti, A. Facchinetti, A. Avogaro, and C. Cobelli. Characterizing multisegment foot kinematics during gait in diabetic foot patients. *Journal of NeuroEngineering and Rehabilitation*, 6:37–37, Oct. 2009.

[102] Z. Sawacha, G. Gabriella, G. Cristoferi, A. Guiotto, A. Avogaro, and C. Cobelli. Diabetic gait and posture abnormalities: a biomechanical investigation through three dimensional gait analysis. *Clinical Biomechanics (Bristol, Avon)*, 24(9):722–728, Nov. 2009.

[103] Z. Sawacha, G. Guarneri, A. Avogaro, and C. Cobelli. A new classification of diabetic gait pattern based on cluster analysis of biomechanical data. *Journal of Diabetes Science and Technology*, 4(5):1127–1138, Sept. 2010.

[104] Z. Sawacha, G. Guarneri, G. Cristoferi, A. Guiotto, A. Avogaro, and C. Cobelli. Integrated kinematicskineticsplantar pressure data analysis: A useful tool for characterizing diabetic foot biomechanics. *Gait & Posture*, 36(1):20–26, May 2012.

[105] Z. Sawacha, A. Guiotto, A. Avogaro, D. Boso, B. Schrefler, A. Scarton, and C. Cobelli. Foot biomechanics model for diabetic ulcer prevention. volume Proceedings, page A120, Bethesda, Maryland, 2012.

[106] Z. Sawacha, F. Spolaor, G. Guarneri, P. Contessa, E. Carraro, A. Venturin, A. Avogaro, and C. Cobelli. Abnormal muscle activation during gait in diabetes patients with and without neuropathy. *Gait & Posture*, 35(1):101–105, Jan. 2012.

[107] J. E. Shaw, C. H. van Schie, A. L. Carrington, C. A. Abbott, and A. J. Boulton. An analysis of dynamic forces transmitted through the foot in diabetic neuropathy. *Diabetes care*, 21(11):1955–1959, Nov. 1998.

[108] J. A. Stebbins, M. E. Harrington, C. Giacomozzi, N. Thompson, A. Zavatsky, and T. N. Theologis. Assessment of sub-division of plantar pressure measurement in children. *Gait & posture*, 22(4):372–376, Dec. 2005.

[109] S. C. Tadepalli, A. Erdemir, and P. R. Cavanagh. Comparison of hexahedral and tetrahedral elements in finite element analysis of the foot and footwear. *Journal of Biomechanics*, 44(12):2337–2343, Aug. 2011.

[110] V. J. Thomas, K. M. Patil, and S. Radhakrishnan. Three-dimensional stress analysis for the mechanics of plantar ulcers in diabetic neuropathy. *Medical & Biological Engineering & Computing*, 42(2):230–235, Mar. 2004.

[111] J. Tong, C. Lim, and O. Goh. Technique to study the biomechanical properties of the human calcaneal heel pad. *The Foot*, 13(2):83–91, June 2003.

[112] L. Uccioli, A. Caselli, C. Giacomozzi, V. Macellari, L. Giurato, L. Lardieri, and G. Menzinger. Pattern of abnormal tangential forces in the diabetic neuropathic foot. *Clinical Biomechanics*, 16(5):446–454, June 2001.

[113] C. H. M. van Schie. A review of the biomechanics of the diabetic foot. *The international journal of lower extremity wounds*, 4(3):160–170, Sept. 2005.

[114] C. L. Vaughan, B. L. Davis, and J. C. O'Connor. *Dynamics of Human Gait*. Kiboho Publishers, Cape Town, South Africa, 2nd edition edition, 1992.

[115] A. Veves, J. M. Giurini, and F. W. LoGerfo. *The Diabetic Foot*. Springer, June 2006.

[116] WHO. Chapter 1 - burden: mortality, morbidity and risk factors. In *Global status report on NCDs 2010*. 2010.

[117] D. A. Winter. *Biomechanics and Motor Control of Human Movement*. John Wiley & Sons, Oct. 2009.

[118] J. S. Wrobel and B. Najafi. Diabetic foot biomechanics and gait dysfunction. *Journal of Diabetes Science and Technology*, 4(4):833–845, July 2010.

[119] L. Wu. Nonlinear finite element analysis for musculoskeletal biomechanics of medial and lateral plantar longitudinal arch of virtual chinese human after plantar ligamentous structure failures. *Clinical Biomechanics*, 22(2):221–229, Feb. 2007.

[120] G. Yarnitzky, Z. Yizhar, and A. Gefen. Real-time subject-specific monitoring of internal deformations and stresses in the soft tissues of the foot: a new approach in gait analysis. *Journal of Biomechanics*, 39(14):2673–2689, 2006.

[121] M. Yavuz, A. Tajaddini, G. Botek, and B. L. Davis. Temporal characteristics of plantar shear distribution: relevance to diabetic patients. *Journal of Biomechanics*, 41(3):556–559, 2008.

[122] P. Young, T. Beresford-West, S. Coward, B. Notarberardino, B. Walker, and A. Abdul-Aziz. An efficient approach to converting three-dimensional image data into highly accurate computational models. *Philosophical Transactions of the Royal Society A: Mathematical, Physical and Engineering Sciences*, 366(1878):3155 –3173, 2008.

[123] Y. Zheng, Y. Choi, K. Wong, S. Chan, and A. Mak. Biomechanical assessment of plantar foot tissue in diabetic patients using an ultrasound indentation system. *Ultrasound in Medicine & Biology*, 26(3):451–456, Mar. 2000.